THREE-DIMENSIONAL FINITE ELEMENT MODELLING IN PILED RAFT
FOUNDATION DESIGN

A THESIS SUBMITTED TO
THE GRADUATE SCHOOL OF NATURAL AND APPLIED SCIENCES
OF
MIDDLE EAST TECHNICAL UNIVERSITY

BY

SINEM SONGÜR

IN PARTIAL FULFILLMENT OF THE REQUIREMENTS
FOR
THE DEGREE OF MASTER OF SCIENCE
IN
CIVIL ENGINEERING

JUNE 2019

Approval of the thesis:

THREE-DIMENSIONAL FINITE ELEMENT MODELLING IN PILED RAFT FOUNDATION DESIGN

submitted by **SINEM SONGÜR** in partial fulfillment of the requirements for the degree of **Master of Science in Civil Engineering Department, Middle East Technical University** by,

Prof. Dr. Halil Kalıpçılar
Dean, Graduate School of **Natural and Applied Sciences**   _____

Prof. Dr. Ahmet Türer
Head of Department, **Civil Engineering**   _____

Assist. Prof. Dr. Nejan Huvaj Sarıhan
Supervisor, **Civil Engineering, METU**   _____

Examining Committee Members:

Prof. Dr. Erdal Çokça
Civil Engineering Department, METU   _____

Assist. Prof. Dr. Nejan Huvaj Sarıhan
Civil Engineering, METU   _____

Assist. Prof. Dr. Onur Pekcan
Civil Engineering Department, METU   _____

Prof. Dr. Sami Oğuzhan Akbaş
Civil Engineering Department, Gazi University   _____

Assoc. Prof. Dr. Berna Unutmaz
Civil Engineering Department, Hacettepe University   _____

Date: 26.06.2019

I hereby declare that all information in this document has been obtained and presented in accordance with academic rules and ethical conduct. I also declare that, as required by these rules and conduct, I have fully cited and referenced all material and results that are not original to this work.

Name, Surname: Sinem Songür

Signature:

ABSTRACT

THREE-DIMENSIONAL FINITE ELEMENT MODELLING IN PILED RAFT FOUNDATION DESIGN

Songür, Sinem
Master of Science, Civil Engineering
Supervisor: Assist. Prof. Dr. Nejan Huvaj Sarıhan

June 2019, 146 pages

This thesis is about optimization of load sharing between piles and raft. Starting with comparison of two pile models named volume pile and embedded pile in a finite element software, verification with an existing building was made. In the next part of the thesis, optimization on pile configuration, pile length, soil type and soil models are presented. Based on the results, it can be concluded that as spacing over diameter ratio increases, settlement reduction ratio also increases and piled raft coefficient, which is ratio of the axial load on piles over total load, decreases. Moreover, increase in single and total pile lengths also increases the piled raft coefficient, whereas it decreases settlement reduction ratio. Lastly, it is implied that a value of "80" for "total length of piles / length of single pile" leads to optimum conditions for all cases analyzed in this study.

Keywords: Piled Raft Foundations, Volume Piles, Embedded Piles, Optimization, Finite Element Modelling

ÖZ

KAZIKLI RADYE TEMEL TASARIMINDA ÜÇ BOYUTLU SONLU ELEMANLAR MODELLEMESİ

Songür, Sinem
Yüksek Lisans, İnşaat Mühendisliği
Tez Danışmanı: Dr. Öğr. Üyesi Nejan Huvaj Sarıhan

Haziran 2019, 146 sayfa

Bu çalışma, kazıklar ve radye arasındaki yük paylaşımının optimizasyonu üzerinedir. Sonlu elemanlar yazılımında hacimsel kazık ve gömülü kazık isimli iki kazık modelinin karşılaştırılması ile başlanarak, var olan bir bina üzerinde doğrulama çalışması yapılmıştır. Sonraki aşamada ise, kazık yerleşimi, kazık boyu, zemin tipi ve zemin modellerinin optimizasyonu sunulmaktadır. Sonuçlara dayanarak, kazık aralığı ve çap oranı arttıkça, oturma azaltma oranının da arttığı ve kazıklara gelen yükün toplam yüke oranı olan kazıklı radye katsayısının azaldığı görülmektedir. Ayrıca, tek kazık uzunluğu ve toplam kazık uzunluğundaki artış, kazıklı radye katsayısını artırırken, oturma azaltma oranını düşürmektedir. Son olarak, "toplam kazık uzunluğu / tek kazık uzunluğu" oranı için "80" değerinin bu çalışmadaki tüm durumlar için optimum koşulları sağladığı sonucu çıkarılmıştır.

Anahtar Kelimeler: Kazıklı Radye Temeller, Hacimsel Kazıklar, Gömülü Kazıklar, Optimizasyon, Sonlu Eleman Modellemeleri

Dedicated to my family

ACKNOWLEDGMENTS

TABLE OF CONTENTS

LIST OF TABLES

TABLES

LIST OF FIGURES

FIGURES

xiv

CHAPTER 1

INTRODUCTION

1.1. General Information

A pile foundation consists of three elements namely pile cap, certain number of piles and the soil. Conventional pile foundation design assumes that piles carry all structural loads and the pile cap does not contribute to the load carrying capacity.

In the last few decades, piled raft design concept has been increasingly used for the foundation design of many buildings especially high rise buildings and towers. Unlike the conventional pile foundation design, this design approach considers the contribution of the raft to the load carrying capacity. In other words, structural load is confronted by both the raft and the piles (Figure 1.1). In this case, piles serve for controlling total and differential settlement in addition to load carrying.

For the piled raft foundation design, several interaction mechanisms are required to be considered, such as the pile-soil, raft-soil, pile-pile and pile-raft interactions (Figure 1.2).
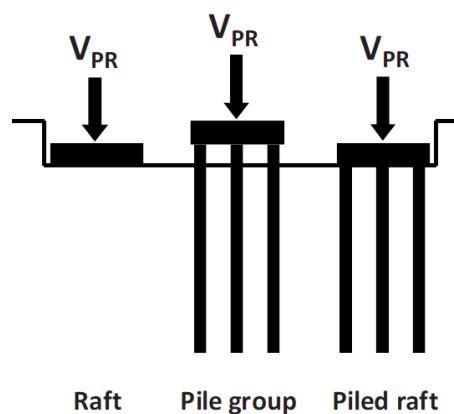
Figure 1.1. Representation of total vertical load 'V_{PR}' carried by different foundation systems (Mandolini et al., 2013)
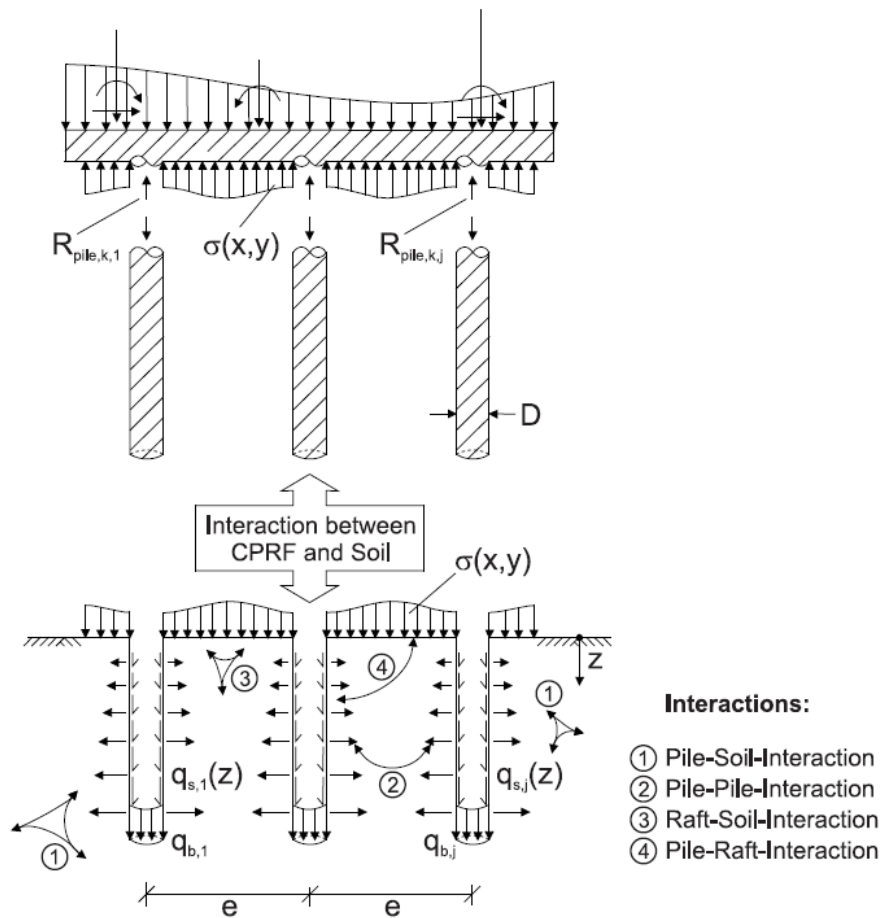
Figure 1.2. Mechanism and interactions of combined pile-raft foundation (CPRF) (ISSMGE, 2013)

Conventional pile foundation design is sometimes more conservative and piled raft foundation design may provide a more economic design approach compared to conventional design. In the case of piled raft, since the piles are used more efficiently and load is shared between piles and raft, unnecessary number of piles may be avoided and a more feasible way of design is provided by ensuring the safety of the structure. It should be noted that in certain cases such as clay soils raft may lose contact with underlying clay when clay undergoes volume change and piled raft may act like pile foundation.

2

1.2. Problem Statement

Finite element method (FEM) is generally used in the design of piled raft foundations. Analytical solutions, laboratory studies-experiments and real case measurements are compared with the results of finite element solutions in various studies in order to provide verification of them. There are many examples of designs conducted via FEM analyses in the literature such as Reul & Randolph (2003), Prakoso & Kulhawy (2001) and Sönmez (2013).

In this study, piled raft foundation is modelled by three-dimensional finite element method, using Plaxis 3D software. In order to provide a guideline for designers, it is essential to combine variables such as soil type, soil model, pile length, pile configuration and pile modelling approach. Therefore, this thesis focuses on examining the effects of these variables.

1.3. Research Objectives

This study aims at investigating the load-sharing and settlement characteristics of piled raft foundations. More specific objectives are as follows:

(1)   To study the load sharing mechanism between the piles and the cap by the help of three-dimensional finite element analyses

(2)   To calculate settlements via finite element analyses and to compare them with the results of real cases

(3)   To provide an optimum design by changing the length, configuration or geometrical positioning of piles in sands and clays under various material models

(4)   To design the piles by both 'Volume pile' and 'Embedded pile' features of Plaxis 3D finite element program and to compare the results of different approaches in order to check whether embedded pile can replace volume pile or not due to time concerns

3

1.4. Scope

This study investigates the design of piled raft foundations by Plaxis 3D finite element software. In Chapter 2, literature review is presented. Design methodology, volume pile and embedded pile properties of software, some numerical and experimental studies are summarized by researching bearing capacity and settlement results. In Chapter 3, methodology and comparison of volume pile and embedded pile properties of Plaxis 3D are provided by verification of a real case. In Chapter 4, two hypothetical cases consisting of either sand or clay are studied by using embedded pile property. Moreover, building and analyzing a model in Plaxis 3D are also presented. In Chapter 5, results of the analyses and conclusions are discussed.

CHAPTER 2

LITERATURE REVIEW

2.1. Design Methodology of Piled Raft Foundation

Mandolini et al. (2013) consider the fact that piles and the raft both carry the total structural load in collaboration in the piled raft foundation design concept. In other words, the total structural load (V_{PR}) is shared among piles and the raft unlike the conventional pile foundation design concept that ignores the load capacity of the raft. Mandolini et al. (2013), represents the aforementioned load sharing behavior with a load sharing ratio (α_{pr}) among piles and the raft and describes the load sharing ratio as the portion of the load carried by the piles. (Eqn 2.1)

$$\alpha_{pr} = \frac{\sum_{i=1}^{n} V_{pile,i}}{V_{PR}} \qquad \text{(Eqn 2.1)}$$

where "n" represents the number of piles and "V_{pile}" represents the load carried by a single pile.

As illustrated in Figure 1.1, $\alpha_{pr} = 0$ implies a raft foundation whereas $\alpha_{pr} = 1$ implies a pile foundation without support of the raft. For a piled raft foundation $0 < \alpha_{pr} < 1$ condition is valid.

In the study, a chart for foundation selection is presented in Figure 2.1 that defines some design approaches including CBD (Capacity Based Design), CSBD (Capacity and Settlement Based Design), SBD (Settlement Based Design), RBD (Raft Based Design) and DSBD (Differential Settlement Based Design).

B_R Raft width

R_{UR} Unpiled raft resistance

w_{UR}, w_{adm} Average settlement of the unpiled raft and admissible average settlement

FS   Factor of safety
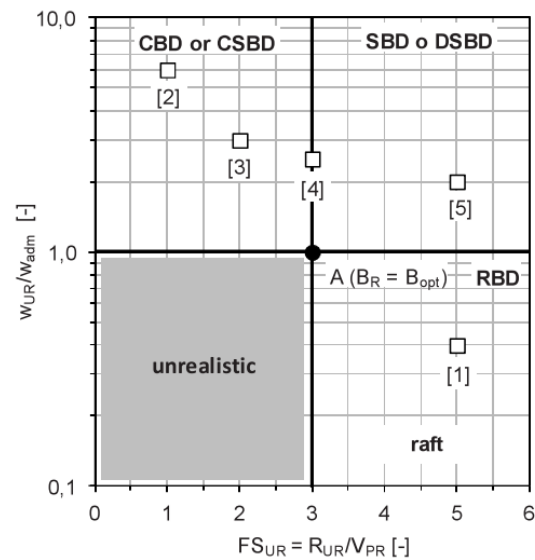
Figure 2.1. Selection chart for design approach (Mandolini et al., 2013)

For a convenient FS=3, "A" point might be considered as optimum where w_{ur}/w_{adm} equals to 1.

Point 1 represents RBD in which w_{ur} and FS_{ur} are acceptable.

For Point 2 and Point 3, both the w_{ur} and FS_{ur} are not acceptable since w_{ur} is greater than w_{adm} and FS_{ur} is under the convenient limit. In order to overcome the FS issue and settlement problem, piles must be added to the system.

For Point 4 and Point 5, FS_{ur} is acceptable. However, w_{ur} is not acceptable since it is greater than w_{adm}. In order to decrease the settlement, piles must be added to the system.

Poulos (2001) explains the design concept and issues of piled raft foundations by defining the stages of the design process with favourable and unfavourable conditions.

Just like the any other foundation systems, the issues of ultimate load capacity under the lateral, vertical and moment loads, total maximum and differential settlements, structural design properties of raft and piles such as moment, shear for raft and axial load for piles must be considered in the design of piled raft foundations.

Poulos (2001) reported that favourable soil conditions in which the piled raft foundations can be successfully applied are stiff clays and dense sands. On the other hand, unfavourable soil conditions include soft clays or loose sands close to the surface, soft compressible layers at the bottom layers and the layers prone to swelling or consolidation. In such cases, raft-soil contact should always exist.

Various design approaches are available related to piled rafts. To be more precise, load and settlement behaviour of piled raft foundation depending on different design approaches can be seen at the Figure 2.2. Curve 0 represents the raft only design with excessive settlements. Curve 1 is the traditional design approach that the piles are assumed to carry the total load. Curve 2 shows the "creep piling" case in which the piles are designed to carry the working load corresponding to 70 - 80% of the ultimate load with a lower factor of safety compared to Curve 1. Curve 3, which belongs to the case in which the piles are placed effectively to control differential settlement, represents the optimum solution by meeting the minimum requirements of design load and allowable solution while the others seem to be over or under-designed.
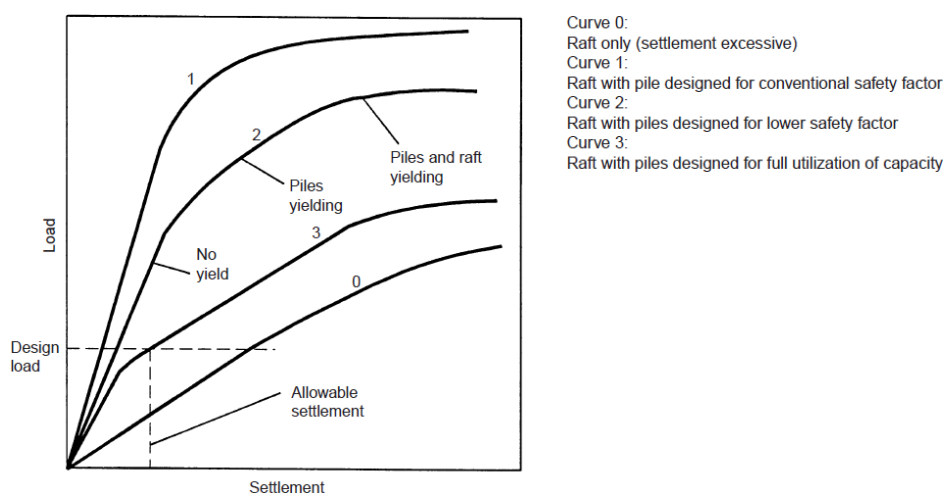
Figure 2.2. Load and settlement curves of diverse design approaches (Poulos, 2001)

7

Finally, the crucial points and stages of the design process are summarized as below:

- In the first stage, necessary number of piles is determined in order to provide to fulfill the requirements of design load and allowable settlements.
- In the second stage, pile location and general properties are determined according to the loading.
- In the last stage, details of the design are presented such as location, configuration and number of the piles and the load, moment and settlement results of raft and piles are computed.

Poulos (2002), discusses the design issues of piled raft foundations by explaining the essential points to be considered by the designers.

Piled raft foundations can effectively be used in cases in which the raft alone can almost meet the load carrying capacity but cannot adequately meet the requirements of allowable total and differential settlements. Therefore, first, the performance of unpiled raft should be analyzed when starting the design. Then, the main points including raft thickness, pile type, pile configuration, pile length and pile diameter must be decided. For this decision, overall vertical load capacity, overall load settlement behaviour and overall differential settlement must be considered.

In overall load settlement part, Poulos (2002) proposes the following equations to determine the stiffness of piled raft and the load taken by raft (Poulos & Davis, 1980; Randolph & Clancy, 1993).

$$k_{pr} = \frac{\left(k_p + k_r(1 - 2\alpha_{pr})\right)}{\left(1 - \alpha_{pr}^2 \frac{k_r}{k_p}\right)} \quad (Eqn\ 2.2)$$

$$\frac{P_r}{P_t} = \frac{k_r(1 - \alpha_{cp})}{k_p + k_r(1 - 2\alpha_{cp})} \quad (Eqn\ 2.3)$$

8

where k_{pr} is piled raft stiffness, k_p is pile group stiffness, k_r is raft stiffness α_{pr} is raft – pile interaction factor, P_r is the load carried by raft and P_t is the total load. Finally, in the result of above equations, following chart is obtained (Figure 2.3.). k_{pr} is calculated from Eqn 2.2 and it is operated until Point A. Beyond Point A, k_r is operated until Point B. After this point, ultimate load capacity of piled raft foundation is reached.
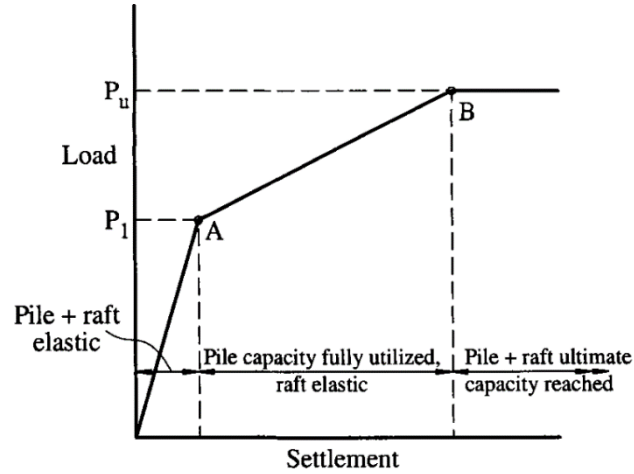
Figure 2.3. Load settlement curve for preliminary design (Poulos, 2002)

The studies of **Clancy & Randolph (1996),** provide a basis for Poulos (2002) and recommend the following parameter range in Table 2.2.

Table 2.1. *Explanations of parameters (Clancy & Randolph, 1996)*

Soil	Pile	Raft
Young's modulus E_s Poisson's ratio ν_s	Young's modulus E_p Length L_p Diameter d_p Spacing s_p	Young's modulus E_r Poisson's ratio ν_r Thickness t_r Length L_r Breadth B_r

Table 2.2. *Recommendations for parameters (Clancy & Randolph, 1996)*

Dimensionless group	Definition	Practical range
Pile slenderness ratio	L_p/d_p	10–100
Pile spacing ratio	s_p/d_p	2·5–8
Pile–soil stiffness ratio	$K_{ps} = E_p/E_s$	100–10 000
Raft plan aspect ratio	L_r/B_r	1–10
Raft–soil stiffness ratio	$K_{rs} = \dfrac{4E_r B_r t_r{}^3(1 - \nu_s{}^2)}{3\pi E_s L_r{}^4(1 - \nu_r{}^2)}$	0·001–10

9

Given chart in Figure 2.4 provides α_{rp} values for various square raft configurations with the values of $L_p/d_p = 25$, $K_{ps} = 1000$ and $K_{rs} = 10$. Moreover, detailed information and different α_{rp} values for other parameters are presented by the charts in the study of Clancy & Randolph (1993).
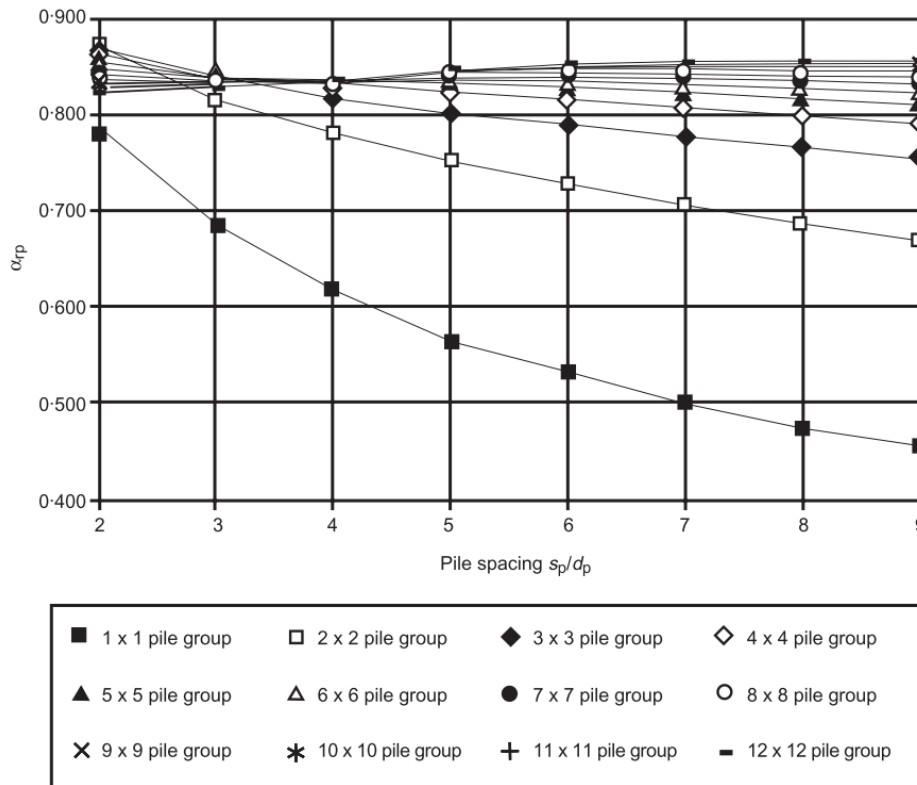
Figure 2.4. α_{rp} values for $L_p/d_p = 25$, $K_{ps} = 1000$ and $K_{rs} = 10$ (Clancy & Randolph, 1996)

Prakoso & Kulhawy (2001), proposes a design method that is the result of a detailed parametric study for piled raft foundations. This design method is presented schematically in the given flowchart in Figure 2.5.
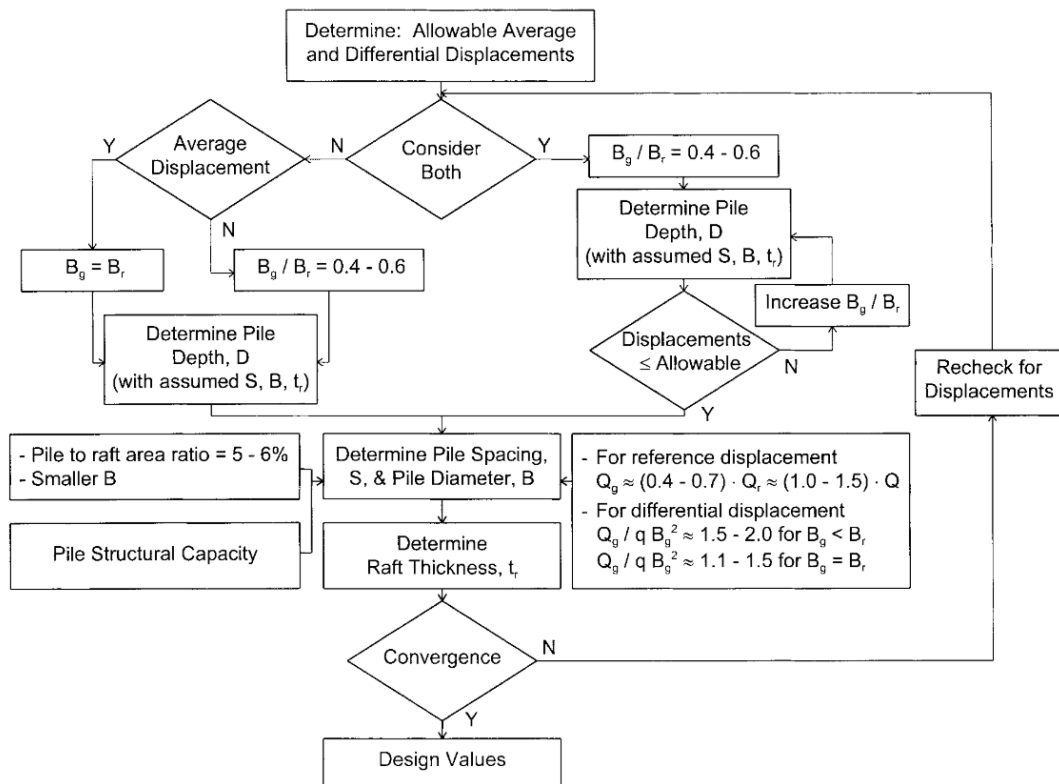
Figure 2.5. Design method flowchart for piled raft foundations (Prakoso & Kulhawy, 2001)

Design method in Figure 2.5 is explained step by step in the following part:

- Firstly, allowable average and differential settlements are determined.
- Pile group to raft width ratio (B_g/B_r) determination is the next step. If the focus is the average settlement, B_g/B_r ratio is assumed as 1. However, if the focus is just the differential settlement or both average settlement and differential settlement, B_g/B_r ratio is assumed as $0.4 - 0.6$. Based on this value, pile depth (D) is determined and settlement values are checked for allowable limits. If it does not fulfill the requirements, B_g/B_r value is increased and the process is repeated until the requirements are met.
- In the next step, pile diameter and pile spacing is determined according to the values pile to raft area ratio (R_{area}), pile group capacity (Q_g), and the pile structural capacity.

11

- In the final step, raft thickness (t_r) is determined based on structural design.

El-Mossallamy et al. (2006) defines the behaviour of piled raft foundation design as in the following figure so that α_s =1 means conventional raft foundation while α_s gets closer to zero, conventional pile foundation is observed. 0< α_s <1 is the region of piled raft foundation. On the other hand, α_L =0 means conventional raft foundation while α_L gets closer to 1, conventional pile foundation is observed. 0< α_L <1 is the region of piled raft foundation.
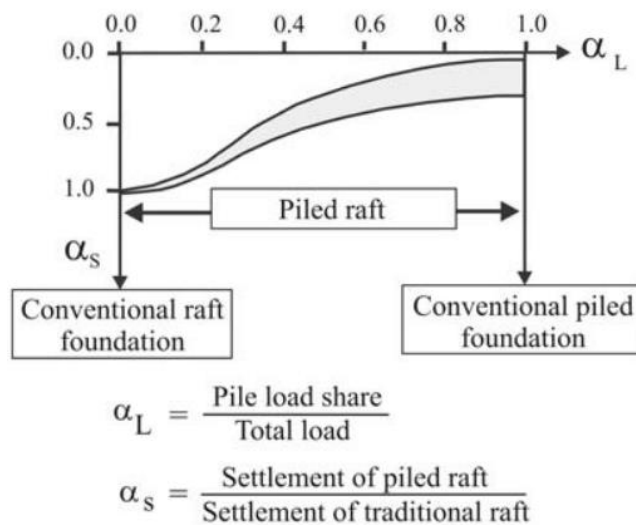
Figure 2.6. α_s and α_L values for piled raft foundation design

2.2. Volume Pile and Embedded Pile Properties

Engin et al. (2008), investigates the reliability of embedded pile property of Plaxis 3D by comparing the finite element software results to field test results.

Embedded pile is a slender beam element which has skin and tip interfaces with the surrounding soil. The advantage of this property is that the piles can be placed in arbitrary direction and location in the soil elements even though 3D finite element mesh has been generated.

In this study, single pile behaviour is examined by both field tests for which the cases of compression pile test case and tension pile test case. These cases are also modelled by embedded pile property of Plaxis 3D.

The first real case is Alzey Bridge pile. The soil profile consists of silt at the upper part underlied by over consolidated stiff plastic clay. Pile load test cells are placed on tip of the pile to measure the compression load. Skin friction is computed by subtracting the tip resistance from the total load.

Tension pile tests are conducted on the bored piles in South Surra, Kuwait where the soil profile consists of cemented desert sand which is detailed in the study of Ismael et al. (1994). Both the compression pile measurements and tension pile measurements are found compatible with embedded pile results as shown in Figure 2.7.
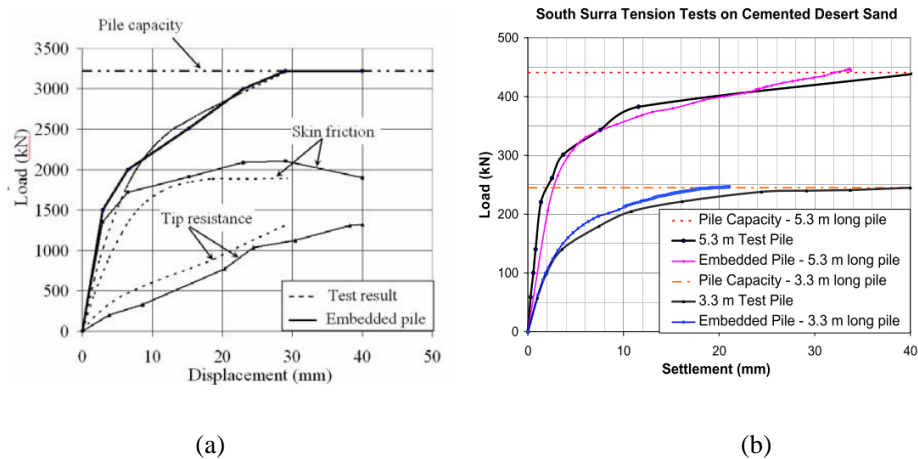
Figure 2.7. (a) Alzey Bridge pile test and embedded pile model load results (b) South Surra pile test and embedded pile model load results (Engin et al., 2008)

In the study of **Dao (2011)**, Plaxis 3D embedded pile property is validated by comparing with Plaxis 3D volume pile property and real measurements in the design of laterally loaded piles.

13

Firstly, a simplified model is created with the boundaries 8 m in x direction, 8 m in y direction and 1 m in z direction. An embedded pile with 1 m length is placed at the origin of the model and the displacement in z direction is restrained while the displacement at the pile foot is allowed in x and y direction. In order to refine the mesh around the embedded pile, a cylinder with 1D diameter is placed around the embedded pile. The cylinder has the same properties with the soil. (Figure 2.8.(a))

Secondly, the same geometry is created for the volume pile as well. However, unlike the embedded pile generation, a material data set for concrete is assigned to the soil volume that represents the volume pile. (Figure 2.8.(b)) R_{inter} value which represents the roughness of the pile soil interaction is assumed as $R_{inter} = 1$ and $R_{inter} = 0.5$ for two different volume pile model.

| (a) | (b) |
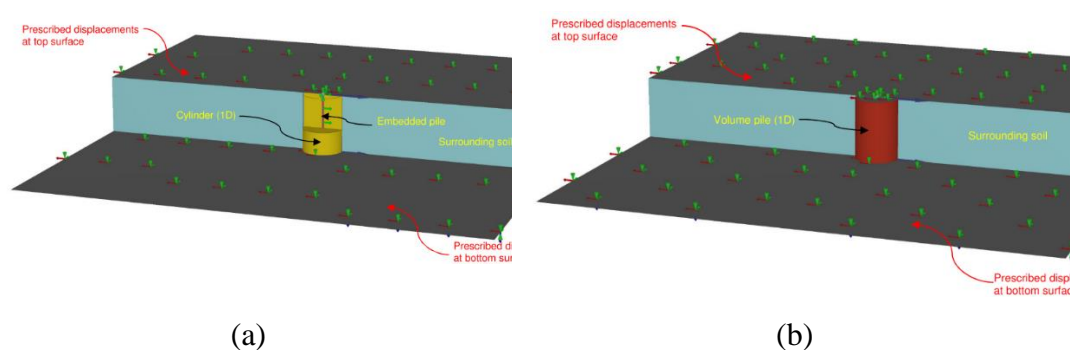
Figure 2.8. (a) Embedded pile model view (b) Volume pile model view (Dao, 2011)

Finally, load and displacement results of embedded pile and volume pile models are compared in Figure 2.9 and embedded pile results are found as nearly same with volume pile results with $R_{inter} = 1$ (without interface).
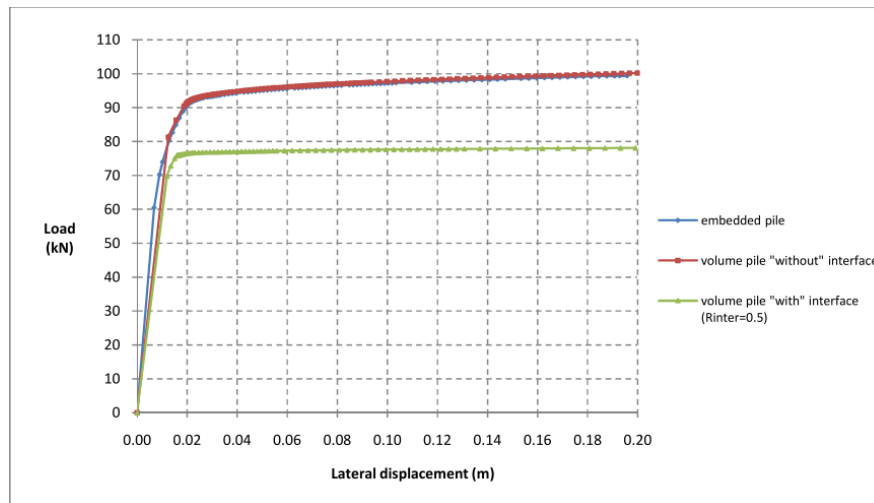
Figure 2.9. Load and displacement curves of embedded pile and volume pile models (Dao, 2011)

Sluis et al. (2014), investigates the use of embedded pile feature in and compare the displacement and bending moment results with the ones of Plaxis 3D analysis for a pile row under lateral load.

They state that piles are used to be modelled as plate or node to node anchor in Plaxis 2D before embedded pile feature of Plaxis. However, these two methods both have disadvantages.

In plate method, plates are created by taking the pile properties for unit width in out of plane. Nevertheless, this causes to decrease the effect of pile soil interaction by interfering the soil mesh and limits the out of plane spacing to lower values.

Node to node anchor method totally ignores the interaction between soil and pile since soil covers all the model including the node to node anchor elements and mesh is continuous that is independent from the pile. In addition, node to node anchor method can only be used for axially loaded piles since it ignores lateral interaction.

Embedded pile feature reflects the benefits of both plate and node to node anchor. Embedded pile behaves like a beam element but in a continuous mesh in the existence of both pile and soil. So, the pile soil interaction is modelled Plaxis 2D well.

15

Finally, embedded pile feature of Plaxis 2D is validated by comparing to Plaxis 3D results in terms of axial load including both compression and tension load; lateral loading resulting from external forces and soil movements. The results are 2D and 3D analyses are found as compatible.

Sheil & McCabe (2012), investigate the single pile and pile group behaviour in soft clay which are modelled by Plaxis 3D embedded pile feature. Pile group finite element results are compared to the field test data in order to see the convenience of embedded pile feature. The comparison presents that this feature provides compatible results with field test data and considered as reasonable due to time saving and less computational effort.

In this study, bearing capacity of embedded pile that is related to the embedded pile properties of maximum skin resistance T_{max} and maximum base resistance F_{max} are also explained. In embedded pile feature, bearing capacity of the pile is not a result of finite element analyses. It must be an input parameter in the material set properties of pile. T_{max} and F_{max} values are generally determined by pile load tests. The skin resistance is considered in three ways including:

- Linear skin friction is defined at pile head and bottom of the pile as $T_{top,max}$ and $T_{bot,max}$
- Multi linear skin friction is used for multi-layered soil profiles with a certain $T_{top,max}$ and varying $T_{bot,max}$ along the pile at different locations.
- Layer dependent skin friction considers the soil strength parameters such as friction angle (φ), cohesion (c) and pile interface factor R_{inter}.

2.3. Various Numerical Studies

In the dissertation of **Ryltenius (2011)**, piled raft foundations are modelled in four ways by Plaxis 3D and Plaxis 2D FEM programs to compare the results of two and

three dimensioned analysis. One model is established in three dimensional and three models are established in two dimensional in soft clay to discuss pile raft interaction.

In piled raft foundations, contrary to the conventional pile foundation design, load distribution between raft and piles is the matter. While raft contributes to the load carrying capacity, piles are used for total and differential settlement reduction.

According to the results of the analysis:

In two dimensional model, raft carries 51 % of the total load. Maximum settlement is 121 mm and the differential settlement is 16 mm.

In three dimensional model, raft carries 36 % of the total load. Maximum settlement is 56 mm and the differential settlement is 11 mm.

A series of analysis are done for different spacing of piles and different raft dimensions for both two and three dimensions. Two dimension analysis results of settlement and load carrying capacity of raft are overestimated compared to three dimensional model.

In the study of **Reul & Randolph (2003)**, foundations of three buildings in Frankfurt, Germany, named Westend 1, Messeturm and Torhaus der Messe, are investigated and back analysis results of piled raft foundations obtained from three dimensional FEM analyses by ABAQUS program, in a subsoil condition of overconsolidated Frankfurt clay underlied by rocky Frankfurt limestone are presented. Measured values are compared to results of analytical solutions and finite element analyses.

First building Westend 1 consists of a 208 m high tower and a 60 m low rise section. Piled raft belongs to the tower part with the raft dimensions of 47 x 62 x 3-4.65 m and 40 bored piles with 1.3 m diameter, 30 m length. Measured center settlement value is 120 mm 2.5 years after the completion of construction whereas the finite element result is 110 mm. according to the measured records, raft carries 50 % of the total load while the finite element result is 44 %.

Second building Messeturm is a 256 m high tower. Foundation is a piled raft with the raft dimensions of 58.8 x 58.8 x 3-6 m and 64 bored piles with 1.3 m diameter,

different lengths of 26.9, 30.9 and 34.9 m. Measured center settlement value is 144 mm whereas the finite element result is 174 mm. according to the measured records, raft carries 57 % of the total load while the finite element result is 40 %.

Third building Torhaus der Messe is a 130 m high tower. Foundation is two piled rafts 10 m apart from each other with the raft dimensions of 17.5 x 24.5 x 2.5 m and 84 bored piles with 0.9 m diameter, 20 m length. Average measured center settlement value of two rafts is 124 mm whereas the finite element result is 96 mm. According to the measured records, raft carries 33 % of the total load while the finite element result is 24 %.

As a result, settlement calculations are compatible with the measured ones but the raft load is underestimated compared to measured values.

In the thesis of **Yılmaz (2010)**, two sets of piled raft foundations with raft dimensions 24x28x2 m and 2.25 m spacing are analyzed by Plaxis 3D program. Number of piles is 143, 120 and 99 alternately and pile length is 25 m for the first set. Number of piles is 120, 99 and 80 alternately and pile length is 30 m for the second set. Effects of number of piles and pile length on settlement values are investigated. Results of the analyses are compared with analytical methods of Butterfield and Douglas (1981) and Shen and Teh (2002) (Table 2.3).

Table 2.3. *Number of piles vs settlement (Yılmaz, 2010)*

		number of piles	settlement (cm)
Set 1 (L = 25 m)	Butterfield and Douglas' 81	143	10,32
		120	10,92
		99	11,61
	Shen and Teh' 02	143	8,91
		120	9,73
		99	10,73
	Plaxis 3D Foundation	143	8,86
		120	9,27
		99	10,00
		80	13,63
Set 2 (L = 30 m)	Butterfield and Douglas' 81	120	9,51
		99	10,11
		80	10,82
	Shen and Teh' 02	120	9,57
		99	10,48
		80	11,51
	Plaxis 3D Foundation	120	7,92
		99	8,39
		80	9,21
		63	12,24

It may be concluded that increasing the number of piles beyond the optimum quantity does not decrease the settlement value significantly. Therefore, optimum number provides an economical design.

A parametric study is done by **Garg et al. (2013)** on optimization of piled raft foundations. The soil profile consists of clay with the properties defined in Table 2.4. 300 kPa uniform load is applied on the system. Some parameters are used as variables which are defined as number of piles (N), aspect ratio (l/d), pile spacing (s/d) and raft thickness (t) shown in Table 2.4.

Table 2.4. *Table of parameters (Garg et al., 2013)*

Property	Unit	Value
Unit weight γ_{unsat}	[kN/m³]	16
Saturated unit weight γ_{sat}	[kN/m³]	19
Young modulus E_{ref}	[kN/m²]	2.000E+04
Poisson ratio μ	[-]	0.35
Shear modulus G_{ref}	[kN/m²]	7407.407
Young modulus E_{oed}	[kN/m²]	3.210E+04
Cohesion c_{ref}	[°]	80
Friction angle φ	[°]	0
Dialantancy angle ψ	[°]	0
Interface strength R_{inter}	[-]	1.0

Aspect ratio (l/d)	Spacing ratio (s/d)	Strip Thickness (t), mm
10	3	300
15	4	400
20	6	500
25	8	600
30	10	700
35	12	800
40	14	900
45	16	1000
50	18	1100
55	20	1200
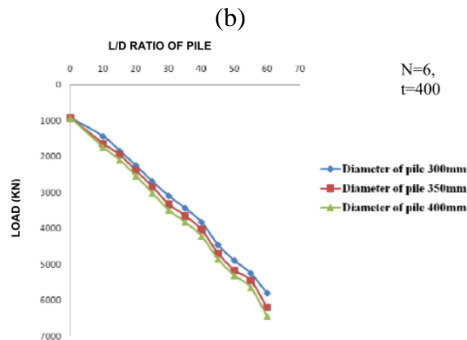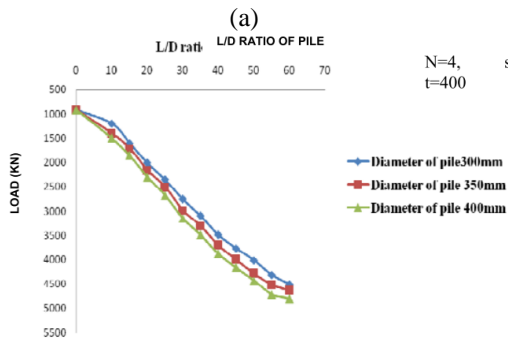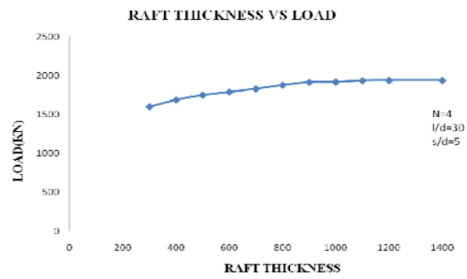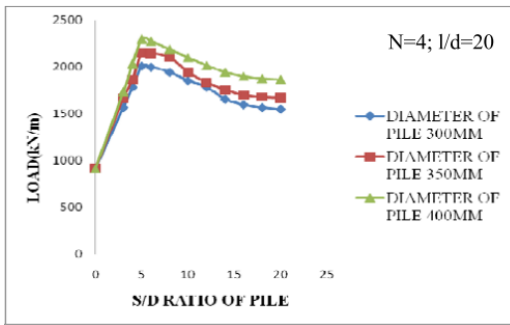
(a)

(b)

(c)

(d)
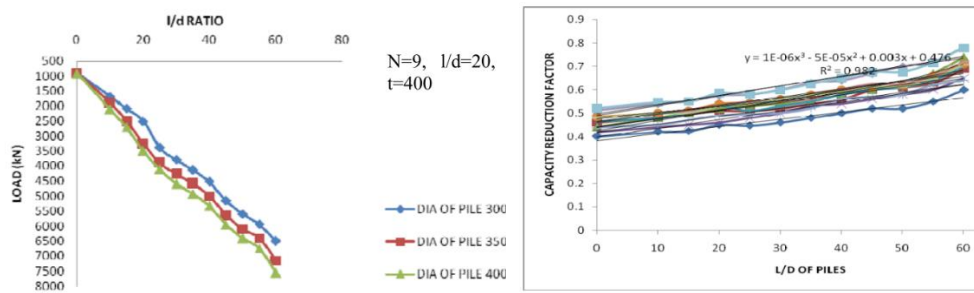
(e)   (f)
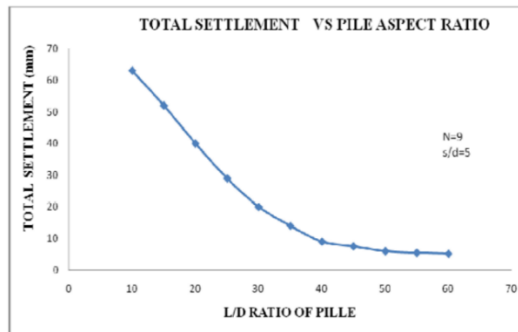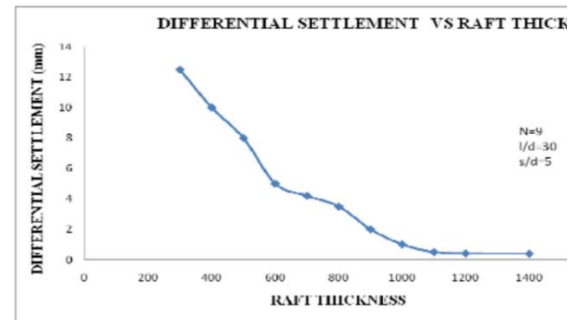
(g)   (h)

Figure 2.10. (a) Impact of s/d ratio on load carrying capacity (b) Impact of s/d raft thickness on load carrying capacity (c), (d), (e) Impact of l/d ratio on load carrying capacity (f) Impact of l/d ratio on α (g) Impact of l/d ratio on total settlement (h) Impact of raft thickness on differential settlement (Garg et al., 2013)

According to the charts in Figure 2.10, followings are concluded:

- Load carrying capacity increases up to s/d is equal to 5, after this point, capacity decreases.

- As the raft thickness increases, load carrying capacity also increases. After a certain point, raft thickness does not have a significant effect on load carrying capacity.

- Increase of the pile diameter from 300 mm to 350 mm to 400 mm, causes increase in load carrying capacity between 15-20%.

- Changing l/d ratio 10 to 55 increases the load carrying capacity nearly by 70%.

21

- Other than the finite element software solution, load on components are calculated by the help of Capacity reduction factor (α). The capacity of the components of the piled raft foundation system is calculated by conventional methods and multiplied by the capacity reduction factor. Capacity reduction factor (α) can be calculated by the following equation of

$$\alpha = 10^{-6} \left(\frac{l}{d}\right)^3 - 5 * 10^{-5} \left(\frac{l}{d}\right)^2 + 0.0003(\frac{l}{d}) + 0.476$$

- Increase of l/d decreases the total settlement up to 90%. Optimum design is provided by choosing l/d as 30.
- Increase of raft thickness decreases the differential settlement.
- Increase in pile to raft area ratio decreases the differential settlement.

In the study of **Alver & Özden (2015)**, method of optimum design of piled raft foundation is investigated which includes two stages. In the first stage, impact of number of piles is examined for a constant pile length. The aim of this stage is determining the minimum number of piles that provides minimum settlement. After determining total pile length by finding the minimum number of piles, pile length and number of piles are changed for a constant total length.

The soil profile of the foundation of a high rise building in Mavişehir, İzmir consists of multiple layers which are 3 m fill at the top underlied by 4 m silty sand and 9 m soft clay with high plasticity at the bottom. Raft sizes are 50 m x 20 m in x and y directions respectively.

Settlement results, which are computed by both Randolph method from literature and finite element analyses, are given at the following Table for different number of piles and spacings.

Table 2.5. *Settlement results for different number of piles (Alver & Özden, 2015)*

Number of piles	s_x (m)	s_y (m)	Settlement, S(mm)	
			Randolph	Finite element (3D)
24 (3x8)	6,8	9,0	48,0	44,3
30 (3x10)	5,3	9,0	35,4	34,4
36 (4x9)	6,0	6,0	31,4	30,2
45 (5x9)	6,0	4,5	29,6	29,0
55 (5x11)	4,8	4,5	28,7	28,1
65 (5x13)	4,0	4,5	28,2	27,8
75 (5x15)	3,4	4,5	28,1	27,5
90 (6x15)	3,4	3,6	27,8	27,4

According to the limit point that the settlements do not significantly decrease beyond, number of piles is determined as 55 for a pile length of 36 m and therefore, the total pile length is calculated as 1980 m. After this point, number of piles and pile lengths are changed for a constant total pile length of 1980 (Table 2.6.).

Table 2.6. *The results of change in pile length and number of piles (Alver & Özden, 2015)*

Number of piles	Pile length, L (m)	s_x (m)	s_y (m)	Settlement, S(mm)
				Finite element (3D)
36 (4x9)	54	6,0	6,0	15,6
44 (4x11)	45	4,8	6,0	20,1
55 (5x11)	36	4,8	4,5	28,1
66 (6x11)	30	4,8	3,6	38,1
80 (5x16)	25	3,2	4,5	46,8
102 (6x17)	20	3,0	3,6	63,0

Conclusions of this study may be listed as following:

- Settlement of the piled raft foundation decrease while the number of piles increase. However, increase in number of piles does not affect the settlement significantly beyond a point where the optimum design is reached.

- Optimum s/d ratio is found as the interval of 4.5-6.

- Increase in pile length decreases the settlement.

Kuwabara (1989), searches for the behavior of piled raft foundation under vertical load by changing the parameters of number of piles (N), pile length over pile diameter ratio (L/d), pile spacing to pile diameter (s/d), $(K=(E_p/E_s)R_A)$ where R_A is the cross section area of pile over area limited by outer circumference. For a model with N=3x3, L/d=25, s/d=5, K=1000; distribution of the contact pressure is investigated at the quarter of the whole model. (Figure 2.11) The percentage of contact pressure on the raft element (p_c) and average contact pressure on the raft (p_{cav}) is shown for various raft elements in Figure 2.11. The results implies that the contact pressure decreases from the area near the corner piles to the area near the edge piles to the center pile.

Figure 2.11. Contact pressure distribution of the raft elements (Kuwabara,

1989)

Mali & Singh (2018) study on the behavior of piled raft foundations in clay under vertical load in terms of settlement, load sharing, bending moment and shear force.

The analyses are conducted by Plaxis 3D software. 15 different pile configurations are arranged with different pile spacing, length, diameter and raft – soil stiffness ratio. A square raft with 45 m x 45 m is loaded 200 kPa.

Conclusions of the study can be summarized as follows;

- The optimum s/d ratio is determined as 5-6 where the settlement and bending moment reach to minimum values.
- The optimum piled group to raft width ratio is found as 0.6 where the bending moment is minimum.
- Increase in pile diameter causes decrease in average and differential settlement and increase in load sharing ratio of pile group.

Increase in raft - soil stiffness ratio causes increase in shear force. However, bending moment is slightly affected by raft - soil stiffness ratio beyond the value of 0.09.

2.4. Experimental Studies

In the paper of **Patil et al. (2014)**, load settlement behaviour and load sharing mechanism of piled raft foundations are presented through an experimental investigation in dry sand by considering different raft thickness and pile configurations. Pile length is selected as 200 mm and slenderness ratio (L/D) is 20. A steel tank is filled with sand and the foundation is placed. Load is applied and vertical displacement is measured by two linear displacement transducers.
Test summary is shown in the table below.

Table 2.7. *Test summary (Patil et al., 2014)*

Test Explanation	Model Raft dimensions (mm x mm x mm)	L/D	S/D	Number of Test Performed
Unpiled raft	160x160x5			1
	160x160x10	-	-	1
	160x160x15			1
Raft + 1 pile	160x160x5			1
	160x160x10	10	-	1
	160x160x15			1
Raft + 4 piles	160x160x5			1
	160x160x10	10	3	1
	160x160x15			1
Raft + 9 piles	160x160x5			1
	160x160x10	10	3	1
	160x160x15			1

Results of the experiments imply that at the beginning of the loading, piles carry the major part of the load. However, as the settlement increases, load is transferred to the raft. Load shared by piles and settlement reduction ratio increase with the increasing number of piles. But, beyond a certain number of piles settlement reduction ratio does not affected much. Increase of raft thickness does not affect the load shared by piles and settlement.

Horikoshi & Randolph (1998) considers the effective placement of the piles under the raft in order to provide an optimum design. Pile group is located at the center of the raft in such a way that total and differential settlements remain in an acceptable range (Figure 2.12).
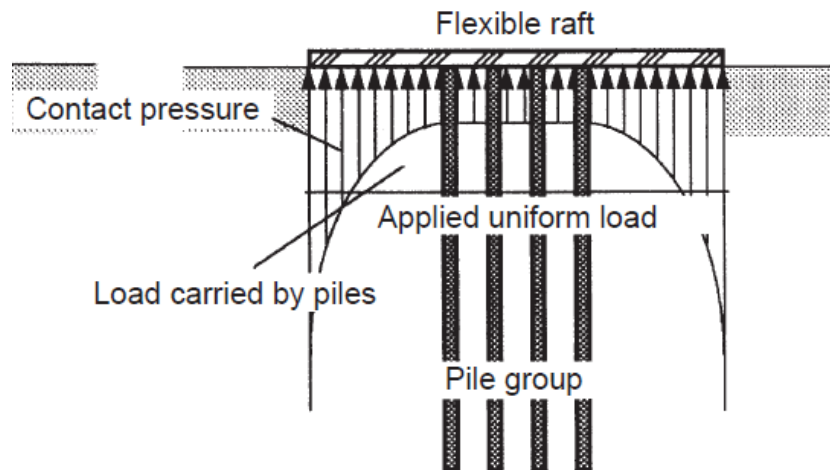
Figure 2.12. Load sharing in piled raft (Horikoshi & Randolph, 1998)

Foundation is modelled by a method of analysis named HyPR based on the word "hybrid" which was developed by Clancy (1993). An important limitation of HyPR is that homogenous soil conditions must be used in model.

Verification of the method is provided by centrifuge test with the following: 9 piles with a diameter of 0.32 m, a length of 15 m and 2.5 m spacing.

According to the results of HyPR and centrifuge test, optimum piled raft design is defined as follows:

- Piles should be located at the 16-25 % of the central area of the raft.
- Raft stiffness and pile group stiffness should be approximately equal.
- Pile group should carry 40-70 % of the total load.

Elwakil & Azzam (2016), perform 23 laboratory tests representing a piled raft foundation in a small scale. Medium dense sand is selected as test soil. Test setup is shown in detail in Figure 2.13. The raft is a steel square plate including 16 piles with a diameter of 16 mm and spacing of 37.5 mm. Different pile lengths are used as 100 mm, 200 mm and 400 mm. Number of piles are also changed as 4, 8, and 16. For each

pile length and number of piles, test is performed in both way that the raft is in contact with the soil surface and free from the soil surface. In addition, piles are placed in both square or staggered configuration.
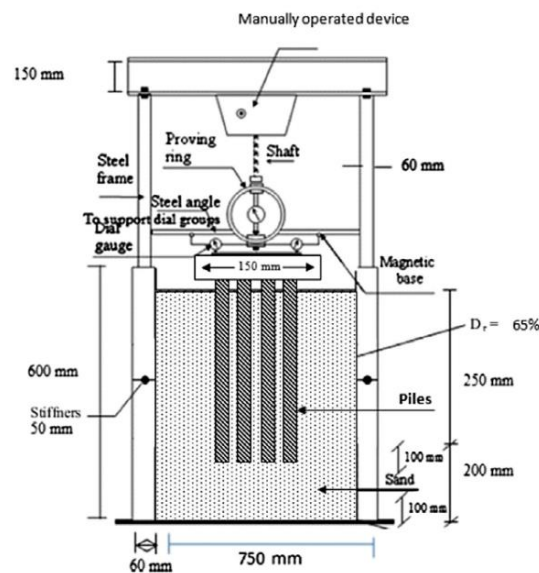
Figure 2.13. Test setup (Elwakil & Azzam, 2016)

The test results propound that;

- Average load carried by the raft is calculated as 39%.
- When the length of piles is reduced, contribution of the raft to load carrying increases.
- When the spacing of piles is reduced, contribution of the raft to load carrying increases.
- Use of few short piles or few long piles with large spacing causes to block failure under the raft. On the other hand, use of long piles with smaller spacing causes block failure under the pile tip.
- Settlement of foundation decreases with number piles and L/D ratio which is the ratio of pile length to pile diameter.

Mosawi et al. (2011), conduct some laboratory tests in order to investigate the behavior of piled raft foundation. The experiment is performed with a soil tank with the length of 0.6 m, width of 0.6 m, height 0.6 m and filled with medium dense sand. The dimensions of the tank is selected in a way so that the boundaries do not limit the failure zone of foundation. The material of piles and the raft is aluminum alloy.

Piled raft geometry is formed by changing some parameters in each test. Pile spacing is selected as 5 cm and kept constant for all the tests. Thickness of raft is determined as 5 mm and 2.5 mm. l/d ratio is changed as 20, 25 and 30. Pile diameters are 9 mm, 12 mm, 15 mm and pile lengths are 200 mm, 250 mm, 300 mm. Pile configurations are formed as 2x1, 3x1, 2x2 and 3x2. The vertical load applied on foundation is either 5 kN or 10 kN. Unpiled raft is also examined for comparison.

The experiment results are as follows;

- The percentage of the load carried by pile group is found as 28%, 38%, 56%, 79% for pile configurations 2x1, 3x1, 2x2, 3x2, respectively with a diameter of 9 mm and a raft thickness of 5 mm. This implies that increase in number of piles also increases the percentage of the load carried by pile group.
- For the unpiled raft, thickness of raft slightly influence the load carrying capacity. On the other hand, raft size increase also raises the load carrying capacity.

Increase in pile diameter, pile length and number of piles also increases the load carrying capacity.

CHAPTER 3

METHODOLOGY AND VERIFICATION

3.1. Introduction

In this chapter, different types of pile modelling in Plaxis 3D that are volume pile and embedded pile are investigated in order to provide the verification of the results of both pile modelling types and determine which one will be used in Chapter 4 for the hypothetical cases.

3.2. Volume Pile and Embedded Pile Properties of Plaxis 3D

3.2.1. Volume Pile

Volume pile comprises three dimensional volume elements, which interact with the surrounding soil.

While modelling the volume pile in Plaxis 3D, the geometry is formed by using *cylinder* command in command line with the properties of radius, height, accuracy which is the number of elements in pile surface (see Figure 3.1) and pointing in direction. Properties are explained with definitions and examples in Table 3.1.

Table 3.1. *Plaxis 3D Reference Manual "cylinder" command definitions*

Purpose
Create a cylinder with a specified radius, height and accuracy at a location (x, y, z) in a specified direction described by a vector.

Example
`cylinder 2 5 10 (1 2 3) (5 7 12)`
    Creates a cylinder with a radius of 2, a height of 5 an accuracy of 10 at coordinates (1, 2, 3) pointing in direction (5, 7, 12).

Signature
`Number' Number' Integer' <Coords: Number' Number' Number'>' <Coords: Number' Number' Number'>'`

Parameters

Number	Radius	Desired radius of the cylinder
Number	Height	Desired height of the cylinder
Integer	Accuracy	Desired accuracy of the cylinder (>1)
Coords		Coordinates
Number	x	x-coordinate
Number	y	y-coordinate
Number	z	z-coordinate
Coords		Vector giving the direction in which the cylinder should be pointing
Number	x	x-value
Number	y	y-value
Number	z	z-value

Volume pile material properties are determined as if it was a soil material with concrete properties. In other words, a material data set for soil is constituted and concrete properties are assigned to the soil material data set. Then, this soil material data set with concrete properties is assigned to the volume pile. However, generating a volume with soil material data set prevents to see the force results of piles unlike embedded piles. In order to overcome this problem, a beam element (Figure 3.1), with the same material properties as volume pile but a Young's Modulus 10^6 times lower than volume pile, is inserted inside the volume element (Dao, 2011). It should be noted that the force results of beam elements needs to be multiplied by 10^6 to reach the real force result of volume pile.
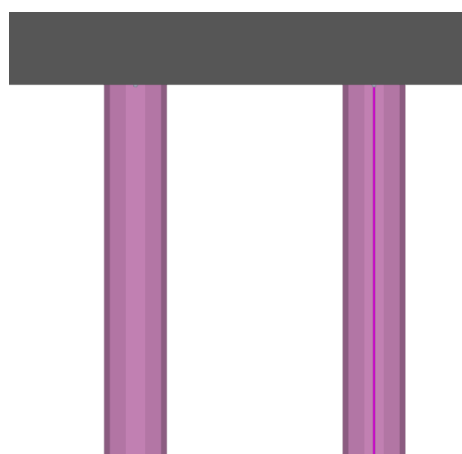
Figure 3.1. Volume pile view with beam element inside it

3.2.2. Embedded Pile

Embedded pile is a beam element that does not occupy any volume and assumes an elastic zone around it in which the plastic soil behavior is not observed. The pile - soil interaction occurs by means of pile skin interaction and pile tip interaction. The beam element is considered to show a linear elastic behaviour.

Since the beam element has no volume, it can easily be located at any point, directed and oriented arbitrarily.

An embedded pile material data set is constituted and the properties of the material data set are assigned to both embedded pile beam element and the elastic zone around it.
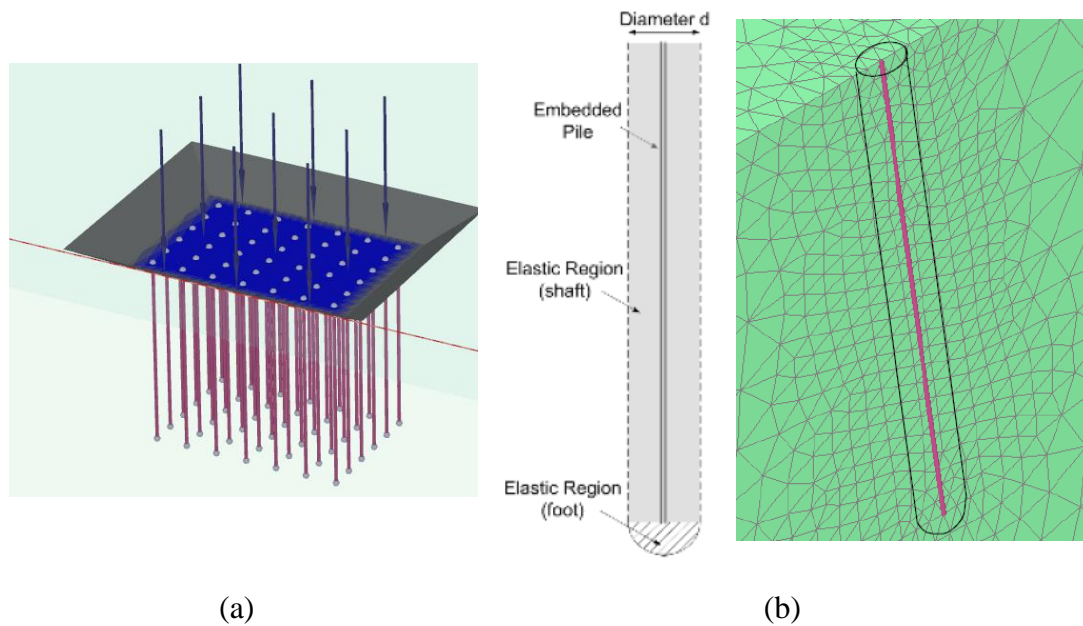
Figure 3.2. (a) Embedded pile view (b) Embedded pile (Brinkgreve, 2014)

Unlike volume pile, embedded pile model can directly give force results. In addition, meshing procedure is not applied to embedded pile since it is a beam element. This provides to shorten the duration of computation and less exertion is needed for analyses.

3.3. A Case Study on Pile Modelling Type

In order to investigate and demonstrate the comparison of volume pile and embedded pile modelling, a case study is conducted on a 130 m high rise building located in Frankfurt and named Torhaus, which was constructed between 1983 and 1986 based on the study of Reul & Randolph (2003).
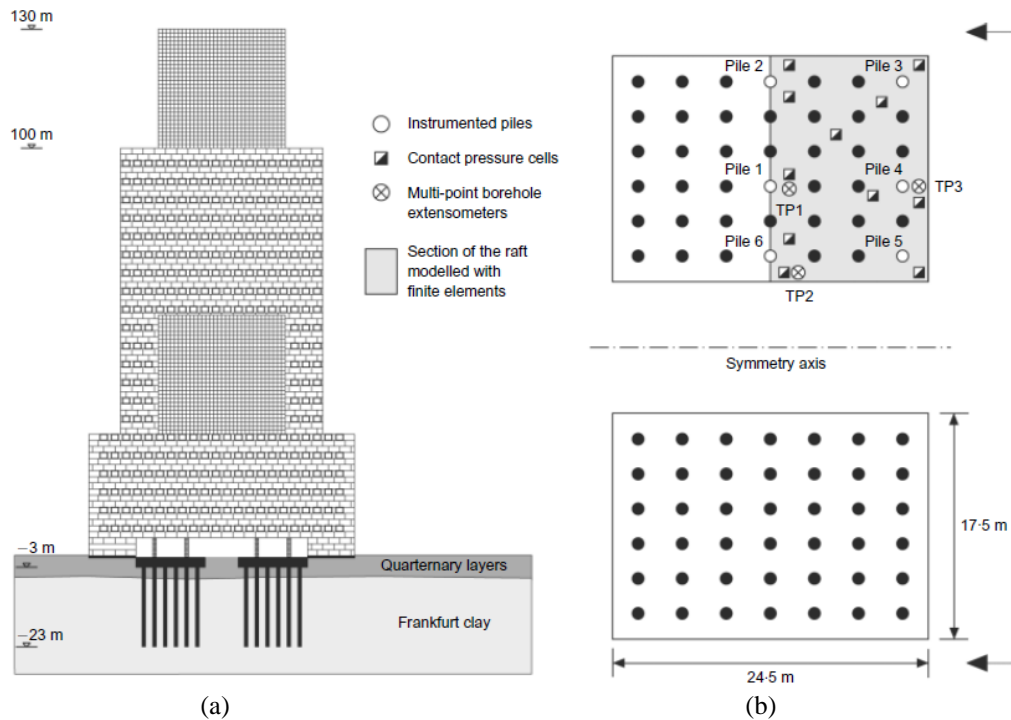
Figure 3.3. (a) Side view of Torhaus building (b) Top view of the foundation (Reul & Randolph, 2003)

The foundation involves two symmetrical rafts and 42 bored piles for each raft as seen in Figure 3.3.(a) and Figure 3.3.(b). In total, 84 piles with 20 m length and 0.9 m diameter are placed under the rafts with the sizes of 17.5 m x 24.5 m x 2.5 m. Raft bottom is located at 3 m depth from ground level. The two rafts are 10 m away from each other.

Structural load is 200000 kN which is uniformly applied on the rafts as 466 kPa.

The soil profile consists of two layers that are quaternary sand and gravel with a depth of 5.5 m and underlying Frankfurt clay. Ground water level is at 3 m depth from ground level. (Figure 3.3.(a))

Material model is selected as Mohr Coulomb Model and other soil parameters used in Plaxis 3D model are tabulated in Table 3.2.

Table 3.2. *Soil parameters (Sönmez, 2013)*

Soil Parameters				
Property Name	**Symbol**	**Sand**	**Clay**	**Unit**
Saturated unit weight	γ_{sat}	19	20	kN/m^3
Initial void ratio	e_{init}	0.5	0.5	-
Young's Modulus	E'	45000	45241	kN/m^2
Poisson's ratio	ν'	0.2	0.2	-
Cohesion	c'_{ref}	0.0001	20	kN/m^2
Internal friction angle	φ'	35	20	^{o}
Dilatancy angle	ψ	0	0	^{o}

Table 3.3. *Raft parameters (Sönmez, 2013)*

Raft Parameters			
Width	B	17.5	m
Length	L	24.5	m
Thickness	d	2.5	m
Unit weight	γ	25	kN/m^3
Young's Modulus	E	37000000	kPa
Poisson ratio	ν	0.2	-

3.3.1. Volume Pile Modelling of Torhaus

In the design of Torhaus model, firstly, volume pile property of Plaxis 3D is used. After the boundaries of the model are selected as 164.5 m in x direction, 150 m in y direction and 110 m in z direction, the model parameters are defined according to the

input parameters in Chapter 3.3 and volume piles are created by using following sample cylinder command in Plaxis 3D:

"cylinder 0.45 20 10 (72.05 6.875 -3) (0 0 -1)"

In order to define the input parameters for the volume pile, a soil material data set is created with the concrete properties and the following parameters are assigned:

Table 3.4. *Volume pile parameters*

Volume Pile Parameters			
Diameter	d	0.9	m
Unit weight	γ	25	kN/m^3
Young's Modulus	E	23500000	kPa
Material model	Linear Elastic		
Drainage type	Non - porous		
Poisson ratio	ν	0.2	-

The parameters for beam element inside the volume pile are defined in following Table:

Table 3.5. *Beam element parameters*

Beam Element Parameters			
Area	A	0.6362	m^2
Unit weight	γ	25	kN/m^3
Young's Modulus	E	23.5	kPa

Because of the "Soil body collapses" error which is explained in "Excavation" stage of Chapter 4.5, the edges of the excavation area are inclined to 2V:5H (Sönmez, 2013).

In the "Mesh" step, "Medium" mesh is preferred in the mesh selection menu due to the numerical problems in "Very fine" or "Fine" mesh resulting from the excessive

element number in model. However, the foundation part of the model is refined to increase accuracy. Therefore, it takes 61 minutes to complete mesh process. Mesh model can be seen in Figure 3.4.
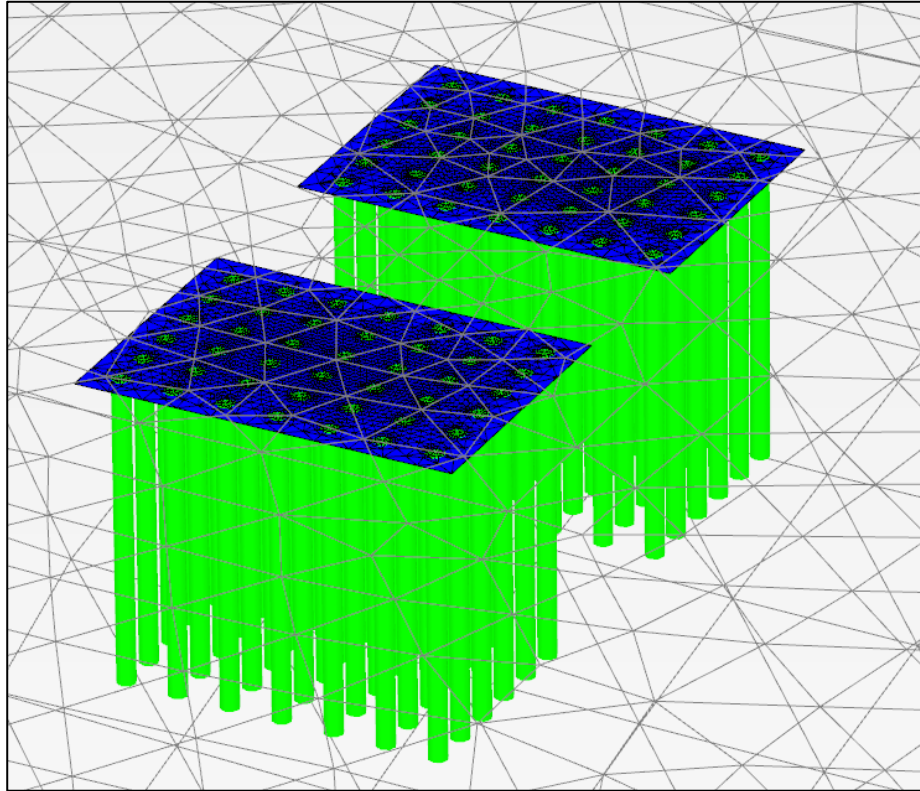
Figure 3.4. Mesh model

Finally, the phases of Excavation, Piles, Raft and Loading are defined respectively. (Figure 3.4) Total computation time for all stages is measured as 193 minutes.

3.3.2. Embedded Pile Modelling of Torhaus

Plaxis 3D model of Torhaus is generated based on the soil profile, geometry, soil and raft parameters of Chapter 3.3. The half of the foundation is modelled according to the symmetry axis in Figure 3.3.(b) due to the decrease of analysis time and computational effort. The boundaries of the model are selected as 164.5 m in x direction, 75 m in y

direction and 110 m in z direction. Apart from that, the embedded pile parameters are tabulated as below:

Table 3.6. *Embedded pile parameters (Engin & Brinkgreve, 2009)*

Embedded Pile Parameters			
Diameter	d	0.9	m
Unit weight	γ	15	kN/m^3
Young's Modulus	E	23500000	kPa
Pile type	Massive circular pile		
Skin friction per unit length	$T_{top, max}$ $T_{bot, max}$	453	kN/m
Tip resistance force	F_{max}	1200	kN

The soil profile, excavated area, the foundation and the surface load are illustrated in Figure 3.5 below:
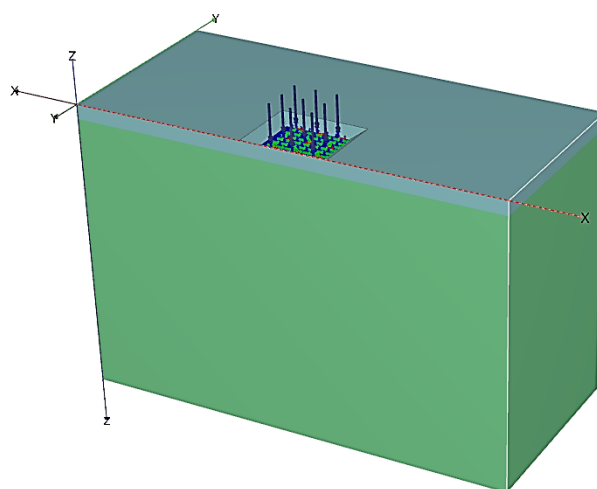
Figure 3.5. General view of Torhaus model

Due to the "Soil body collapses" error that is explained in "Excavation" stage of Chapter 4.5, the edges of the excavation area is inclined to 2V:3H.

After the geometry is generated, mesh size is selected as "Very fine" and the foundation is refined to provide more accurate results; then, "Mesh" step is completed.

In final step, staged construction stages are defined as Initial phase, Excavation, Piles, Raft and Loading respectively. (Figure 3.6)
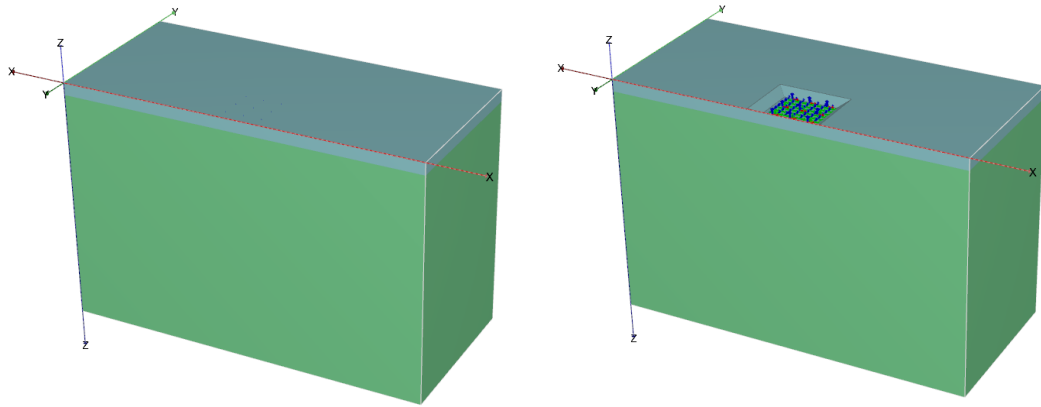
(a)

(b)
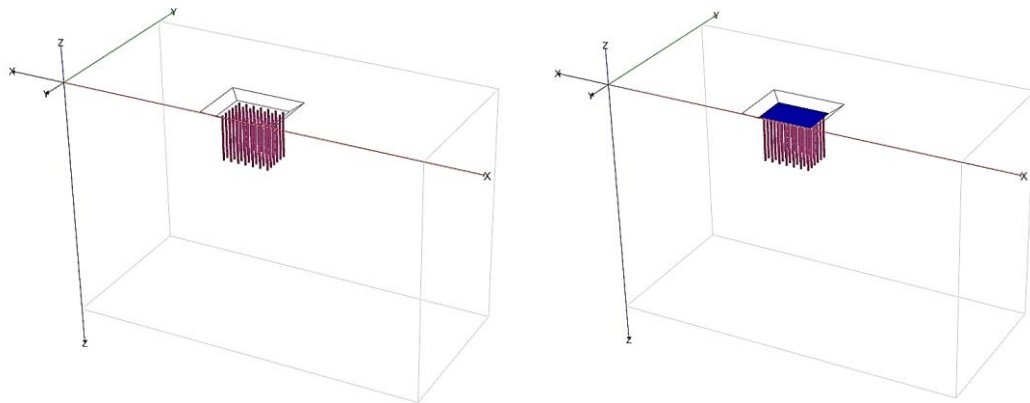
(c)

(d)
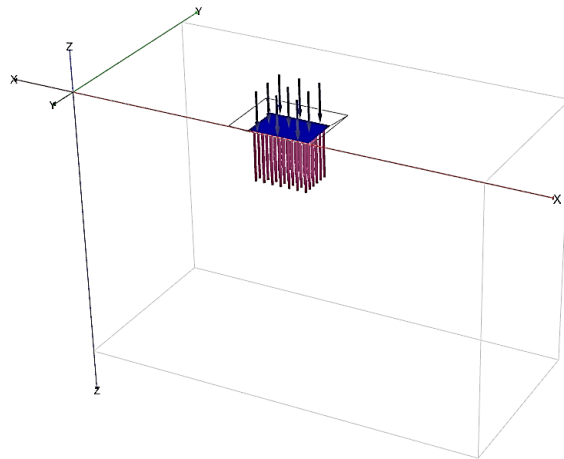
(e)

Figure 3.6. (a) Initial phase (b) Excavation phase (c) Piles phase (d) Raft phase (e) Loading phase

3.4. Evaluation of Conclusions and Verification of the Embedded Pile Property

The results are investigated in terms of settlement of the piled raft foundation and the axial load of piles and raft.

According to Katzenbach et al. (2000), in a piled raft foundation design, the assumption of "loading the piles to their ultimate capacity and distributing the rest of the load to the raft" is valid. Therefore, in this study, the load carried by the piles are viewed by the help of software and compared to the total structural load in order to determine the load sharing mechanism between raft and pile group.

Since Reul & Randolph (2003) and Engin & Brinkgreve (2009) have studied on analyzing Torhaus building, the results of this study might be compared to settlement and load results of aforementioned studies that include both finite element analysis results and real measurements.

Reul & Randolph (2003) present the results of finite element analysis software named ABAQUS and real measurements of Torhaus in their study. The numbering of certain

40

piles, which are used for comparison of finite element analysis results to the measured ones, is given in the following Figure 3.7.
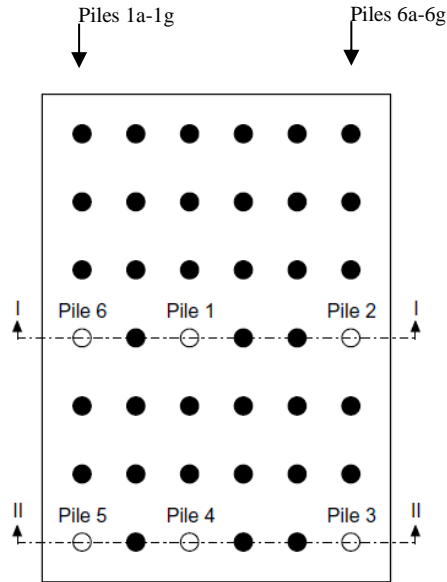
Figure 3.7. Torhaus building pile pattern (Reul & Randolph, 2003)

The axial loads of piles that are located in 6x7 configuration are tabulated below in Table 3.7.

Table 3.7. *Axial loads of piles*

Numbers are given in kN.					
Piles 1a-1g	Piles 2a-2g	Piles 3a-3g	Piles 4a-4g	Piles 5a-5g	Piles 6a-6g
8016	5490	5225	5165	5229	7771
5939	3848	3430	3504	3865	5789
5707	3591	3340	3340	3589	5623
5803	3509	3378	3275	3620	5654
5854	3590	3322	3352	3607	5486
5734	3840	3550	3535	3930	5705
7861	5308	5074	5117	5096	7966

Comparison of all load results of certain piles are given in the Figure 3.8 below. Finite element results of this study, consisting of Plaxis 3D embedded pile model and Plaxis 3D volume pile model, in addition to literature findings, namely, Plaxis 3D embedded pile model (Engin & Brinkgreve, 2009), ABAQUS model (Reul & Randolph, 2003) and the real measurements of February 1986 are presented in the Figure 3.8.
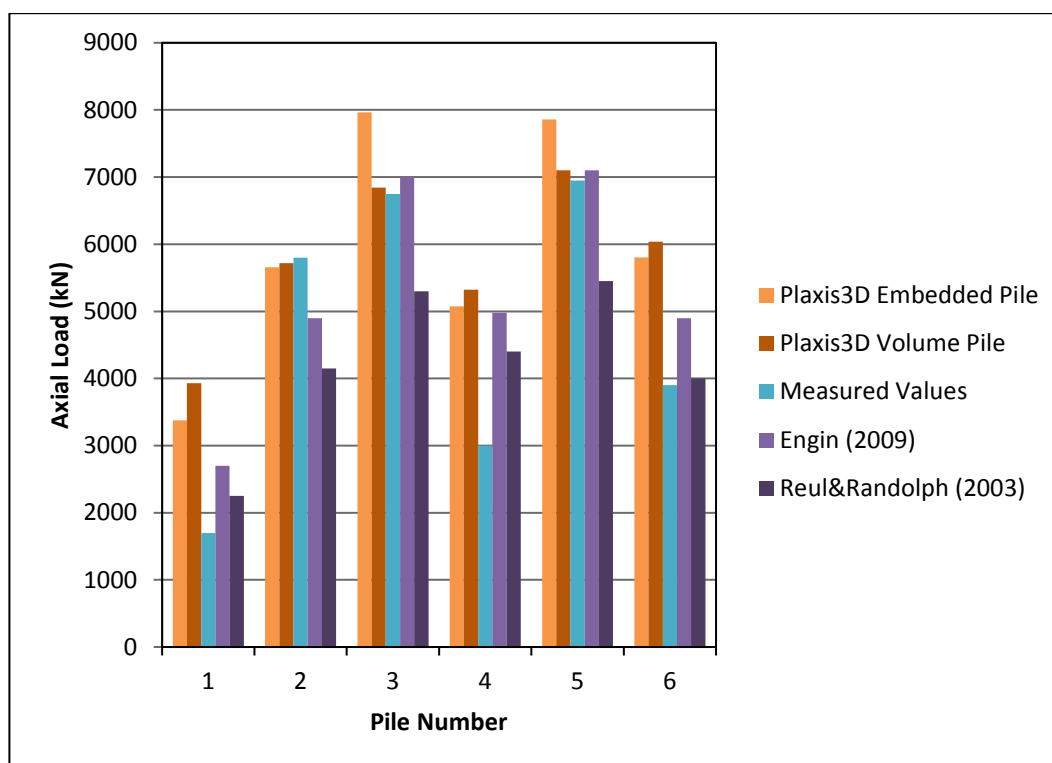
Figure 3.8. Comparison of axial load results

It can be concluded from Figure 3.8 that all the finite element analysis axial load results for Pile 1, Pile 4 and Pile 6 overestimate the pile loads compared to the measured values. On the other hand, Pile 2, Pile 3 and Pile 5 loads give approximate results to the measured values.

Reul & Randolph (2003) also give the finite element analysis results for Cross-section I and Cross-section II that is shown in Figure 3.7. In this study, piles are named as 1d, 2d, 3d, 4d, 5d and 6d for Cross-section I; 1g, 2g, 3g, 4g, 5g and 6g for Cross-section

II. In figure 3.9 and Figure 3.10, the results of Plaxis 3D embedded pile model and Plaxis 3D volume pile model are compared to the results of Reul & Randolph (2003) study. If all of the piles share the total load uniformly (raft takes zero load) each pile would take 200000 kN /42 piles = 4762 kN. This number can also be seen in Figure 3.9 and 3.10 for comparison purposes.
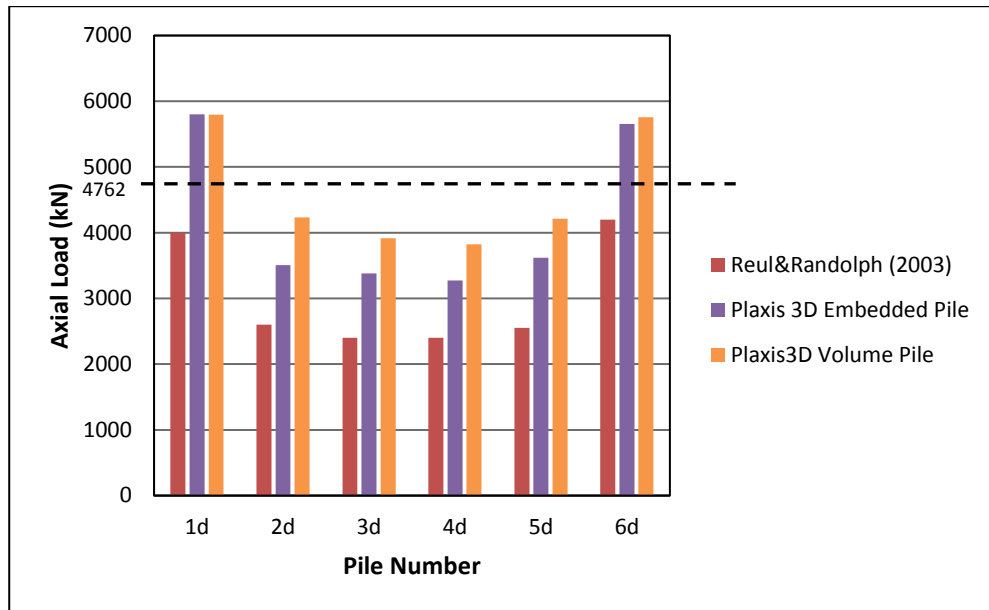
Figure 3.9. Comparison of Pile 1d to Pile 6d axial load results
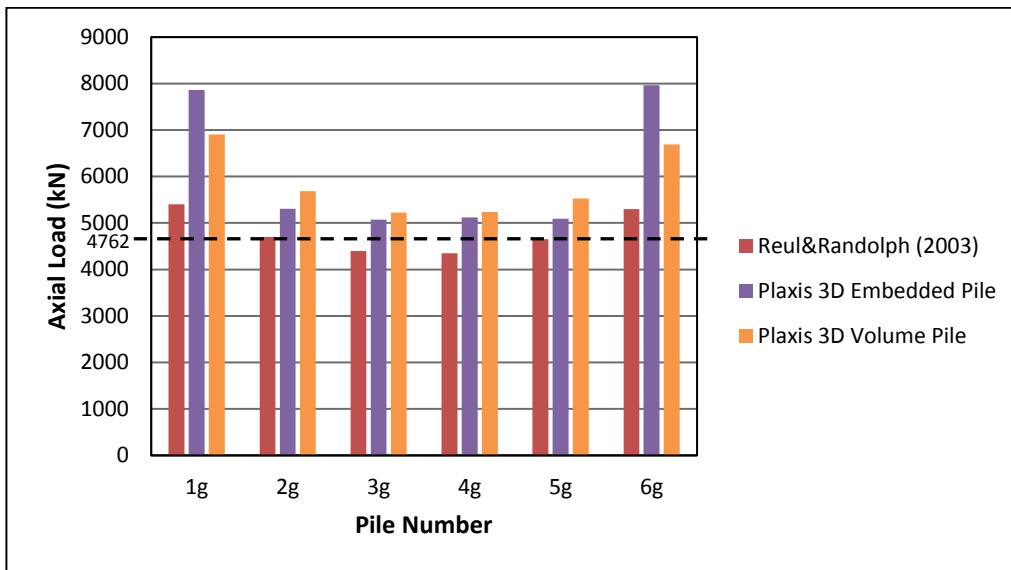
Figure 3.10. Comparison of Pile 1g to Pile 6g axial load results

Evaluation of Figure 3.9 and Figure 3.10 implies that Plaxis 3D estimates higher pile loads compared to Reul & Randolph (2003). While there is a slight difference in central pile loads, a distinct difference is observed for edge and corner piles. However, general behaviour of center pile (Pile 1), edge piles (Pile 2, Pile 4, Pile 6) and corner piles (Pile 3 and Pile 5) are similar to the one of Reul & Randolph (2003). It can also be concluded that the load increases from central pile to edge piles to corner piles.

Finally, settlement values that are measured at the center of the raft are given in Table 3.8. Moreover, the ratio of the load carried by the piles over the total load, α is presented in Table 3.8.

Table 3.8. *Summary of results*

Name of the study	Maximum settlement (mm)	α
Plaxis 3D Embedded Pile	78	0.88
Plaxis 3D Volume Pile	78	0.94
Reul & Randolph (2003)	96	0.76
Sönmez (2013)	76	0.81
Engin & Brinkgreve (2009)	60	0.92
Measured values	124	0.80

Settlement values are similar for finite element analyses. Yet, they underestimate the settlement compared to the measured values.

The ratio of the load carried by the piles over the total load, α values are similar and changes between 80% and 90% nearly.

All in all, it can be stated that comparison of the load and settlement results of volume pile and embedded pile models in Plaxis 3D provides approximate results. If the duration of the finite element analysis and the computational effort for both models are considered, embedded pile property in pile design can safely be used for the analysis of hypothetical cases in Chapter 4.

CHAPTER 4

PARAMETRIC STUDY

4.1. Model Size, Boundary Conditions and Initial Conditions

It is vital that a proper model size and boundary conditions are chosen for the design of foundations in order to provide reasonable results. On one hand, highly close boundaries to the foundation prevent observing the deformation and stress for a sufficient region around the foundation. To illustrate, in Figure 4.1.(a), the boundaries are positioned 0.5B distance from the raft which results in misleading deductions. On the other hand, extending the boundaries beyond the necessary requirements causes ineffectual use of finite element software since it is time consuming to solve a large model. Figure 4.1.(c), in which the boundaries are positioned 2B from the raft and Figure 4.1.(d), in which the boundaries are positioned 4B distance from the raft, can be considered as an unnecessarily huge model.

(a)

(b)

Total displacements |u|
Maximum value = 0,1087 m (Element 6128 at Node 50604)
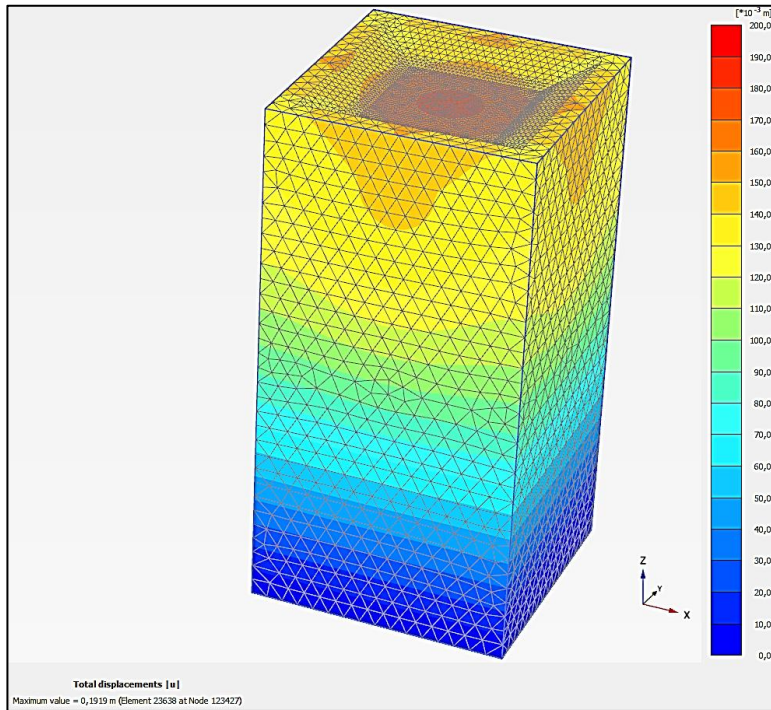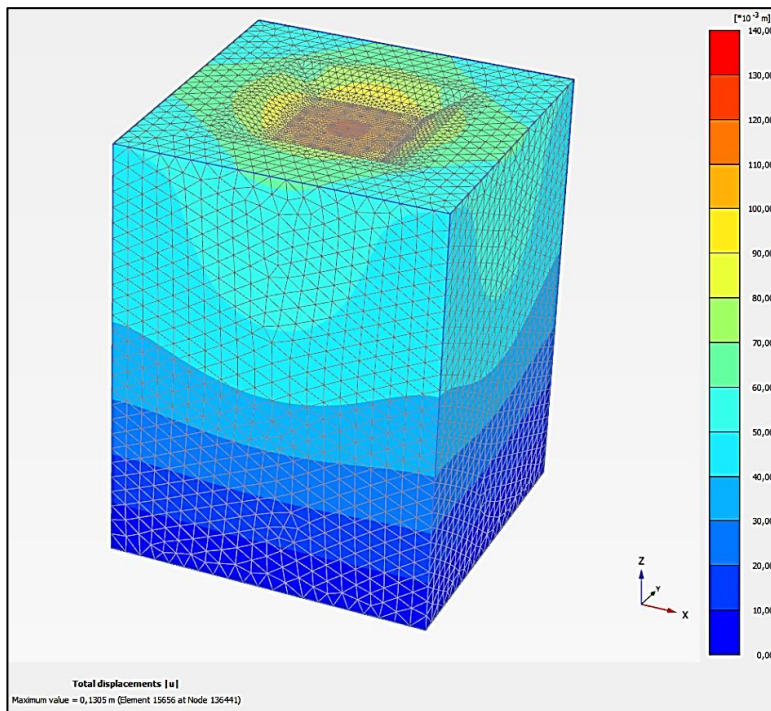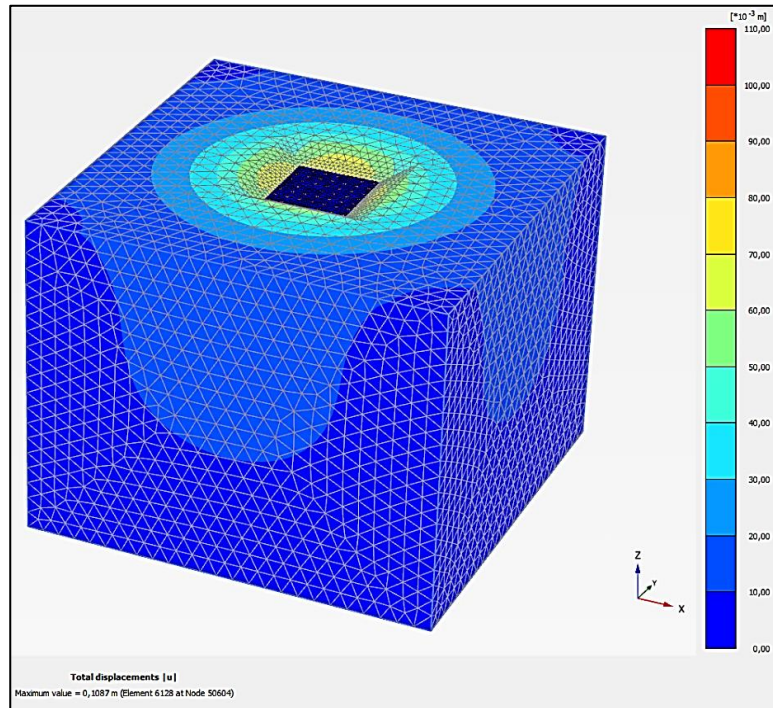
(c)
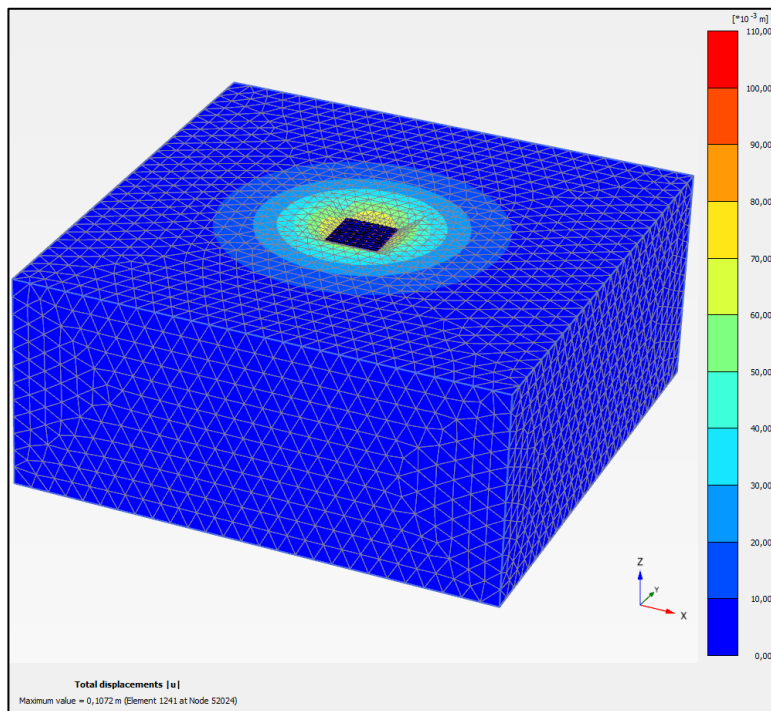
(d)

Figure 4.1. (a) Displacement of 0.5B distanced boundaries (b) Displacement of B distanced boundaries (c) Displacement of 2B distanced boundaries (d) Displacement of 4B distanced boundaries

A proper model size and boundary conditions for a piled raft foundation with raft sizes of "B x B" and pile length "L" might be decided at B distance from raft and 2L distance from the tip of the pile. Therefore, model size of 90 m x 90 m x 120 m is applied for a piled raft foundation with raft sizes of 30 m x 30 m and pile length 40 m (Figure 4.2).
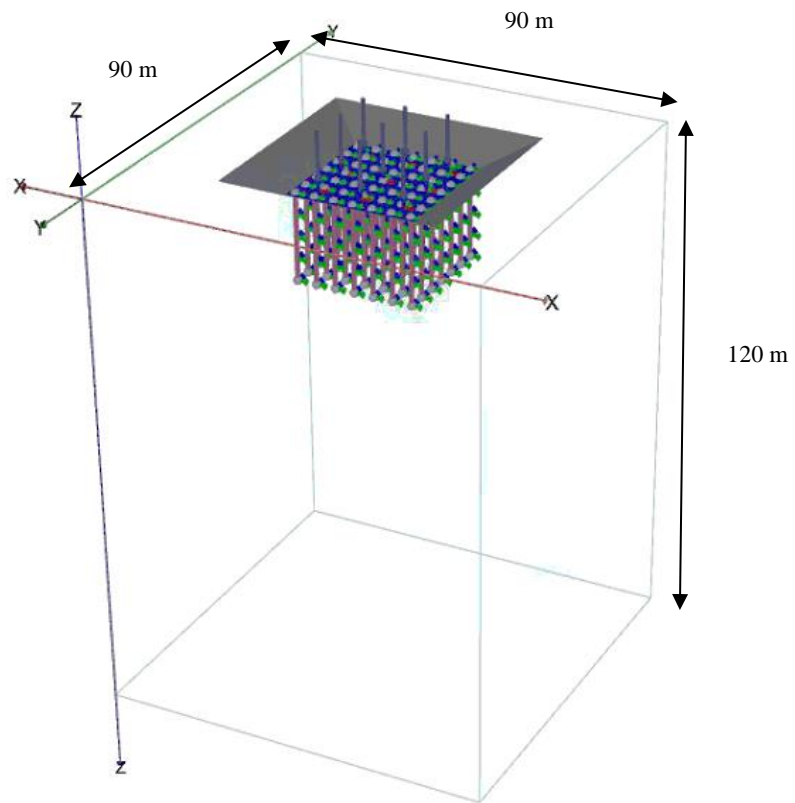
Figure 4.2. General view of the model

4.2. Material Model and Input Parameters

Selection of proper material model according to the soil type is the next step in Plaxis 3D. Considering that the analyses are conducted for two different soil types that are medium dense sand and medium stiff – stiff clay, Table 4.1 might be shown as reference for applicability of the material models.

Table 4.1. *Plaxis 3D Material Models Manual (2013) - Appendix B*

Considering different types of soils								
Model	Concrete	Rock	Gravel	Sand	Silt	OC clay	NC clay	Peat (org)
Linear Elastic model	C	C						
Mohr-Coulomb model	A	B	C	C	C	C	C	C
Hardening Soil model			B	B	B	B	B	
HS small model			A	A	A	A	B	
Soft Soil Creep model							A*	A*
Soft Soil model							A*	A*
Jointed Rock model		A**						
Modified Cam-Clay model							C	C
NGI-ADP model							A*	A*
Hoek-Brown model		A**						

A : The best standard model in PLAXIS for this application

B : Reasonable modelling

C : First order (crude) approximation

* : Soft Soil Creep model in case time-dependent behaviour is important; NGI-ADP model for short-term analysis, in case only undrained strength is known

** : Jointed Rock model in case of anisotropy and stratification; Hoek-Brown model for rock in general

For the first hypothetical case that includes medium dense sand, Mohr Coulomb model, which is the first order approximation, and Hardening Soil model, which is the reasonable modelling, are selected for use in design.

For the design of second hypothetical case that includes medium stiff – stiff clay, Mohr Coulomb model, which is the first order approximation, and Hardening Soil model which is the reasonable modelling and Soft Soil Creep model which is the best standard model are selected for use in design.

Mohr Coulomb model shows linear elastic perfectly plastic behaviour which means totally elastic, reversible and yield surface is not impressed by plastic straining. Basic parameters of Mohr Coulomb model are explained as follows: (Plaxis 3D Manual, 2013)

E': Young's Modulus kN/m^2

ν': Poisson ratio -

c'_{ref}: Cohesion kN/m^2

φ': Friction angle   o

ψ: Dilatancy angle   o
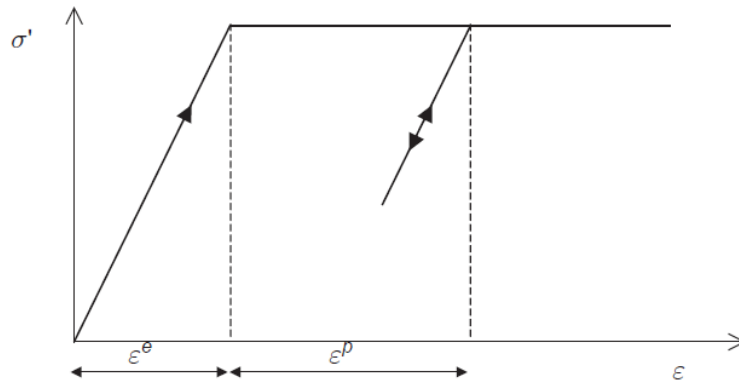
Figure 4.3. Stress – strain behaviour of Mohr Coulomb model (Plaxis 3D Manual, 2013)

Hardening Soil model constitutes two types of hardening used for modelling irreversible plastic strains namely shear hardening resulting from primary deviatoric loading and compression hardening resulting from primary compression in oedometer loading and isotropic loading. Basic parameters of Hardening Soil model are explained as follows: (Plaxis 3D Manual, 2013)

E_{50}^{ref} : Plastic straining due to primary deviatoric loading kN/m^2

E_{oed}^{ref} : Plastic straining due to primary compression kN/m^2

E_{ur}^{ref} : Elastic unloading and reloading kN/m^2

m : Power for stress level dependency of stiffness
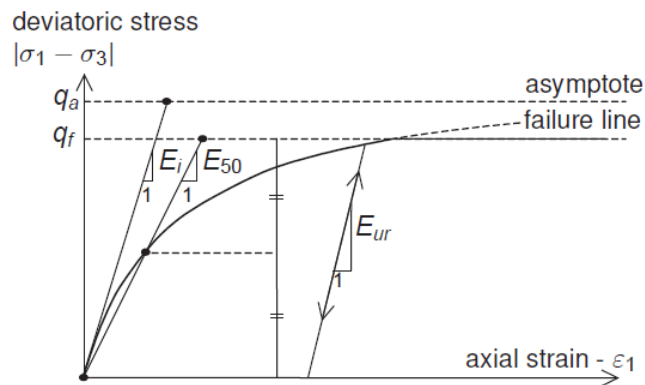
Figure 4.4. Stress – strain behaviour of Hardening Soil model (Plaxis 3D Manual, 2013)

Soft soil problems can mostly be solved by Hardening Soil model. However, Hardening Soil model is not convenient to compute creep that is the secondary compression of soft soils in long term. Soft Soil Creep model operates the process of the time dependent behavior and computes the secondary compression. Basic parameters of Soft Soil Creep model are explained as follows: (Plaxis 3D Manual, 2013)

C_c: Compression index

C_s: Swelling index

C_α: Creep index for secondary compression

e_{init}: Initial void ratio
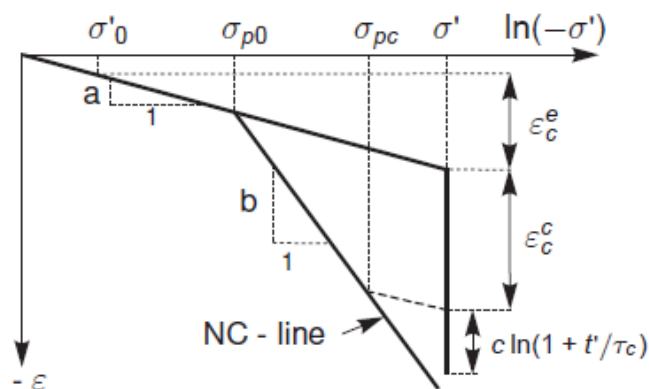
Figure 4.5. Stress – strain behaviour of Soft Soil Creep model (Plaxis 3D Manual, 2013)

54

Soil parameters for both soil types and each material model are listed in the table below (Table 4.2):

Table 4.2. *Soil parameters*

Soil Parameters				
Property Name	Symbol	Sand	Clay	Unit
Unsaturated unit weight	γ_{unsat}	19	19	kN/m^3
Saturated unit weight	γ_{sat}	19	19	kN/m^3
Initial void ratio	e_{init}	0.5	0.7	-
Young's Modulus	E'	35000	50000	kN/m^2
Secant stiffness for CD triaxial test	E_{50}^{ref}	35000	50000	kN/m^2
Tangent oedometer stiffness	E_{oed}^{ref}	35000	50000	kN/m^2
Unloading / reloading stiffness	E_{ur}^{ref}	105000	150000	kN/m^2
Power for stress level dependency of stiffness	m	0.5	0.5	-
Poisson's ratio	ν'	0.25	0.2	-
Cohesion	c'_{ref}	0.0001	10	kN/m^2
Internal friction angle	φ'	35	28	^{o}
Dilatancy angle	ψ	5	5	^{o}
Compression index	C_c	-	0.3	-
Swelling index	C_s	-	0.06	-
Creep index for secondary compression	C_α	-	0.12	-

The parameters given in the Table 4.2 are selected as representative from widely used ones in the literature.

Sand parameters are determined as follows:

c'$_{ref}$ is selected to be very close to zero, but not exactly zero, because of computational limitations of software. Therefore it is selected as 0.0001.

Accordingly, Stroud (1988) and Bowles (1996) provide similar ranges for internal friction angle for medium dense sand; so, it is selected as $\varphi'=35^0$.

Using $\varphi'=35^0$ for sand ranges, various sand gradations, an average of e=0.5 (US Navy, 1982).

Lambe & Whitman (1969) suggests that E' for medium dense sand varies between 30000 to 50000 kPa. so, it is selected as E'=35000 kPa.

With an initial assumption of stiff clay undrained shear strength, $c_u = 75$ kPa (Terzaghi et al., 1996) is found appropriate. For drained shear strength parameters,

$$c' = 0.1 * c_u \text{ (Danish Standard DS 415)}$$

$$c' = 0.2 * c_u \text{ (Sorensen \& Okkels, 2013)}$$

which gives a range of 7.5 to 15 kPa for c'. So, c' is selected as 10 kPa.

Assumption of Plasticity Index PI=25% helps in finding φ', E_u and E'.

Accordingly, φ'=28 (Terzaghi et al., 1996) is selected. In addition to assumption of PI=25%, OCR=2 gives a range of E_u values (Duncan & Buchignani, 1976). A proper selection of E_u results in E'=5000 kPa determination as follows (v=0.2):

$$\frac{E'}{E_u} = \frac{1 + v}{1 + v_u}$$

For inorganic clays with the assumption of water content, w=25% based on Terzaghi et al. (1996):

$$\frac{C_\alpha}{C_c} = 0.4$$

$$\frac{C_s}{C_c} = 0.2$$

$$C_c = 0.3$$

$$C_s = 0.06$$

$$C_\alpha = 0.012$$

Finally, basic phase relations with fully saturated soil and $G_s = 2.65$ leads to a $e_{init} = 0.7$.

For both sand and clay, dilation angle is selected as 5^0.

4.3. Structural Model and Input Parameters

A certain raft whose sizes, length (B) x width (B) x thickness (d), are determined as 30 m x 30 m x 2 m respectively is used in the design of the piled raft foundation.

Pile length (L) is changed as L=20 m, L=30 m and L=40 m and for each pile length, nine different pile spacing over pile diameter ratios (s/d) which are $2 - 2.25 - 2.5 - 3 - 3.5 - 4.5 - 5.5 - 7 - 9$ are applied. Pile diameter (d) is selected as d=1m. Top view and three dimensional view of each foundation are shown below.
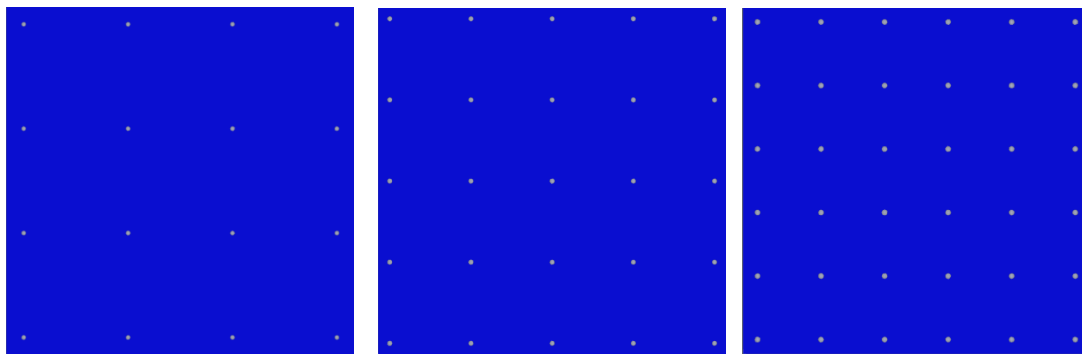
| s/d=9 | s/d=7 | s/d=5.5 |
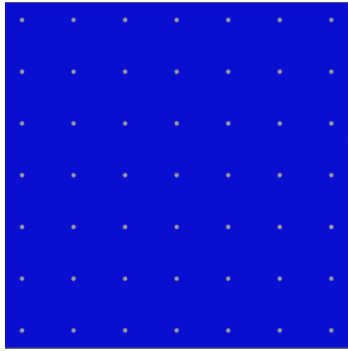
s/d=4.5
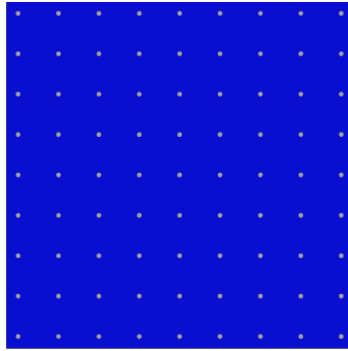
s/d=3.5
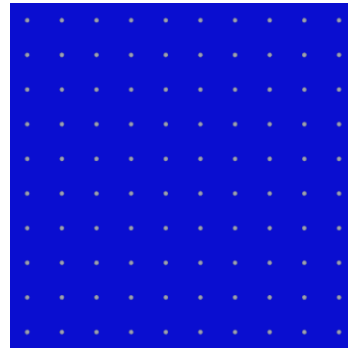
s/d=3
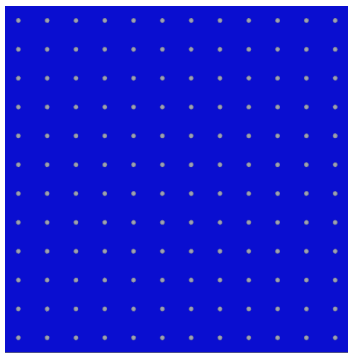
s/d=2.5

s/d=2.25

s/d=2

s/d=9

s/d=7

s/d=5.5

58

s/d=4.5   s/d=3.5   s/d=3
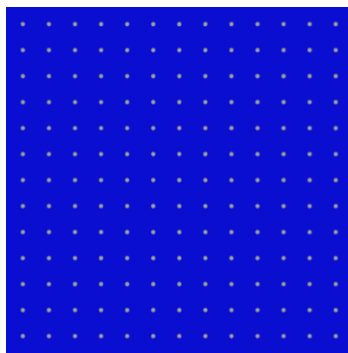
s/d=2.5   s/d=2.25   s/d=2
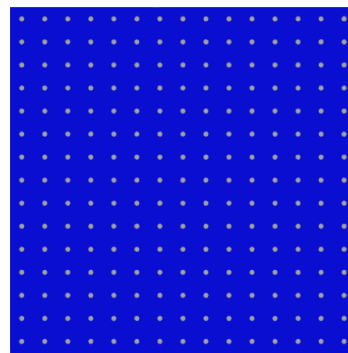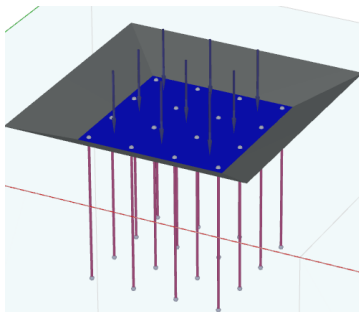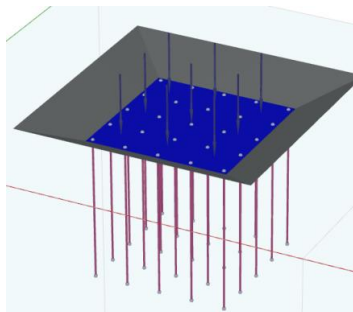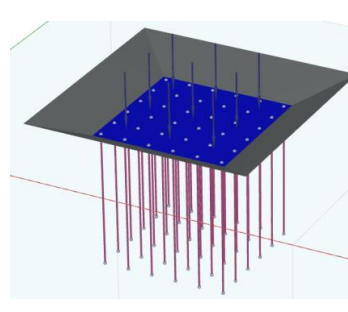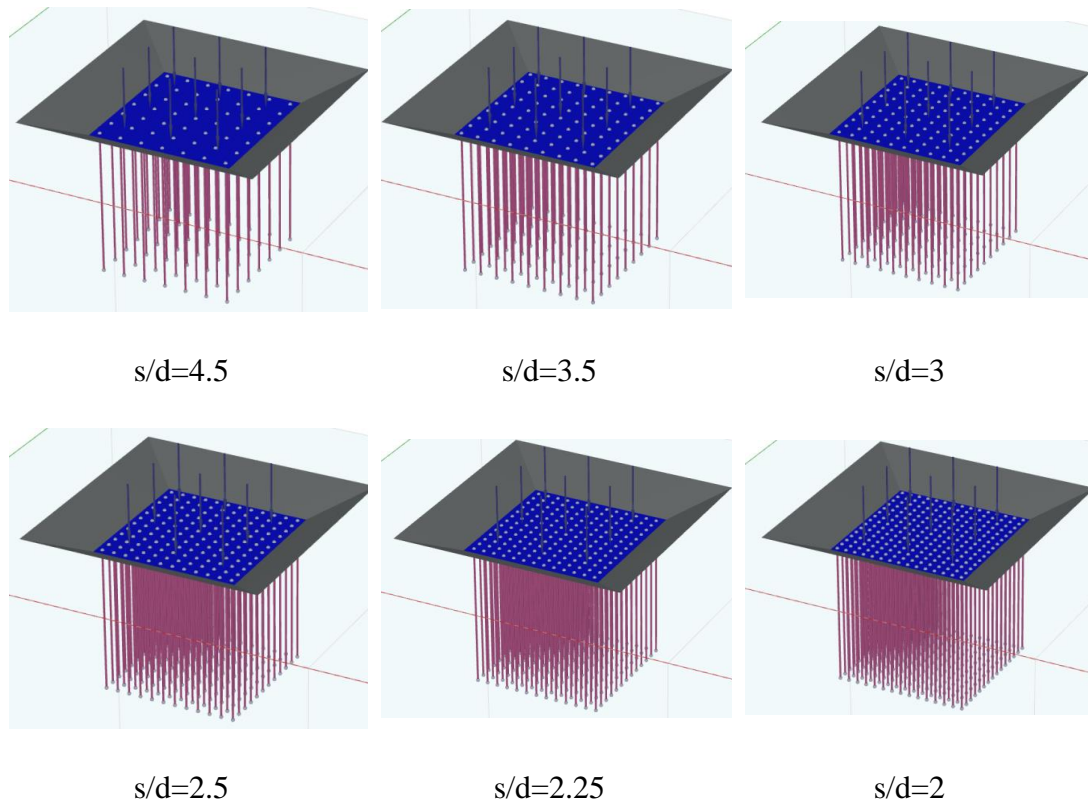
Figure 4.6. Top view and 3 dimensional view of each foundation

All of the cases depending on the soil types, material models, drainage types, pile lengths and pile spacing over pile diameter ratios (s/d) that are modelled and analyzed in this study are summarized in the below Model Case Table (Table 4.3).

Table 4.3. *Model case table*

Model Case Table						
Soil Type	**Material Model**	**Drainage Type**	**Pile Length**	**L=20**	**L=30**	**L=40**
Sand	Mohr Coulomb	Drained	s/d	2	2	2
				2.25	2.25	2.25
				2.5	2.5	2.5
				3	3	3
				3.5	3.5	3.5
				4.5	4.5	4.5
				5.5	5.5	5.5
				7	7	7
				9	9	9
	Hardening Soil	Drained	**Pile Length**	**L=20**	**L=30**	**L=40**
			s/d	2	2	2
				2.25	2.25	2.25
				2.5	2.5	2.5
				3	3	3
				3.5	3.5	3.5
				4.5	4.5	4.5
				5.5	5.5	5.5
				7	7	7
				9	9	9
Clay	Mohr Coulomb	Undrained A	**Pile Length**	**L=20**	**L=30**	**L=40**
			s/d	2	2	2
				2.25	2.25	2.25

		Pile Length	L=20	L=30	L=40
			2.5	2.5	2.5
			3	3	3
			3.5	3.5	3.5
			4.5	4.5	4.5
			5.5	5.5	5.5
			7	7	7
			9	9	9
		Pile Length	**L=20**	**L=30**	**L=40**
			2	2	2
			2.25	2.25	2.25
			2.5	2.5	2.5
Hardening Soil	Undrained A		3	3	3
		s/d	3.5	3.5	3.5
			4.5	4.5	4.5
			5.5	5.5	5.5
			7	7	7
			9	9	9
		Pile Length	**L=20**	**L=30**	**L=40**
			2	2	2
			2.25	2.25	2.25
			2.5	2.5	2.5
Soft Soil Creep	Drained		3	3	3
		s/d	3.5	3.5	3.5
			4.5	4.5	4.5
			5.5	5.5	5.5
			7	7	7
			9	9	9

Modelling a raft in Plaxis 3D requires to select the material set as "Plate" and assign the raft parameters to the "Plate" that are tabulated as below Table 4.4:

Table 4.4. *Raft parameters*

Raft Parameters			
Width	B	30	m
Length	L	30	m
Thickness	d	2	m
Unit weight	γ	25	kN/m^3
Young's Modulus	E	25000000	kPa
Poisson ratio	ν	0.2	
Behaviour		Linear, Isotropic	

Modelling the piles in Plaxis 3D requires to select the material set as "Embedded piles" and assign the pile parameters to the "Embedded piles" that are tabulated as below Table 4.5:

Table 4.5. *Pile parameters*

Pile Parameters			
Diameter	d	1	m
Unit weight	γ	6	kN/m^3
Young's Modulus	E	23500000	kPa
Pile type		Massive circular pile	
Skin friction per unit length	$T_{top,\ max}$ $T_{bot,\ max}$	Calculated for each case	kN/m
Tip resistance force	F_{max}	Calculated for each case	kN

When defining the unit weight of an embedded pile, it has to be noted that the embedded pile is a beam element, which does not occupy a volume itself and overlaps with the soil around it. In order to overcome the overlapping problem, the unit weight of an embedded pile is calculated by subtracting the soil unit weight from the concrete pile unit weight. Hence, the unit weight of an embedded pile is calculated as 6 kN/m^3 by subtracting the soil unit weight which is 19 kN/m^3 for this case, from the concrete pile unit weight which is 25 kN/m^3.

Skin friction $T_{top, max}$ - $T_{bot, max}$ and tip resistance F_{max} contribute to the resistance of piles. In finding appropriate values for each of these parameters, conventional soil mechanics and foundation engineering formulations are used (Eqns. 4.1, 4.2, 4.3, 4.4).

Sand equations:

$$Skin\ friction: f_s = K_s * \sigma_v * tan\delta\ (Eqn\ 4.1)$$

$$Tip\ resistance: f = N_q * \sigma_v\ (Eqn\ 4.2)$$

Clay equations:

$$Skin\ friction: f_s = \alpha * C_u\ (Eqn\ 4.3)$$

$$Tip\ resistance: f = 9 * C_u\ (Eqn\ 4.4)$$

4.4. Mesh and Fineness Effect

After completing the geometry and input parameters of soil and structure model, finite element mesh generation step is proceeded. Mesh generation is the process of dividing the model consisting of soil and structural elements into the volume elements in order to make computations.

Plaxis 3D generates 10 - node tetrahedral elements in mesh procedure of soil volume as it is seen below Figure 4.7.
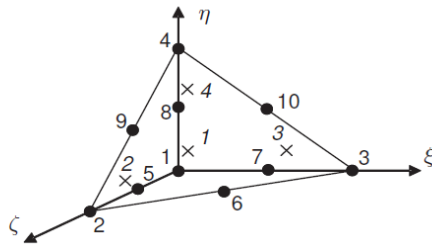
Figure 4.7. 10 - node tetrahedral element (Plaxis 3D Scientific Manual, 2013)

Plates, which are used for modelling of the raft, are generated by 6 - node triangular elements in Plaxis 3D (Figure 4.8).

Figure 4.8. 6 – node triangular element (Plaxis 3D Scientific Manual, 2013)

The embedded pile is considered as a beam element that has an interaction with the surrounding soil. The beam element passes through the 10 - node tetrahedral volume element and 3 extra nodes are added inside the 10 - node tetrahedral element.
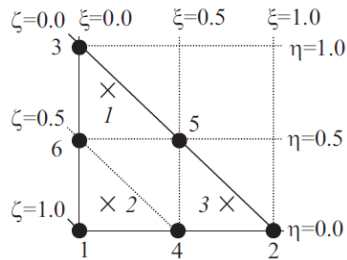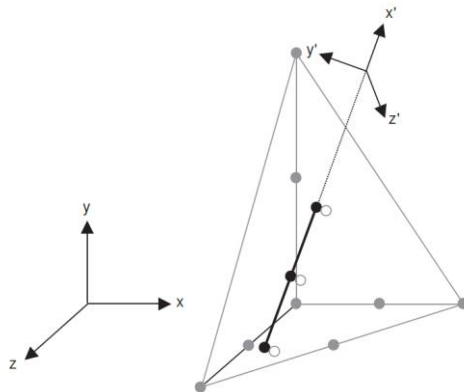

Figure 4.9. 10 - node tetrahedral element (Plaxis 3D Scientific Manual, 2013)

64

Mesh size influences run time and accuracy of the computations. As the size of the elements gets smaller, run time of analyses and accuracy of results increase. Size options of the mesh elements are ordered below.

- Very coarse
- Coarse
- Medium
- Fine
- Very fine

A piled raft foundation model with pile length L=30 m and spacing over diameter ratio (s/d) = 4,5 is analyzed in sand with Mohr Coulomb material model as an example for each mesh size and the results are tabulated in Table 4.6 in order to examine the mesh size effects on run time of model, number of soil elements, number of nodes, average element size, settlement of foundation and settlement reduction ratio (SRR) which is the ratio of settlement of piled raft foundation over unpiled raft foundation.

Table 4.6. *Mesh size effect*

Mesh Size	Run Time (min)	Number of soil elements	Number of nodes	Average element size (m)	Settlement (m)	SRR
Very Coarse	3	8164	13901	10.91	0.1082	0.475
Coarse	4	11063	17662	9.373	0.108	0.474
Medium	8	21462	33206	6.73	0.1085	0.476
Fine	13	44594	65943	4.669	0.109	0.479
Very Fine	87	157606	223679	2.483	0.1119	0.491

In this study, mesh size is mainly selected as "Very Fine" for the mesh generation of the models in Table 4.3 and the structural parts are refined again in order to provide more accurate results as it is seen in Table 4.6. However, decreasing the size of the element leads to extend run time highly and this may sometimes cause run time error in Plaxis 3D which is a numerical problem in software. Enlarging the mesh size by

selecting "Fine" mesh size instead of "Very Fine" provides to overcome run time error in software.

(a)   **(b)**
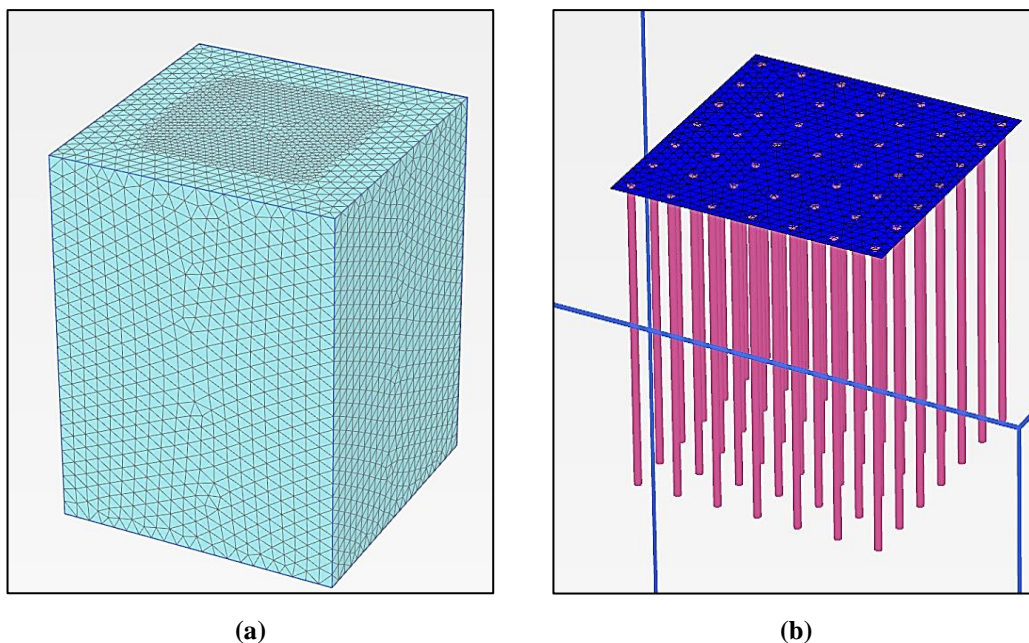
Figure 4.10. (a) Whole model mesh view   (b) Structural model mesh view

4.5. Staged Construction

The last step of the calculation is staged construction. In this step, phases of the construction are defined like a real life simulation comprising initial conditions, excavation, generation of piles, generation of raft and application of structural load.

Firstly, the initial conditions involving initial geometry, initial effective stresses and pore pressures are generated in initial phase. In this phase, all the soil volumes are activated and all the structural elements and loads are inactivated. General view of the initial phase is given in Figure 4.11.(a).

(a)

(b)

(c)

(d)

(e)

Figure 4.11. (a) General view of the initial phase (b) General view of the excavation phase (c) General view of the pile phase (d) General view of the raft phase (e) General view of the loading phase

The next stage is the excavation phase. Since the bottom of the raft is located at 5 meters below the ground, the site has to be excava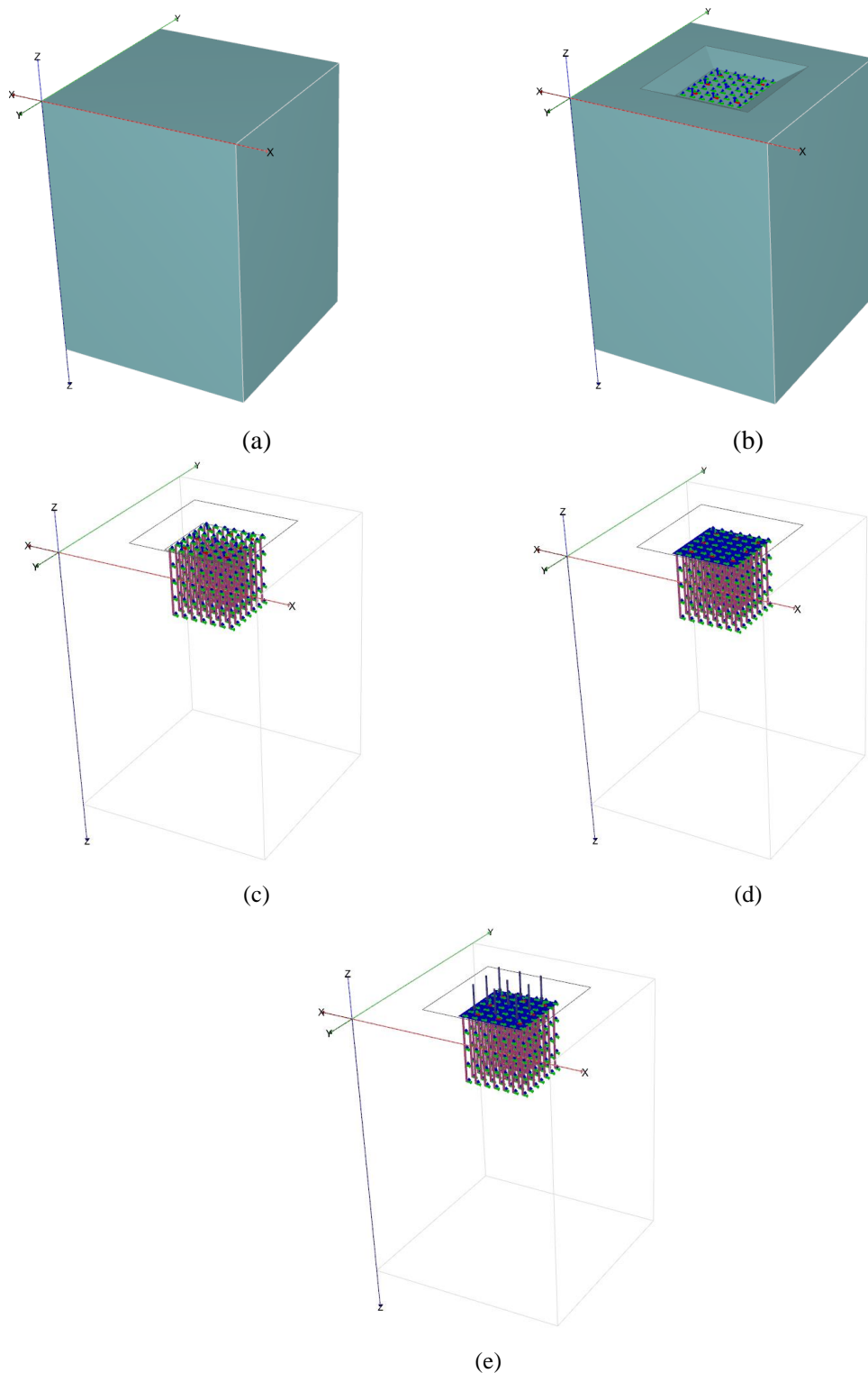ted for 5 meters from top to bottom. However, 5 meter deep excavation may not be possible because of stability problems. Therefore, "Soil body collapses" error may occur during the excavation phase. In order to overcome this stability problem, 1V:2H approach is applied by excavating the ground angularly.

In excavation phase, the excavated soil volume is inactivated; also, all the structural elements and loads are inactivated. General view of the excavation phase is given in Figure 4.11.(b).

The third stage is pile phase. In addition to the soil volume except excavated part, piles are also activated in this phase. However, raft and load have still been inactive (Figure 4.11.(c)).

The next stage is raft phase. In addition to the soil volume except excavated part and piles, raft is also activated in this phase. However, load has still been inactive (Figure 4.11.(d)).

The last stage is loading phase. In addition to the soil volume except excavated part, piles and raft, load is also activated in this phase. 300 kPa surface load for a 20 - storey high rise building is applied on the foundation uniformly (Figure 4.11.(e)).

4.6. Solution of an Example Analysis

In this part, a sample model is solved in Plaxis 3D and the computations are examined in detail. Results are also introduced at the end of this section.

Geometric, structural and material input parameters are demonstrated in the given Table 4.7.

Table 4.7. *Geometric, structural and material input parameters*

	Input Parameters			
	Property Name	**Symbol**	**Type/ Value**	**Unit**
Soil	Soil	-	Sand	-
	Material model	-	Mohr Coulomb	-
	Unsaturated unit weight	γ_{unsat}	19	kN/m^3
	Saturated unit weight	γ_{sat}	19	kN/m^3
	Initial void ratio	e_{init}	0.5	-
	Young's Modulus	E'	35000	kN/m^2
	Power for stress level dependency of stiffness	m	0.5	-
	Poisson's ratio	ν'	0.25	-
	Cohesion	c'_{ref}	0.0001	kN/m^2
	Internal friction angle	φ'	35	^{o}
	Dilatancy angle	ψ	5	^{o}
Pile	Length	L	30	m
	Spacing	s	3.5	m
	Diameter	d	1	m
	Spacing over diameter ratio	s/d	3.5	-

	Number of piles	-	81	-
	Pile type	-	Massive circular pile	-
	Young's Modulus	E	23500000	kN/m^2
	Unit weight	γ	6	kN/m^3
	Skin friction per unit length	$T_{top,max}$ $T_{bot,max}$	294	kN/m
	Tip resistance force	F_{max}	10184	kN
Raft	Width	B	30	m
	Length	L	30	m
	Thickness	d	2	m
	Unit weight	γ	25	kN/m^3
	Young's Modulus	E	25000000	kPa
	Poisson ratio	ν	0.2	-
	Behaviour	-	Linear, Isotropic	-

Pile skin friction and tip resistance for are calculated by following formulas:

$$Skin\ friction: f_s = K_s * \sigma_v * tan\delta\ (Eqn\ 4.1)$$

$$Tip\ resistance: f = N_q * \sigma_v\ (Eqn\ 4.2)$$

where K_s=0.5 $tan\delta$=0.49 σ_v=380 kPa f_s=93.7 kPa $T_{top,max}$ and $T_{bot,max}$=294 kN/m

where N_q=19.5 σ_v (at tip)=665 kPa   f=12967.5 kPa F_{max}=10184 kN

The first step in creating the model is determining the boundaries. Boundaries are defined in Project properties window as below Figure 4.12.
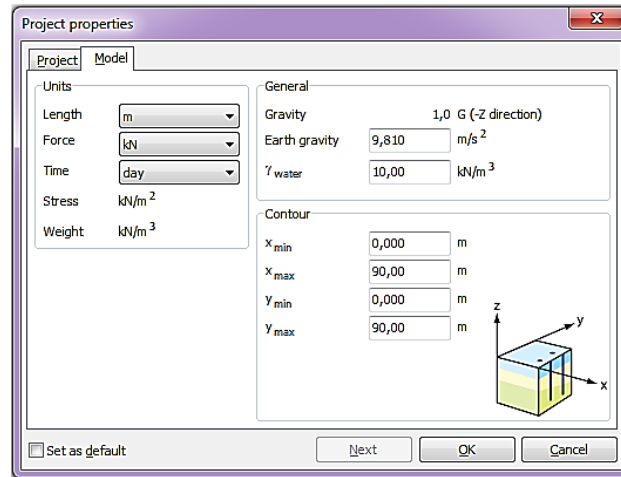

Figure 4.12. Project properties window

Model depth, soil layers and ground water level are defined in Modify soil layers window at "Soil" tab as below Figure 4.13.
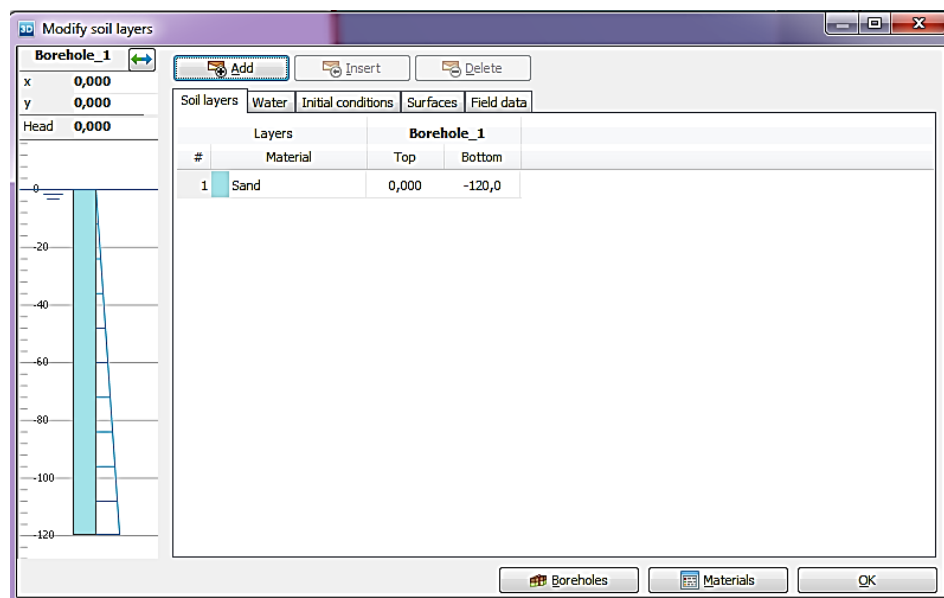

Figure 4.13. Modify soil layers window

Then, sand properties are defined under Material sets window at "Soil" tab as below Figure 4.14.
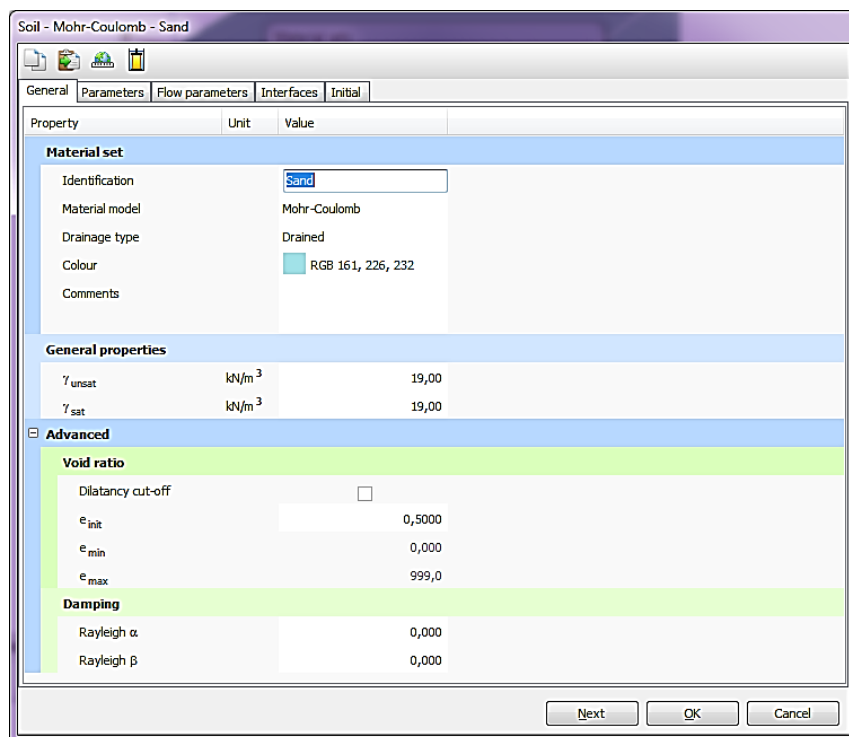
Figure 4.14. Soil material set – General tab
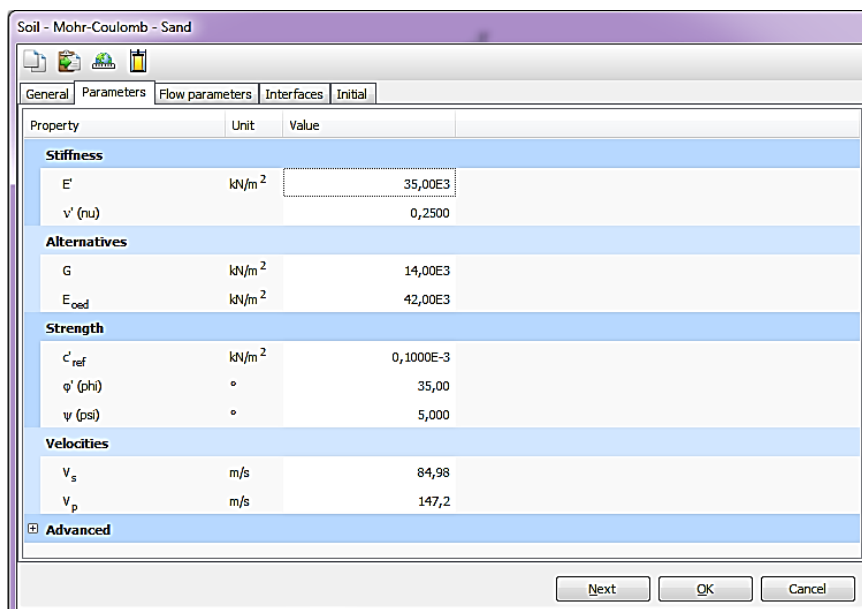
Figure 4.15. Soil material set – Parameters tab

In another step, excavation and foundation is generated in geometry and structural properties are assigned to related elements in "Structures" tab. Firstly, the ground is excavated with 1V:2H angle (Figure 4.13) and then, raft is placed as a plate element at the bottom of the excavated soil where is 5 m below ground and piles are located under the raft as embedded pile elements from -5 m to -35 m. After the geometry is formed, pile and raft material properties are defined in Material sets window as it is seen in Figure 4.14 and Figure 4.15. Moreover, surface load is also created and put on the foundation and the magnitude of surface load is assigned as $\sigma_z = 300$ kN/m^2. Final view of the model is illustrated in Figure 4.16.
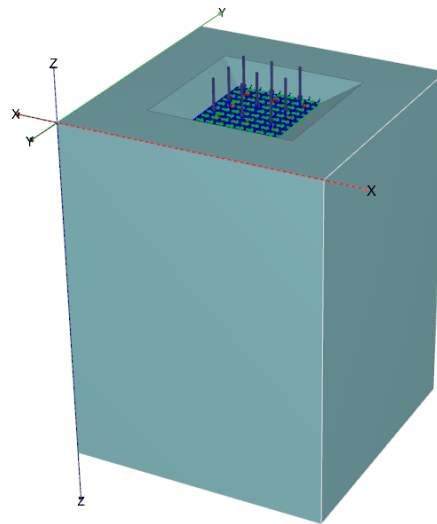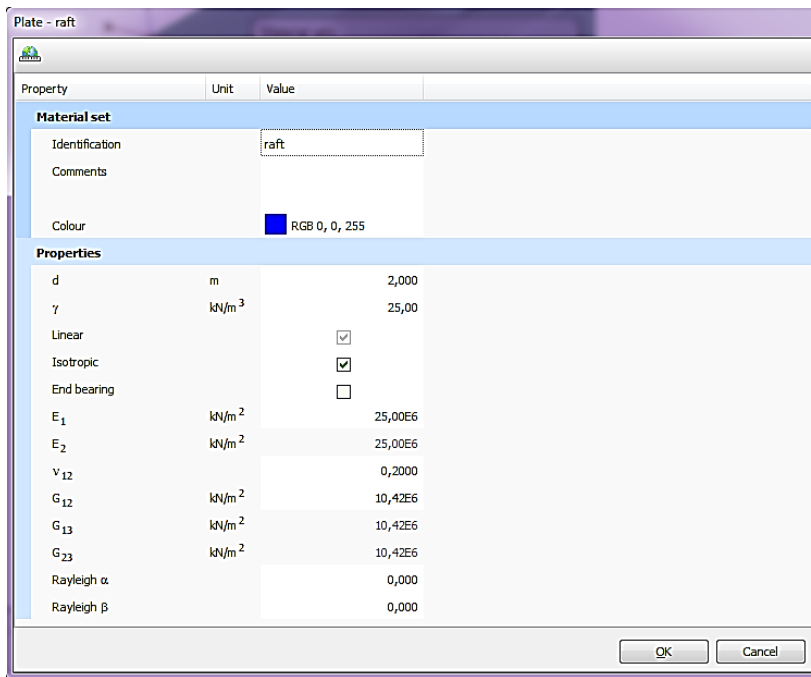

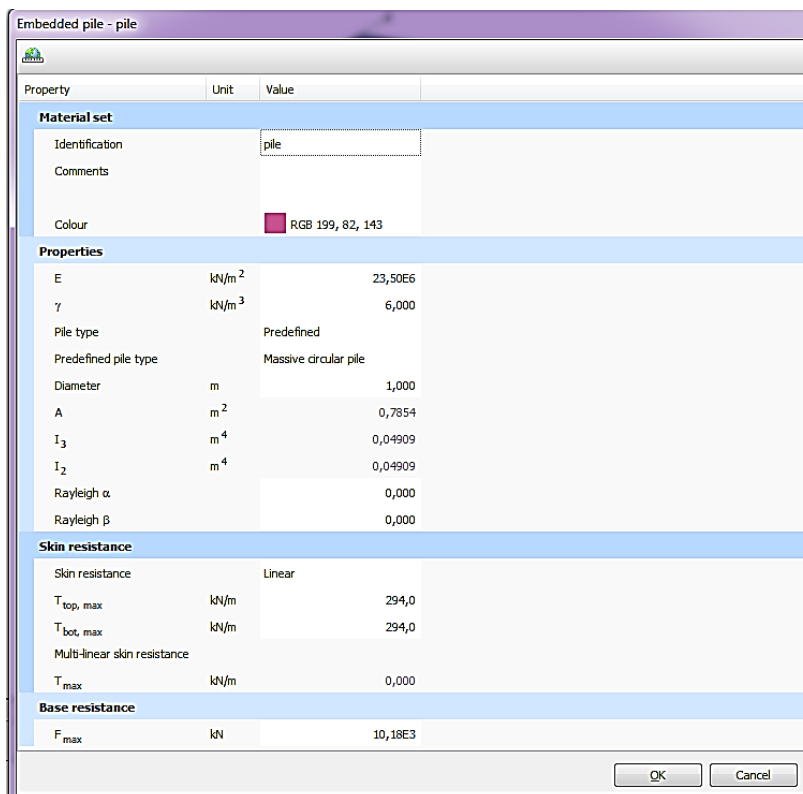*Figure 4.16.* Final view of the model

Figure 4.17. Raft material set

Figure 4.18. Pile material set

74

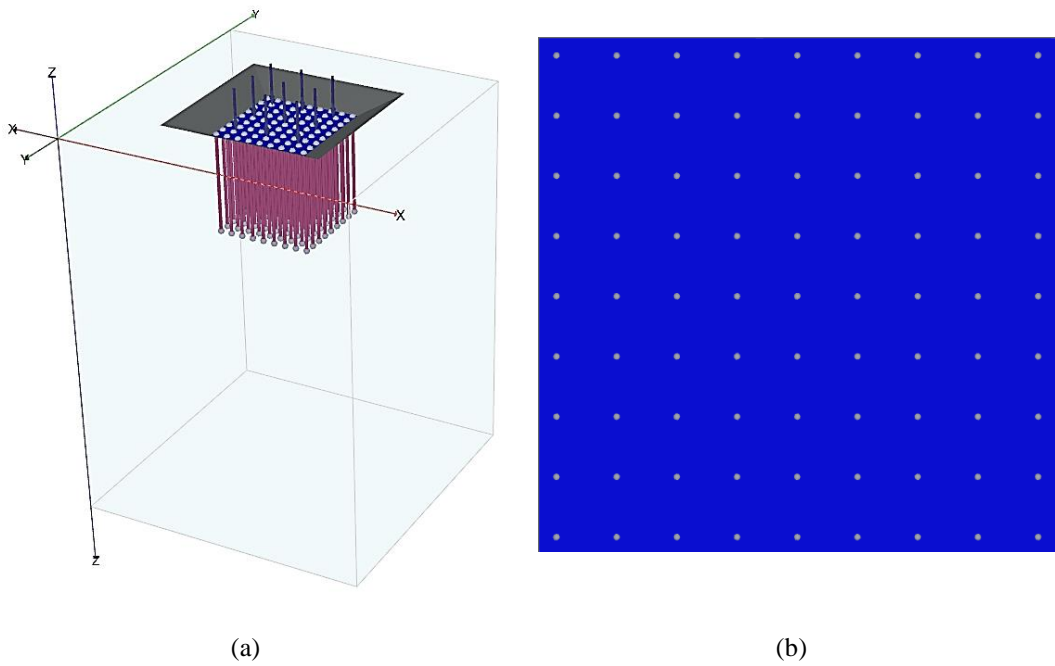<center>(a)</center>

<center>(b)</center>

Figure 4.19. (a) Perspective view of the structural model (b) Top view of the structural model

After completing the soil and structural model, mesh is generated under the "Mesh" tab. Element distribution selected as "Very fine" in Mesh options window and structural elements are refined to get more accurate results at that region. Mesh view is given in Figure 4.20.
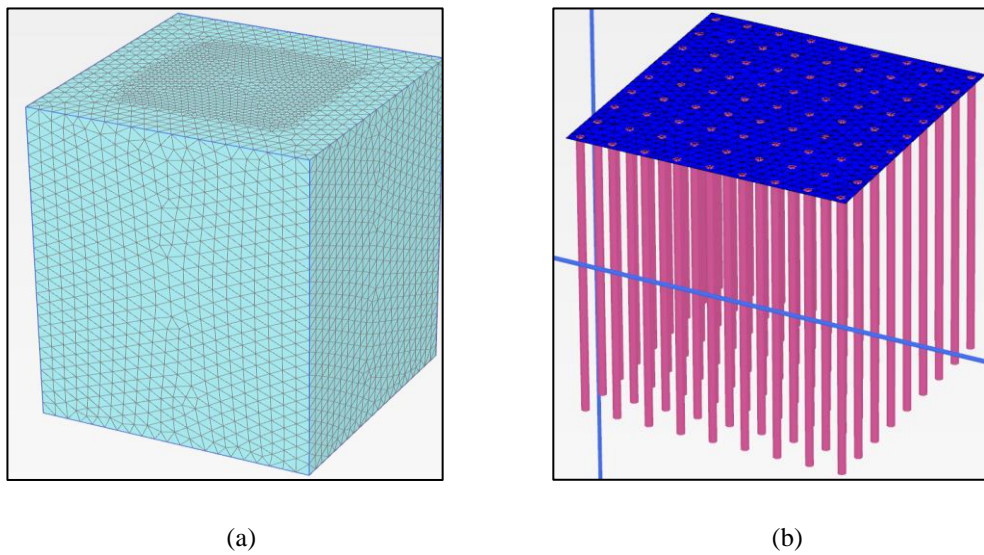

<center>(a)</center>

<center>(b)</center>

Figure 4.20. Mesh view

Finally, in the "Staged construction" tab, all the stages that comprises:

- Initial phase
- Excavation
- Piles
- Raft
- Load

are generated as explained in Section 4.5 in detail and the model is calculated.

Results of calculation are examined and evaluated with regards to settlement and bearing capacity of the structural elements. Displacement and deformation in vertical direction (u_z) is illustrated as below in Figure 4.21.
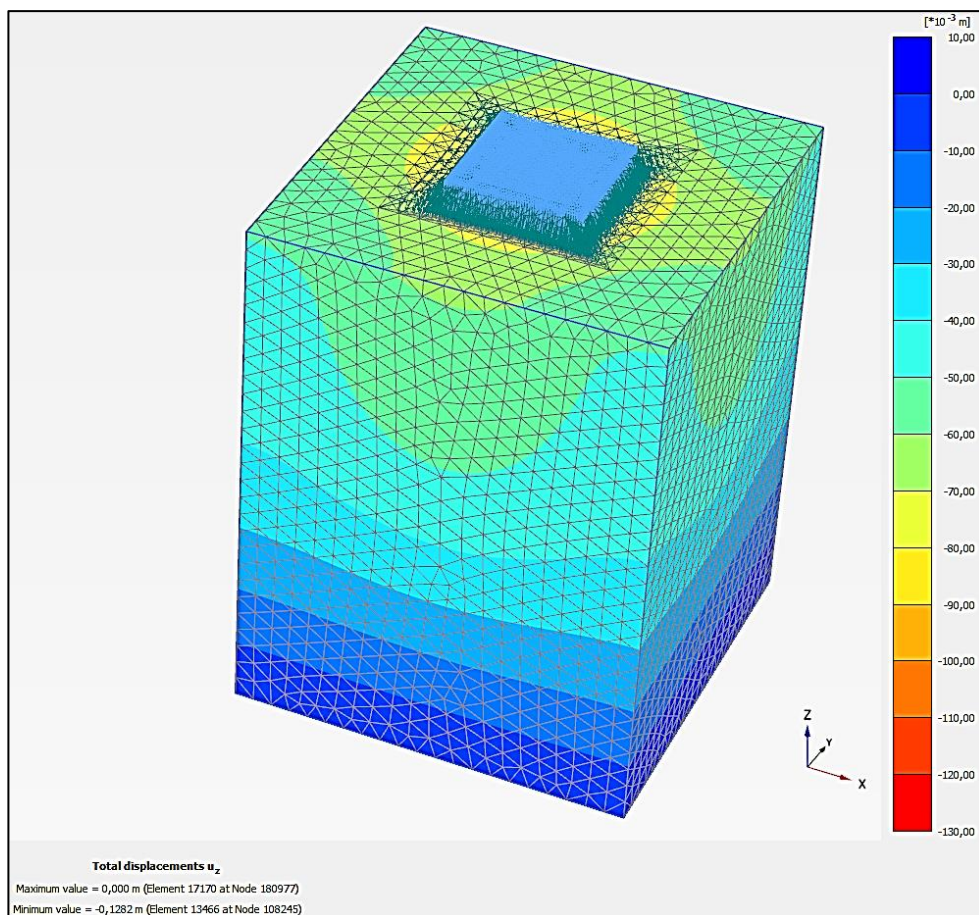

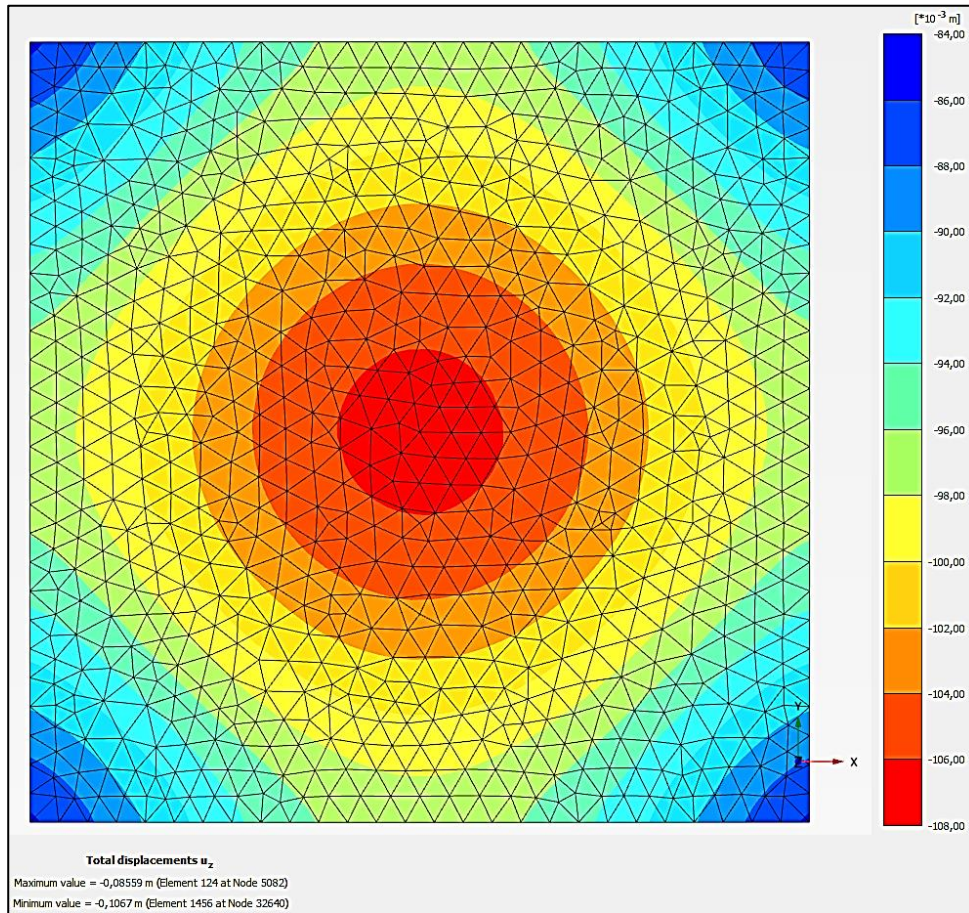*Figure 4.21.* Displacement in vertical direction (u_z)

Figure 4.22. Top view of the displacement in vertical direction (u_z)

Pile contribution to decrease of settlement of foundation is defined as settlement reduction ratio (SRR) which is the ratio of piled raft foundation settlement over unpiled raft foundation settlement. The settlement of unpiled raft foundation is computed as 0.228 m. Therefore, settlement reduction ratio (SRR) of piled raft foundation is calculated as 0.47.

$$SRR = \frac{\text{settlement of piled raft foundation}}{\text{settlement of unpiled raft foundation}}$$

Another criterion that is considered in piled raft foundation design is the contribution of piles to the load sharing. In order to determine the aforementioned contribution, axial load on piles is computed and ratio of the axial load on piles over total load (α) is determined.
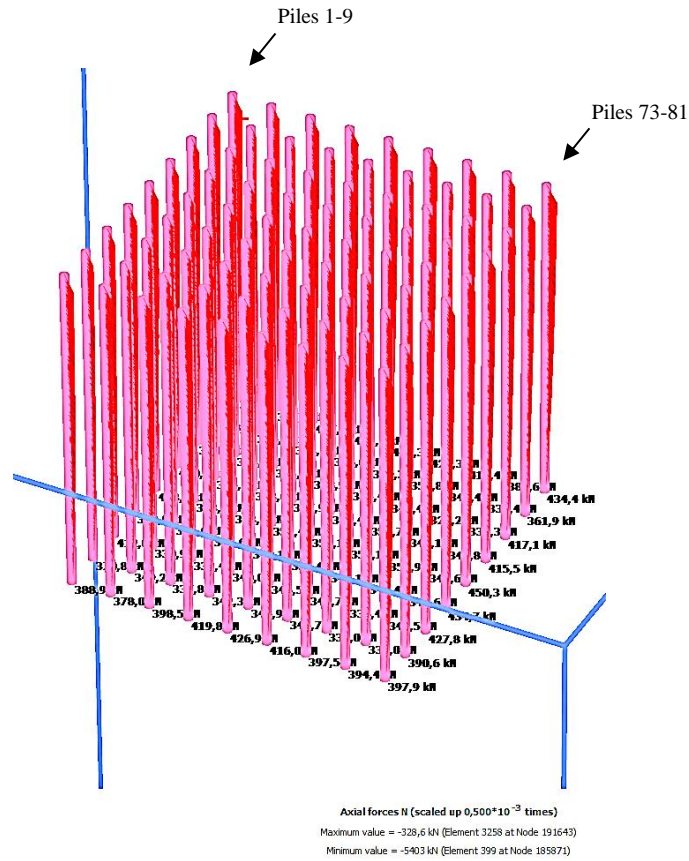
Figure 4.23. Axial forces of piles

The axial loads of piles that are located in 9x9 configuration are tabulated below in Table 4.8. The ratio of edge or corner piles over center pile ranges between 1.37 to 1.73 which means edge or corner piles take 1.37-1.73 times higher load compared to the center pile.

Table 4.8. *Axial force on each pile*

| Numbers are given in kN.								
Piles 1-9	Piles 10-18	Piles 19-27	Piles 28-36	Piles 37-45	Piles 46-54	Piles 55-63	Piles 64-72	Piles 73-81
5403	4343	4467	4706	4847	4726	4468	4293	5257
4312	2843	2840	2950	3001	2961	2861	2897	4357
4451	2851	2792	2915	2956	2904	2811	2872	4494
4722	2931	2913	3043	3088	3029	2917	2965	4691
4851	2981	2950	3082	3124	3089	2947	3019	4813
4743	2934	2902	3040	3081	3032	2887	2971	4687
4488	2861	2777	2903	2976	2868	2826	2848	4465
4381	2844	2837	2971	2999	2933	2848	2857	4360
5287	4302	4533	4779	4725	4792	4492	4369	5280
Total load of piles (kN)								292611
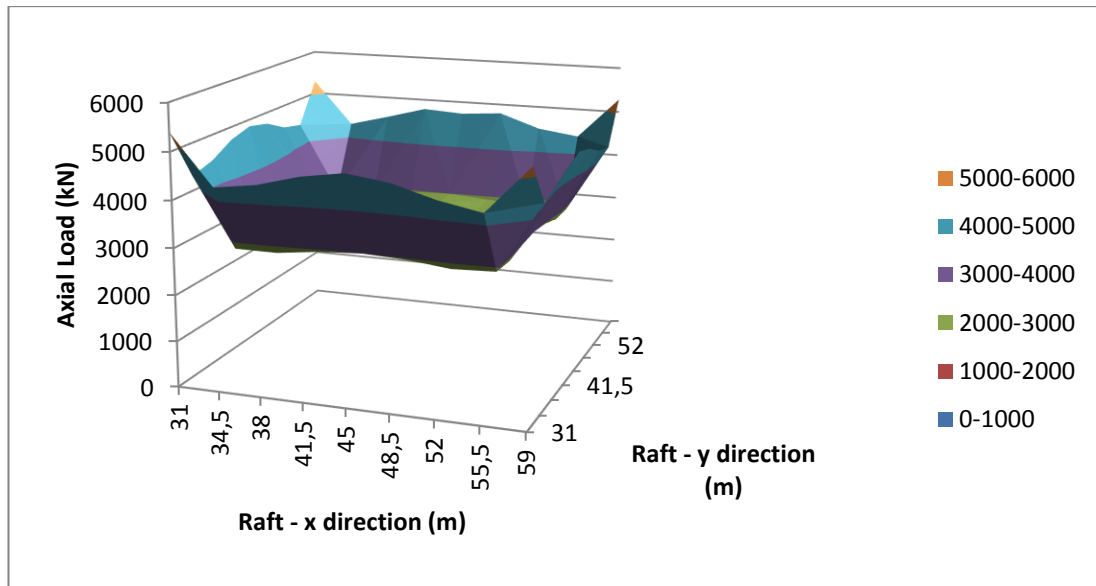
Figure 4.24. 3 - dimensional illustration of axial loads on piles

Total load on piles is calculated as sum of the structural load and raft load.

Structure load: 300 kPa × 30 m × 30 m= 270000 kN

Raft load: 25 kN/m^3 × 30 m × 30 m × 2 m = 45000 kN

Total load on piles: 315000 kN

Average load on each pile: 315000 kN / 81 piles = 3889 kN / pile

Hence, the ratio of the load carried by piles over total load (α) is computed as % 92.

$$\alpha = \frac{\text{load carried by piles}}{\text{total load}}$$

Based on Eqn 2.2 and Eqn 2.3, finite element result can be verified by Clancy & Randolph Method (1993).

$$k_{pr} = \frac{\left(k_p + k_r\left(1 - 2\alpha_{pr}\right)\right)}{\left(1 - \alpha_{pr}^2 \frac{k_r}{k_p}\right)} \quad (Eqn\ 2.2)$$

$$\frac{P_r}{P_t} = \frac{k_r\left(1 - \alpha_{pr}\right)}{k_p + k_r\left(1 - 2\alpha_{pr}\right)} \quad (Eqn\ 2.3)$$

where $k_r = \frac{(\beta\sqrt{BL})}{(1-v_s^2)} E_s,$ β=1.1shape factor for square raft, B and L are raft dimensions (30 m x 30 m), v_s and E_s Poisson's ratio and Young's Modulus of soil from Table 4.7, α_{pr} is interaction factor and generally taken as 0.8 for most cases.

k_r= 1.232 MN/mm

k_p= Total load / Pile group settlement (S_{gr}) where $S_{gr} = S_i \times R_s$ and

$R_s = (R_{25}-R_{16})(\sqrt{n}-5) + R_{25}$

$$R_A = \frac{(A_p)}{(\pi D^2/4)} = 1 \qquad K = \frac{(E_p R_A)}{(E_s)} = 671$$

P_{ave} for each pile=3.889 MN

$$s_i = \frac{(P_{ave} * I)}{(d * E_s)}$$

where $I = I_O \times R_K \times R_V \times R_H$

$I = 0.065 \times 1.4 \times 0.915 \times 1 = 0.083$ for L/d=30, K=671, n=81, s/d=3.5

$s_i = 9.28$ mm

$R_s = (7.22 - 5.565) (\sqrt{81}\text{-}5) + 7.22 = 13.84$

$S_{gr} = 9.28 \times 13.84 = 128.4$ mm

$k_p = 315$ MN / 128.4 mm = 2.45 MN/mm

$$k_{pr} = \frac{(2.45 + 1.232(1 - 2x0.8))}{\left(1 - 0.8^2 \frac{1.232}{2.45}\right)} = 2.52 \, MN/mm$$

$$\frac{P_r}{P_t} = \frac{1.232(1 - 0.8)}{2.45 + 1.232(1 - 2x0.8)} = 0.14$$

Calculations give the results of 0.14 for raft load sharing ratio, hence 0.86 for pile group load sharing ratio whereas the finite element result is 0.92 for pile group load sharing ratio which makes it reasonable.

CHAPTER 5

DISCUSSION OF RESULTS

In Chapter 4, a parametric study is conducted on two hypothetical cases that comprise different pile lengths with various pile configurations. Indeed, in Chapter 4.3, summary of all cases that are handled in this study is presented. In addition, generating a model geometry, defining material sets and all calculation steps are explained in detail from Chapter 4.1 to Chapter 4.6.

In Chapter 5, calculation results of Chapter 4 and evaluation of the conclusions are presented and discussed in order to obtain the optimum design.

The results are evaluated with regards to maximum settlement of the piled raft foundation and axial load capacity of piles and the raft. Furthermore, some other parameters that are derived from aforementioned settlement and axial load capacity are defined as following and used in given charts in this Chapter.

Settlement reduction ratio (SRR) and piled raft coefficient (α) are also evaluated.

Total length is the product of "number of piles at the piled raft foundation" and "the single pile length", which has a unit of meter (m).

Individual values of settlement and loads from which SRR and α calculated can be seen in Appendix B.

For sand condition, drainage type is selected as "Drained" and maximum settlement of unpiled raft foundation is calculated as 0.228 m. Following charts are given in Figure 5.1, Figure 5.2, Figure 5.3, Figure 5.4 Figure 5.5 and Figure 5.6 for both material models that are Mohr Coulomb and Hardening Soil and pile lengths of L=20 m, L=30 m and L=40 m.

For clay condition, drainage type is selected as "Undrained A" and maximum settlement of unpiled raft foundation is calculated as 0.1103 m. Following charts are

given in Figure 5.7, Figure 5.8, Figure 5.9 and Figure 5.10, Figure 5.11 and Figure 5.12 for both material models that are Mohr Coulomb and Hardening Soil and pile lengths of L=20 m, L=30 m and L=40 m.

For clay condition, drainage type is selected as "Drained" and maximum settlement of unpiled raft foundation is calculated as 4.353 m for 1000 days after construction. Following charts are given in Figure 5.13, Figure 5.14, Figure 5.15 and Figure 5.16, Figure 5.17 and Figure 5.18 for Soft Soil Creep model and pile lengths of L=20 m, L=30 m and L=40 m.

Mohr Coulomb and Hardening Soil Model results for sand:
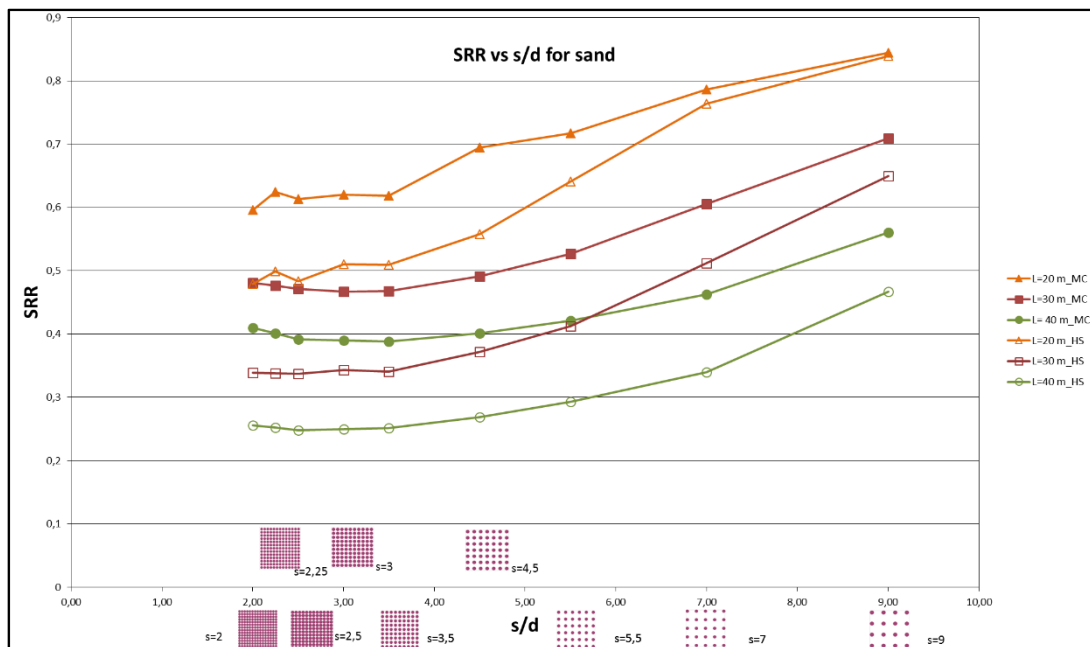
Figure 5.1. SRR vs s/d chart for sand

SRR value equals to "1" refers to unpiled raft. Therefore, lower SRR numbers are desired for reducing settlements. As we can see in Figure 5.1, as s/d increases (as spacing increases), SRR increases for both Hardening Soil and Mohr Coulomb model. For a given length of piles, Mohr Coulomb model always gives larger SRR value for all s/d values. For a given soil constitutive model, as single pile length increases, SRR decreases for a given s/d ratio. For all piles lengths (20 m, 30 m, 40 m), for all s/d

ratios between 2 and 9, for both Hardening Soil and Mohr Coulomb models, SRR values are in the range of 0.25 to 0.85.

It should be noted that there will be an allowable settlement value in piled raft design. For example, if an allowable settlement value of 15 cm is assumed, in Figure 5.1, L=20 m, Mohr Coulomb Soil model, s/d=9, 7, 5.5, 4.5 and Hardening Soil model s/d=9 piled raft designs would be unacceptable. So, such analyses should be evaluated together with allowable settlement.
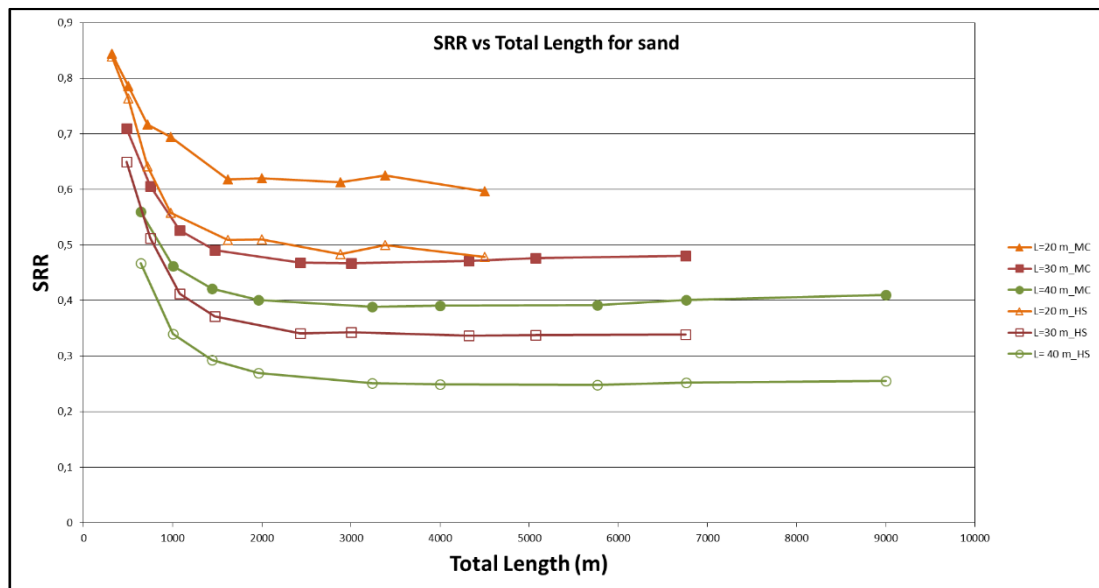

Figure 5.2. SRR vs Total Length chart for sand

Figure 5.2 indicates that, as total length of piles increase, SRR values decrease for all analyzed cases in this study. It can be deduced from Figure 5.2, there is an optimum total length of piles, which provides lowest SRR value (i.e. the most benefit in reducing settlement). There seems to be an optimum total length of piles, which is the most efficient length for reducing settlement. For example, for L=30 m, Mohr Coulomb soil model Figure 5.2 shows that SRR decreases from 0.7 to 0.48 for total length of 500 m to nearly 7000 m. An optimum value of "total length of piles / length of single pile" "80" provides benefit for all cases analyzed in this study. For example,

for L=30 m, SRR does not change significantly after the value of total length of pile of 2400 m. (i.e. 80 x L=2400 m)
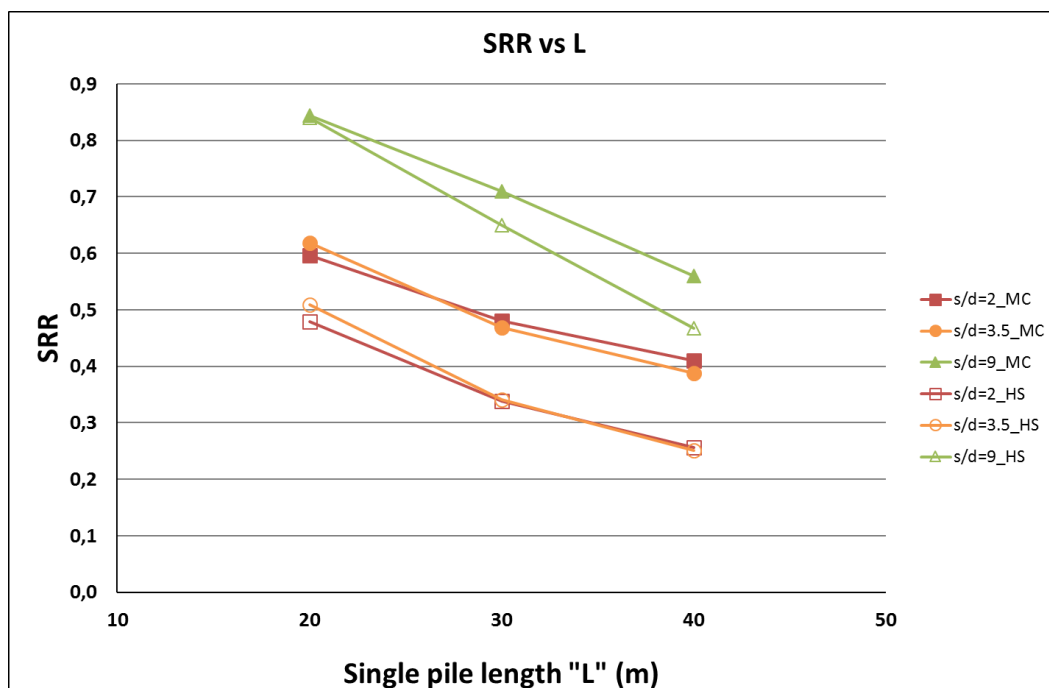

Figure 5.3. SRR vs L chart for sand

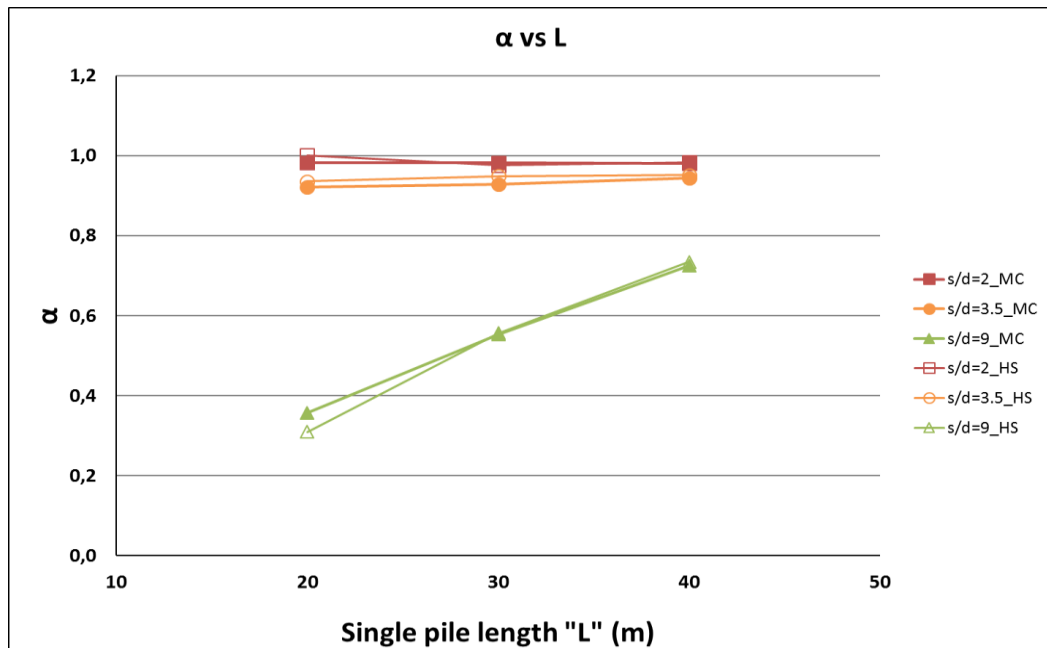According to Figure 5.3, SRR values decrease with increasing single pile length (L) values for both soil models.

Figure 5.4. α vs L chart for sand

According to Figure 5.4, α values slightly increase with increasing single pile length (L) values for s/d=2 and s/d=3.5 while they significantly increase with increasing single pile length (L) values for s/d=9 for both soil models. This may indicate between s/d=9 and s/d=3.5 pile group efficiency and pile soil interaction behaviour changes significantly i.e. there is a certain spacing less than which controls pile soil group behaviour.
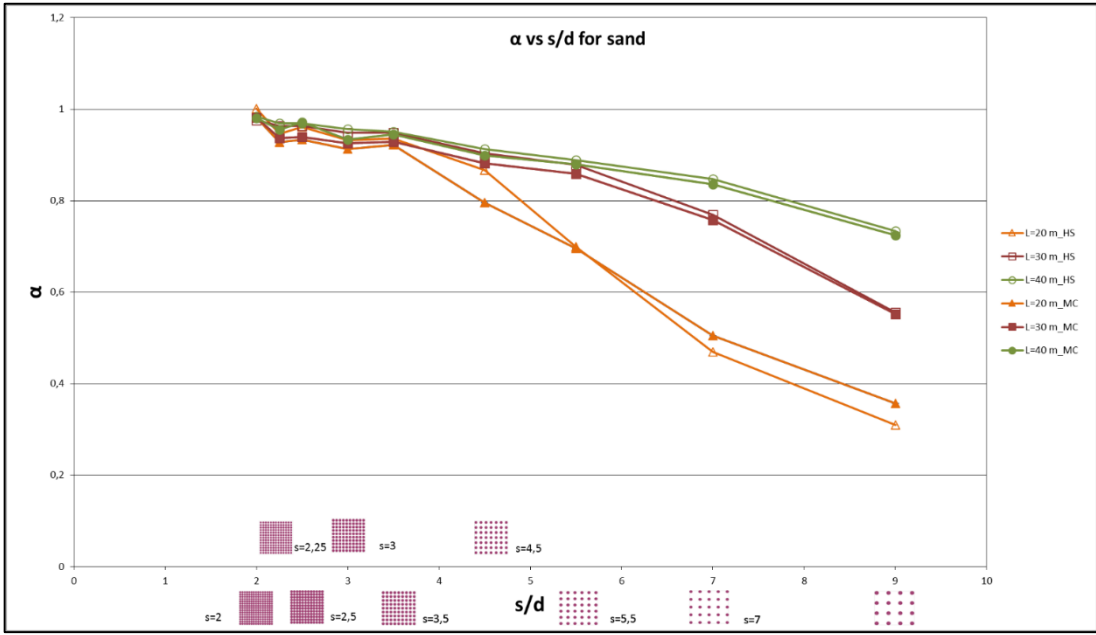
Figure 5.5. α vs s/d chart for sand

α indicates load sharing between piles and raft. A value close to "1" means only piles carry the load, raft does not contribute. According to Figure 5.5, as s/d increases (as spacing increases), α value decreases. When we compare Mohr Coulomb and Hardening Soil model, α value does not seem to be affected by the soil model used. For a given s/d, as single pile length increases, α increases, which means in order to transfer more loads to raft, length of a single pile should be shorter for a given s/d ratio. For L=40 m, α reduces from near 1 to near 0.75 whereas for L=20 m, α reduces to near 0.35 for s/d=9. Therefore, for a chosen target α value (for example 0.60) L=20 m and s/d=6 or L=30 m and s/d=8.5 can be selected. This indicates charts such as in Figure 5.3 can be used for optimum design of piled raft for target load sharing conditions.
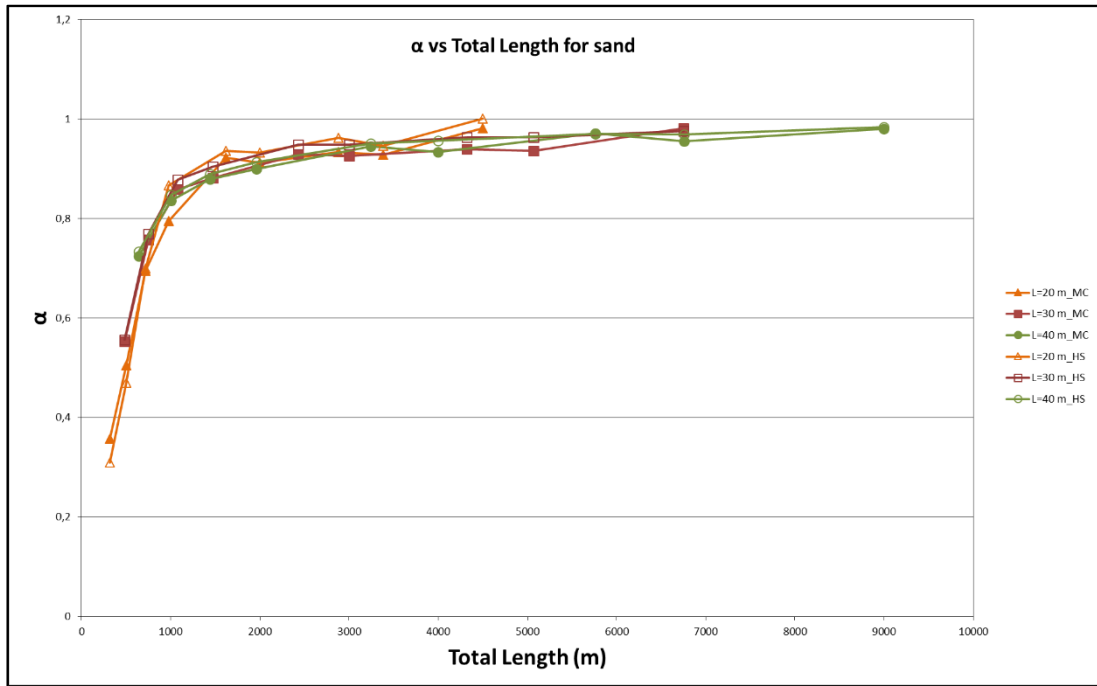
Figure 5.6. α vs Total Length chart for sand

Optimum ratio of "total length of piles / single length of pile" value of 80 seems to provide α value near 0.90-0.95 which means most of the load is carried by the piles (Figure 5.6). Figure 5.6 indicates that as total length of piles increase, α increases, for all cases analyzed in this study.

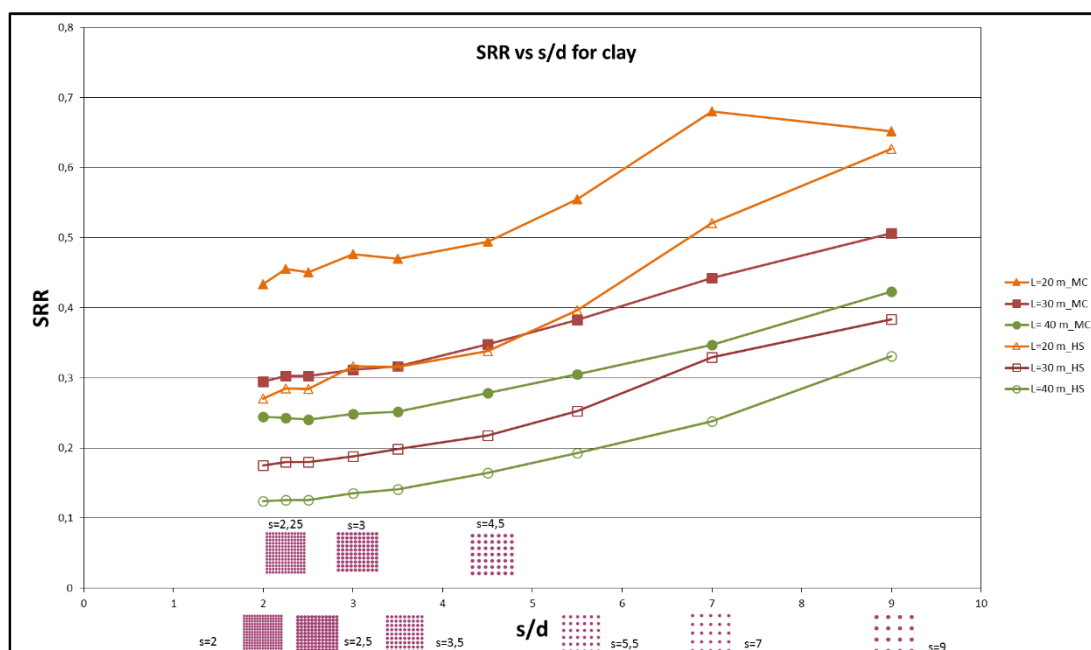Mohr Coulomb and Hardening Soil Model results for clay:

Figure 5.7. SRR vs s/d chart for clay

As we can see in Figure 5.7, as s/d increases (as spacing increases), SRR increases for both Hardening Soil and Mohr Coulomb model. For a given length of single piles, Mohr Coulomb model always gives larger SRR value for all s/d values. For a given soil constitutive model, as single pile length increases, SRR decreases for a given s/d ratio. For all piles lengths (20 m, 30 m, 40 m), for all s/d ratios between 2 and 9, for both Hardening Soil and Mohr Coulomb models, SRR values are in the range of 0.12 to 0.68 in clay.
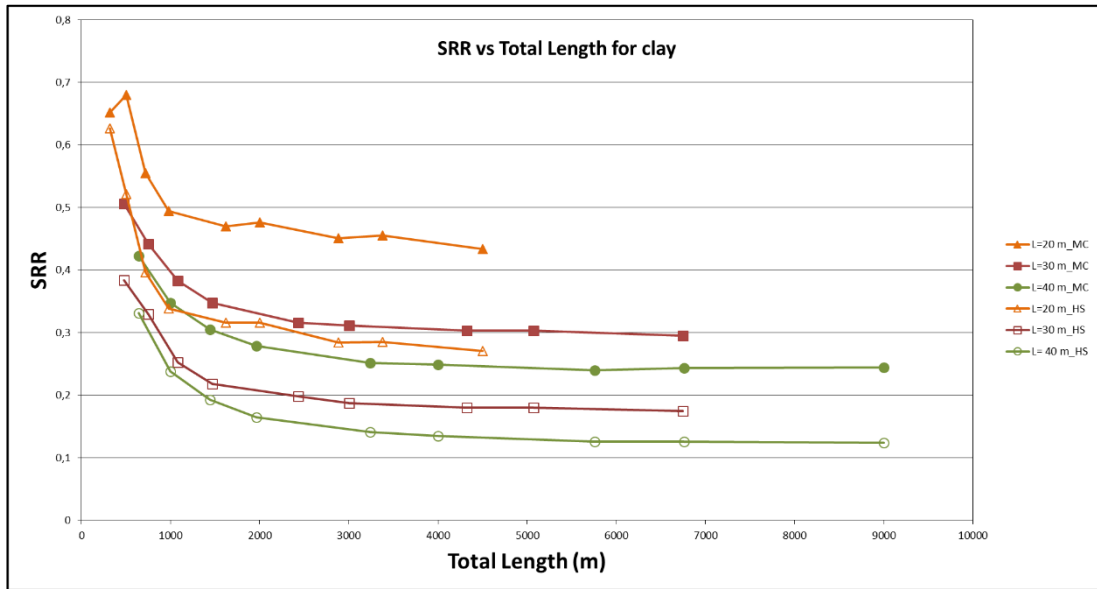
Figure 5.8. SRR vs Total Length chart for clay

Figure 5.8 indicates that, as total length of piles increase, SRR values decrease for all analyzed cases in this study. It can be deduced from Figure 5.8, there is an optimum total length of piles, which provides lowest SRR value (i.e. the most benefit in reducing settlement). There seems to be an optimum total length of piles, which is the most efficient length for reducing settlement. For example, for L=30 m, Mohr Coulomb soil model Figure 5.8 shows that SRR decreases from 0.5 to 0.3 for total length of 500 m to nearly 7000 m. An optimum value of "total length of piles / length of single pile" 80 provides benefit for all cases analyzed in this study. For example, for L=30 m, SRR does not change significantly after the value of total length of pile of 2400 m. (i.e. 80 x L=2400 m)
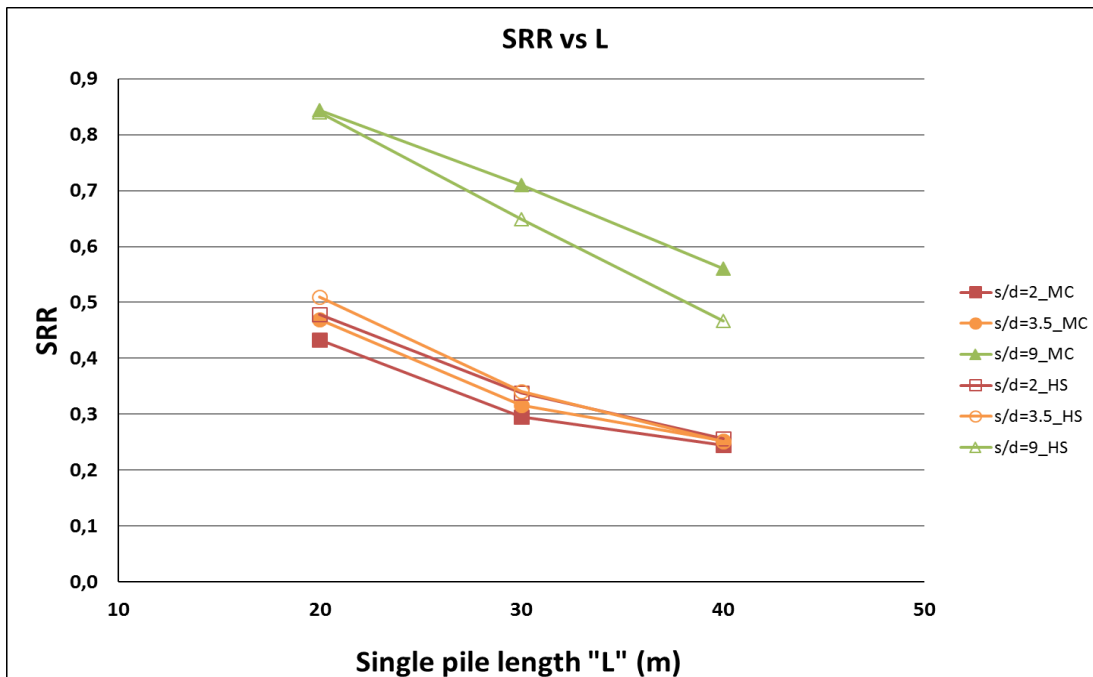
Figure 5.9. SRR vs L chart for clay

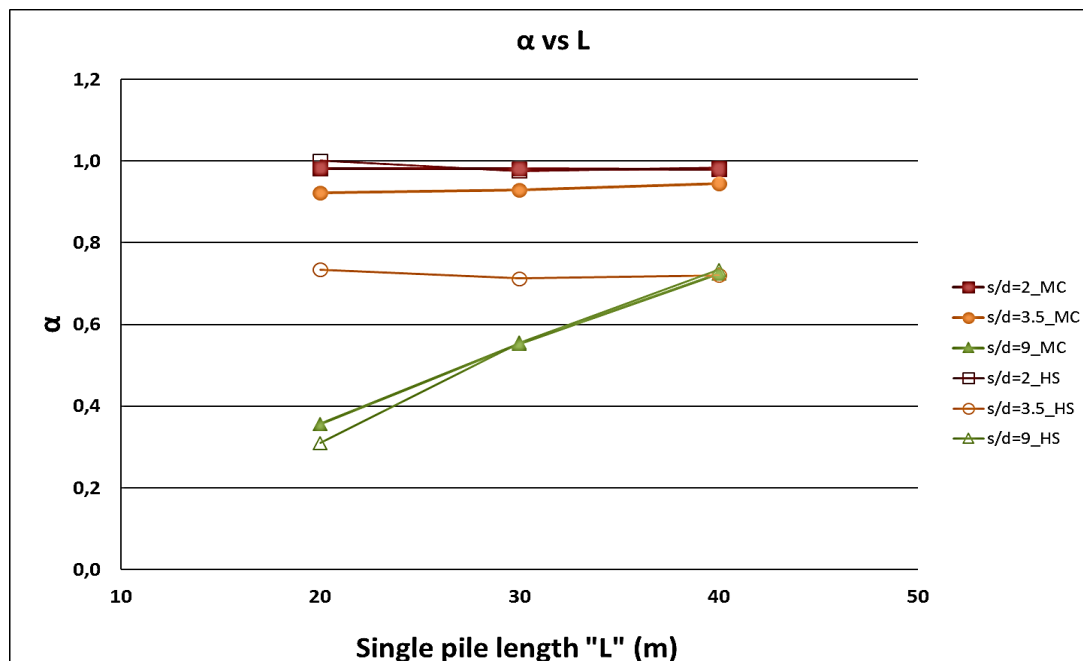According to Figure 5.9, SRR values decrease with increasing single pile length (L) values for both soil models.

Figure 5.10. α vs L chart for clay

92

According to Figure 10, α values slightly increase with increasing single pile length (L) values for s/d=2 and s/d=3.5 while they distinctly increase with increasing single pile length (L) values for s/d=9 for both soil models.
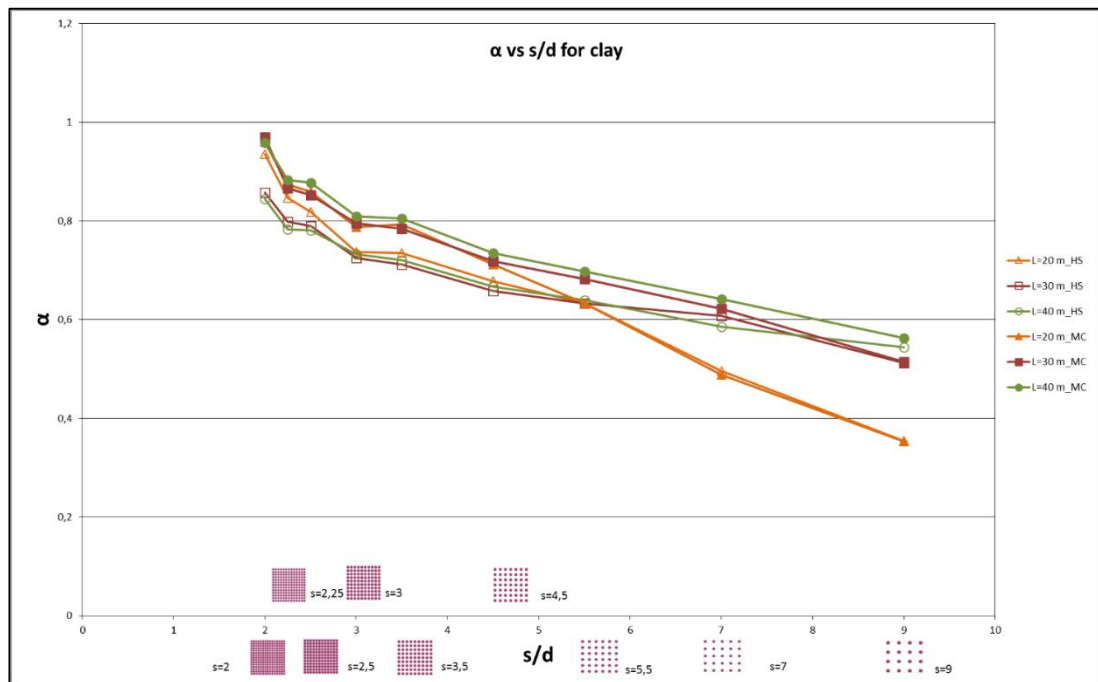

Figure 5.11. α vs s/d chart for clay

According to Figure 5.11, as s/d increases (as spacing increases), α value decreases. When we compare Mohr Coulomb and Hardening Soil model, α value does not seem to be affected by the soil model used. For L=40 m, α reduces from near 1 to near 0.55 whereas for L=20 m, α reduces to near 0.35 for s/d=9. Therefore, for a chosen target α value (for example 0.60), L=20 m and s/d=5.5 or L=30 m and s/d=7 can be selected. This indicates charts such as in Figure 5.11 can be used for optimum design of piled raft for target load sharing conditions.

93

Figure 5.12. α vs Total Length chart for clay

Figure 5.12 indicates that as total length of piles increase, α increases for all cases analyzed in this study. For a given total length of piles, as single pile length increases, α decreases slightly.

Soft Soil Creep Model results for clay are presented in Figure 5.13-5.18. Similar trends can be concluded as for the analysis of Mohr Coulomb and Hardening Soil models. However, some outliers on L=30 m and L= 40 m graphs can be observed.
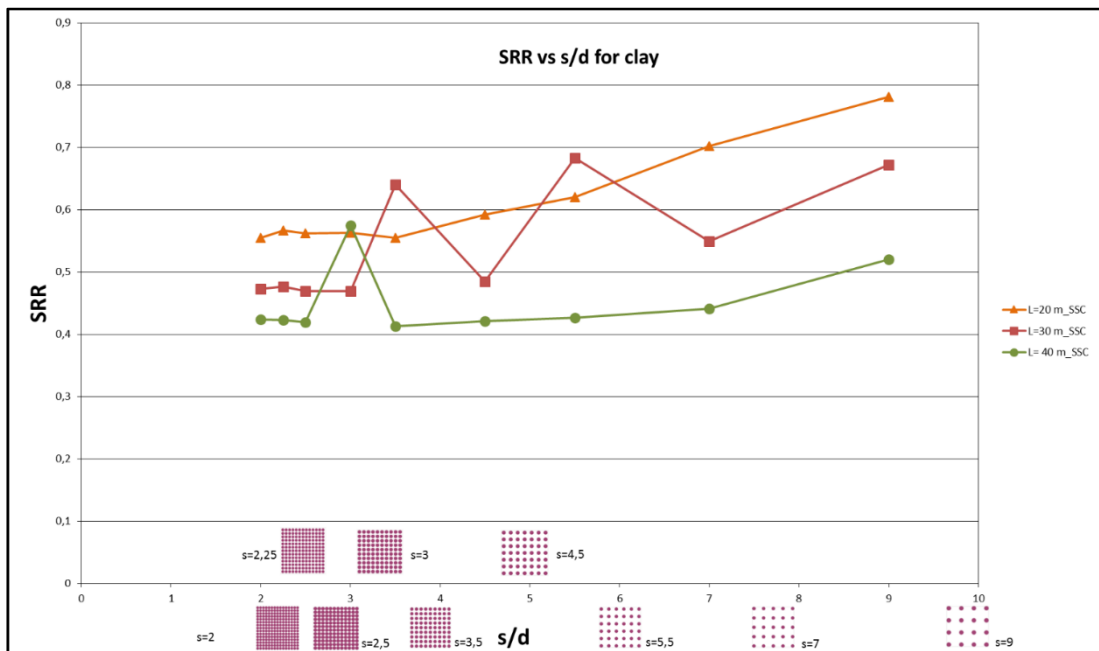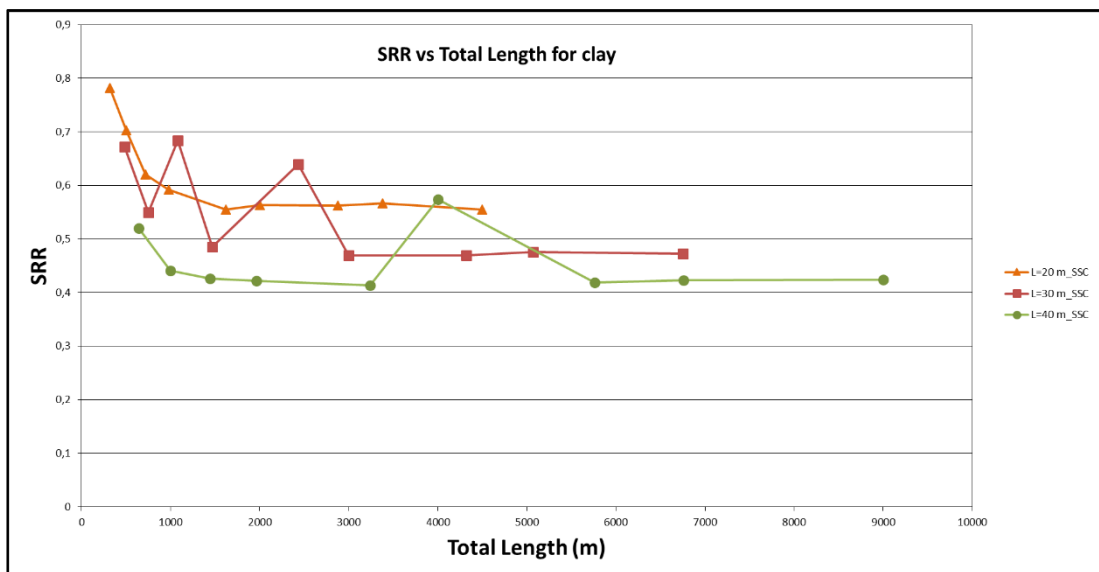
Figure 5.13. SRR vs s/d chart for clay
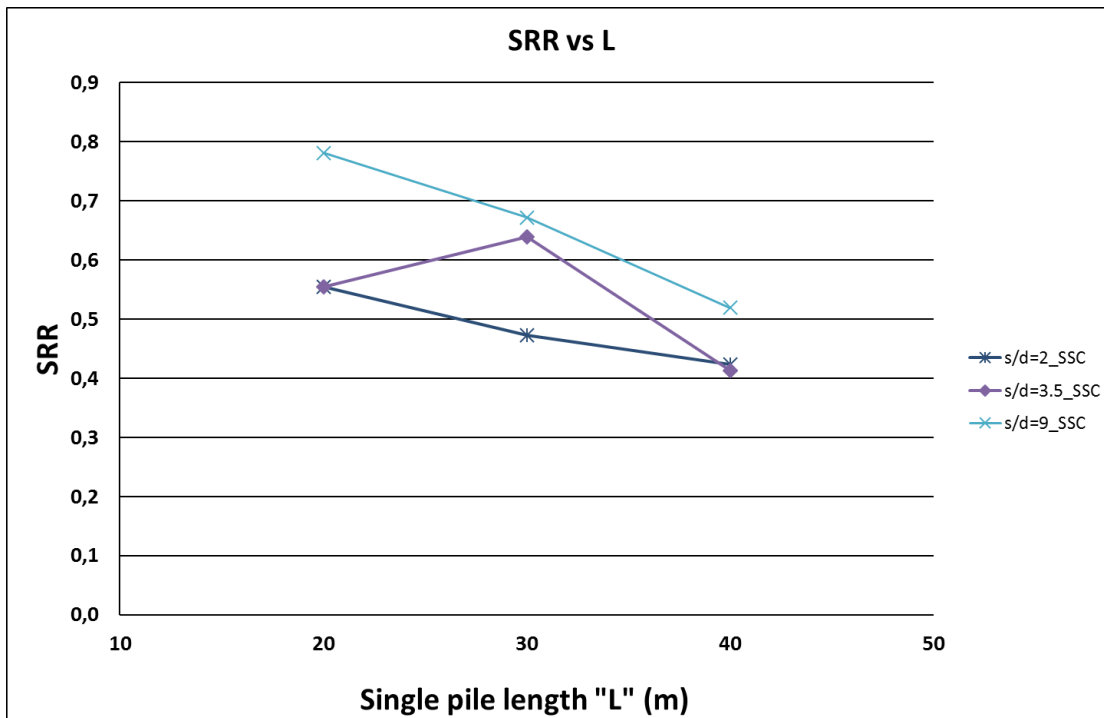

Figure 5.14. SRR vs Total Length chart for clay

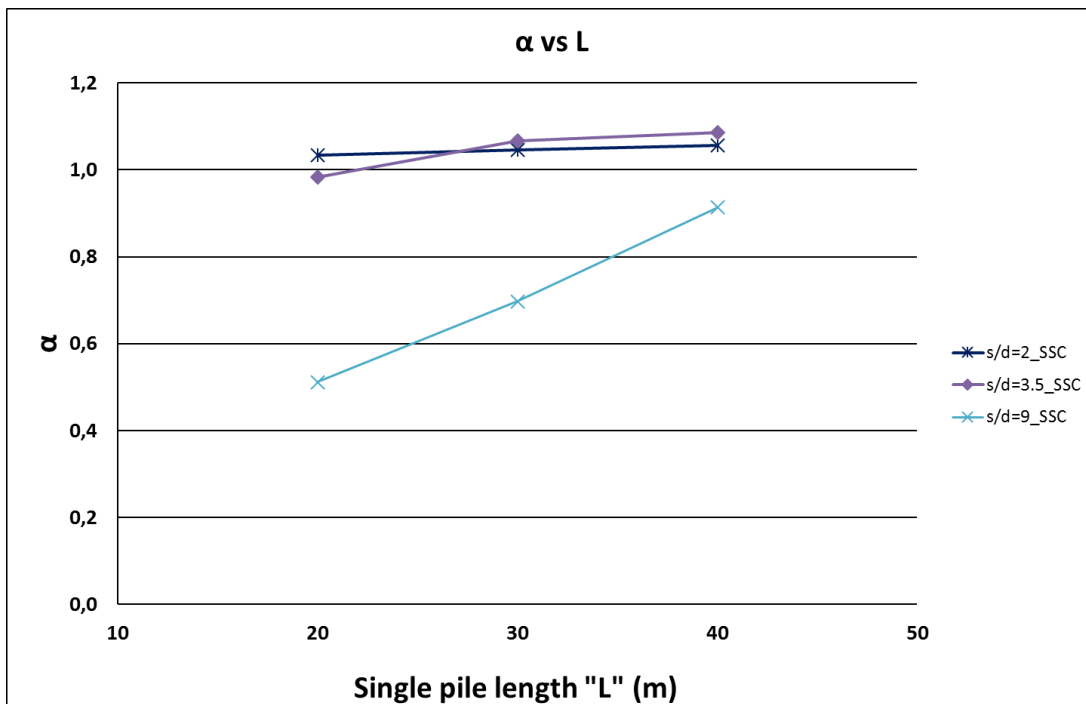*Figure 5.15.* SRR vs L chart for clay

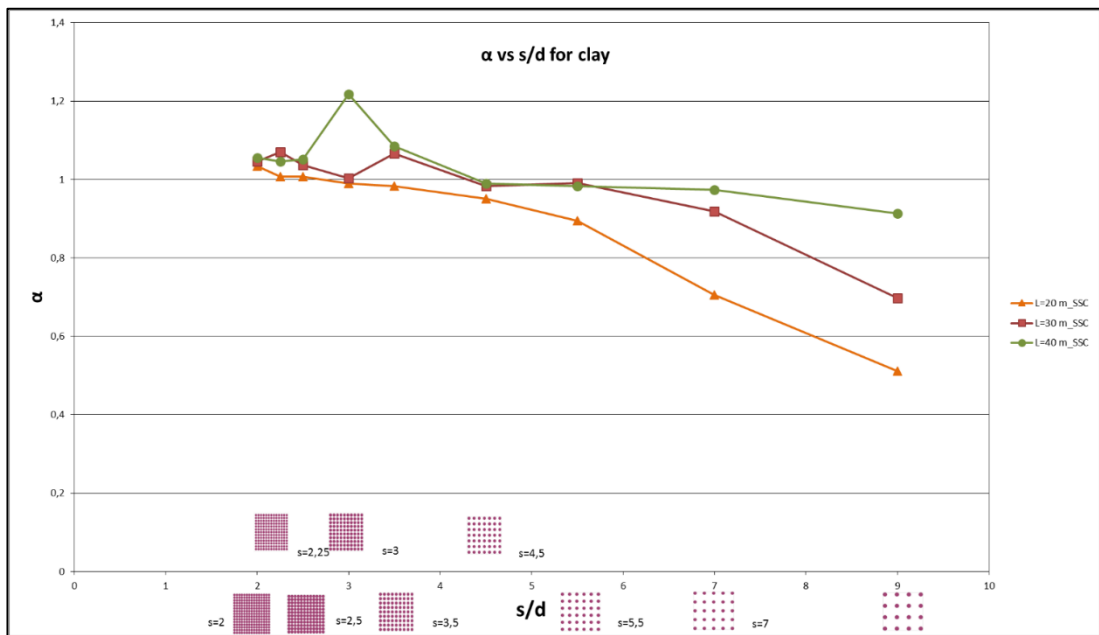*Figure 5.16.* α vs L chart for clay
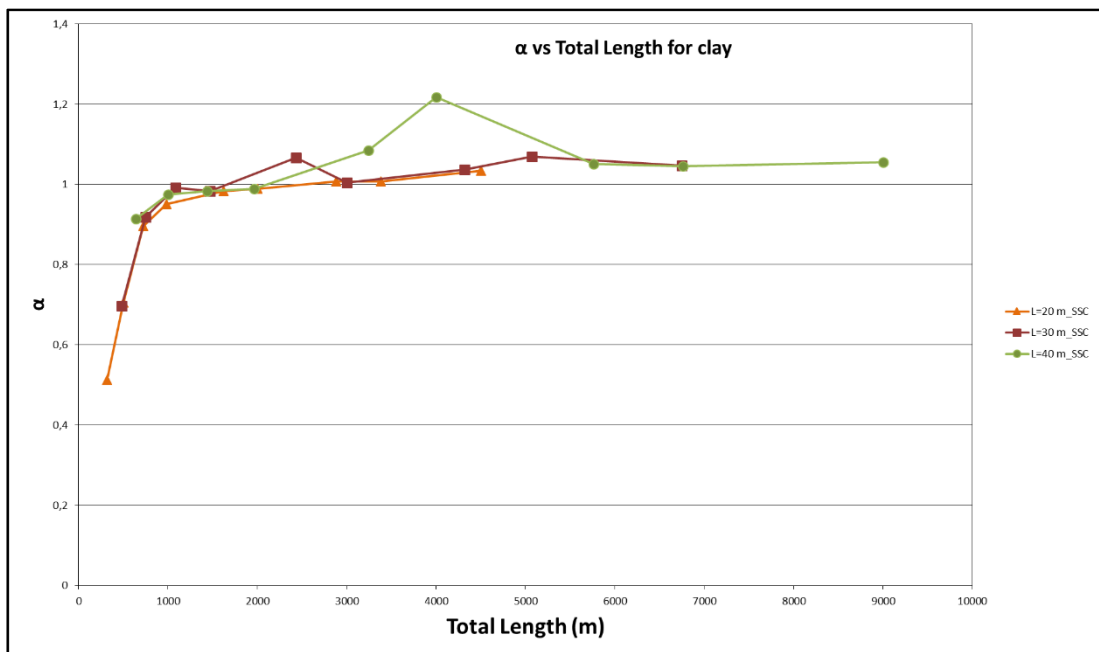
Figure 5.17. α vs s/d chart for clay

Figure 5.18. α vs Total Length chart for clay

97

Figure 5.19 and 5.20 show the relation between SRR and α for both sand and clay. The result show that as α increases SRR also increases for all analyses results. The relation between SRR and α seems to follow general behaviour suggested by El-Mossallamy et al. (2006). Such charts can be used in optimum design of piled rafts to satisfy required SRR and α values.
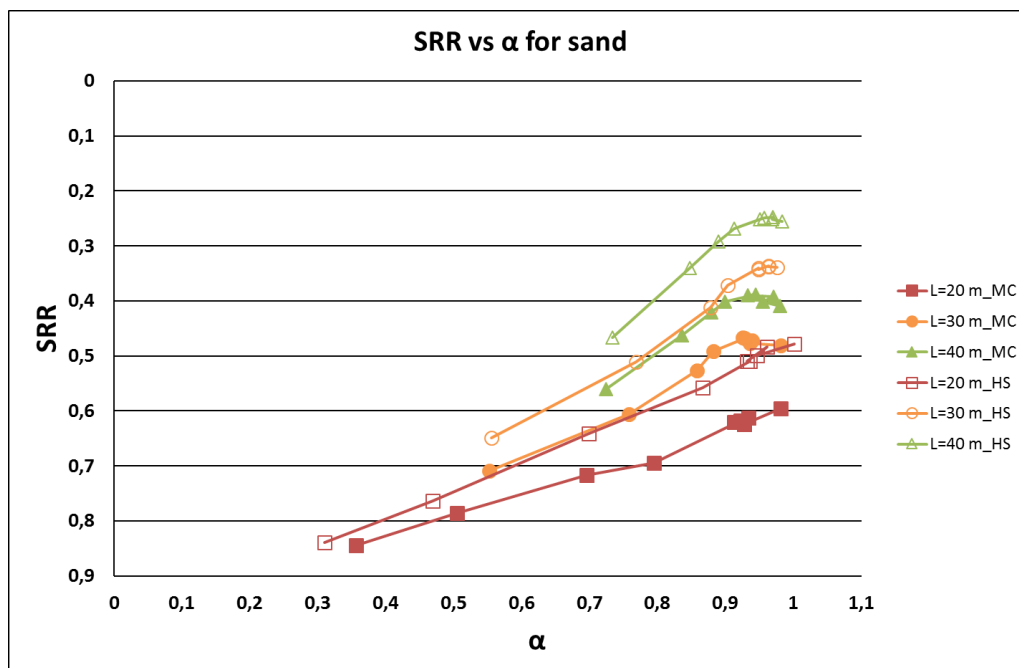

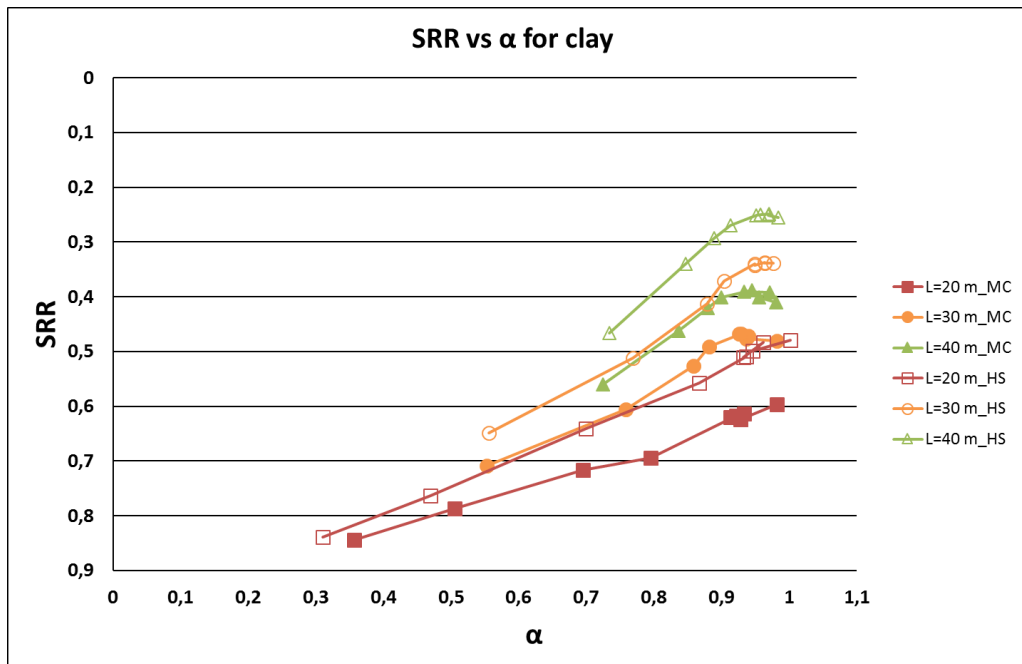*Figure 5.19.* SRR vs α chart for sand

Figure 5.20. SRR vs α chart for clay

In order to demonstrate the three dimensional axial load profile of the pile group, the axial load on each pile, which is located by the actual x and y coordinates on the figures, is computed and following figures are obtained. L=20 m and s/d=2.5 m, L=20 m and s/d=2.25 m, L=40 m and s/d=2.5 m, L=40 m and s/d=2.25 m for Mohr Coulomb material model are available at Figure 5.21, 5.22, 5.23 and 5.24. All of the three dimensional axial load profile figures can be seen at the Appendix A. We can see from Figure 5.21 to 5.24 that piles under the central part of raft takes less load as compare to piles near the edges. This was also stated in the literature by other researchers.
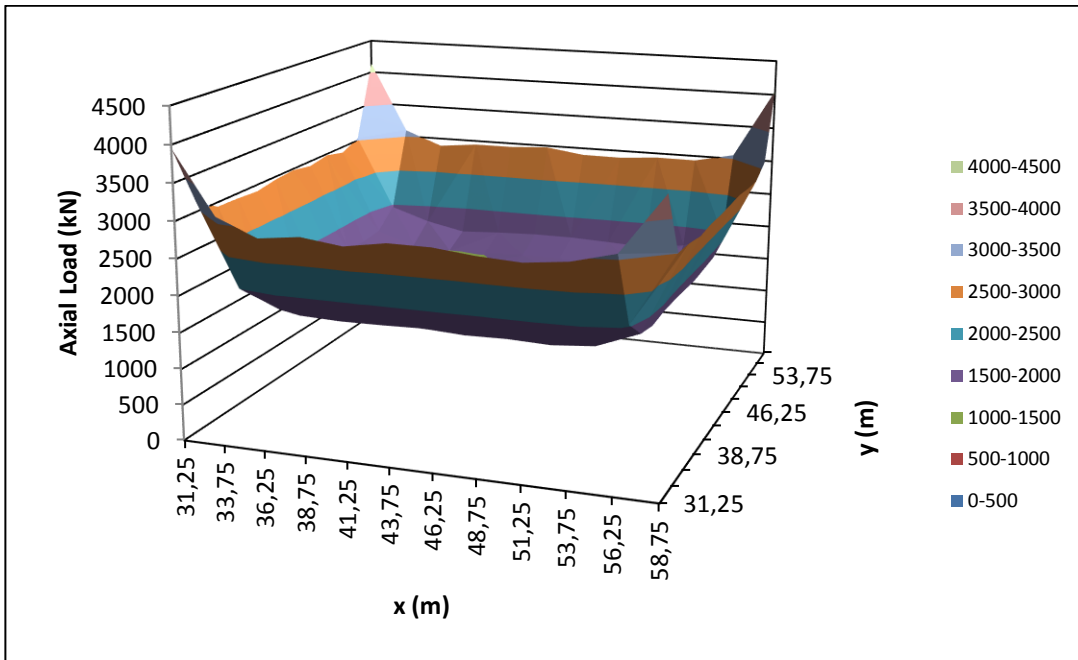
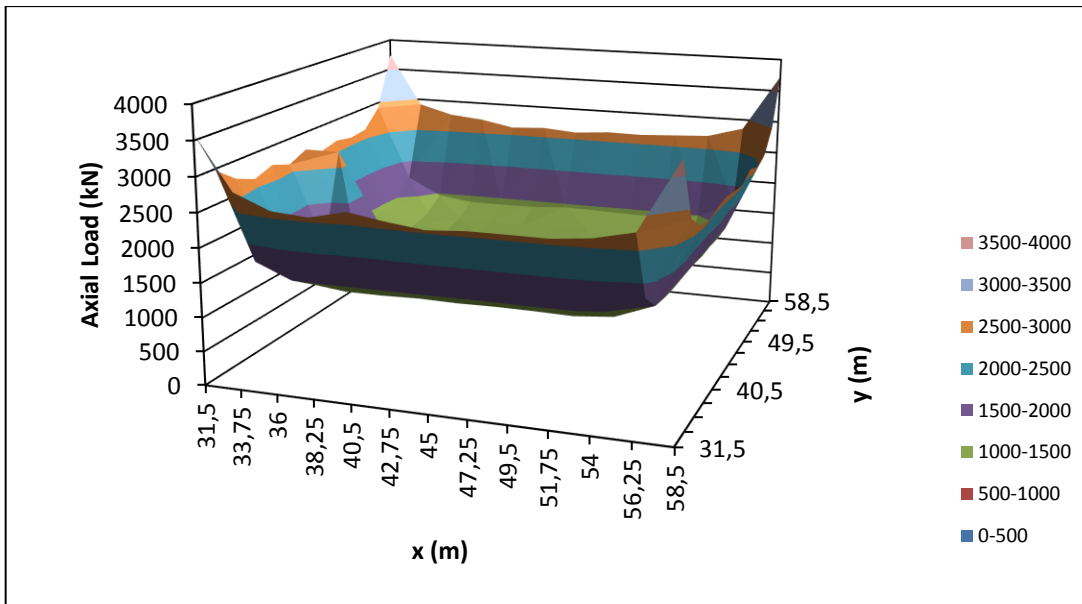*Figure 5.21.* 3D axial load profile of piled raft foundation with L=20 m and s/d=2.5

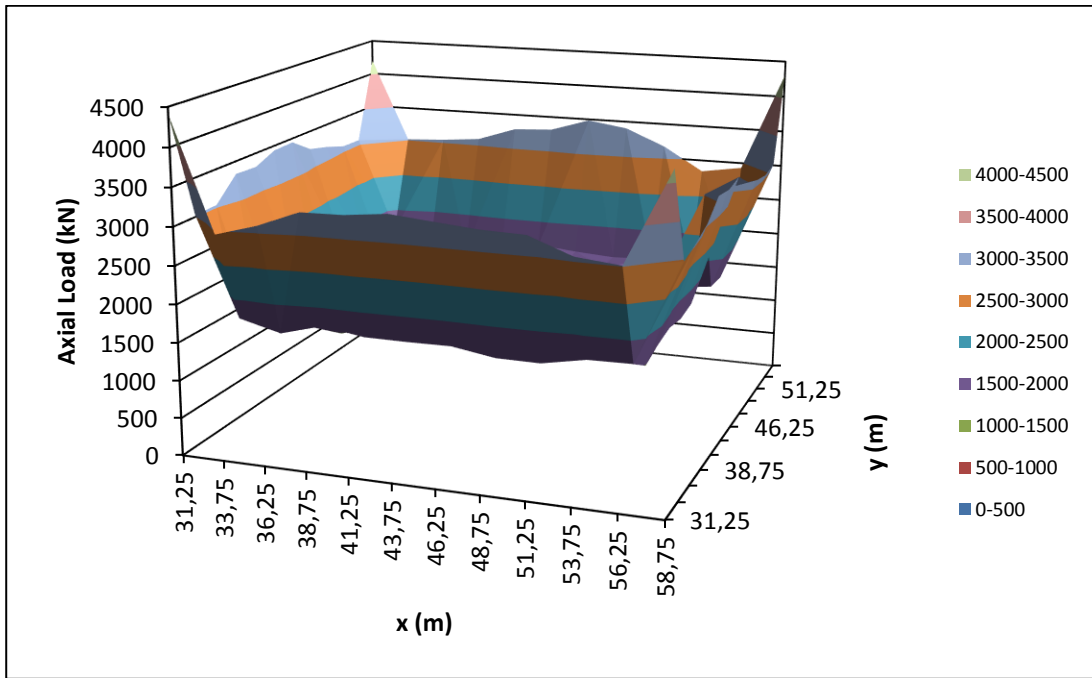*Figure 5.22.* 3D axial load profile of piled raft foundation with L=20 m and s/d=2.25

Figure 5.23. 3D axial load profile of piled raft foundation with L=40 m and s/d=2.5
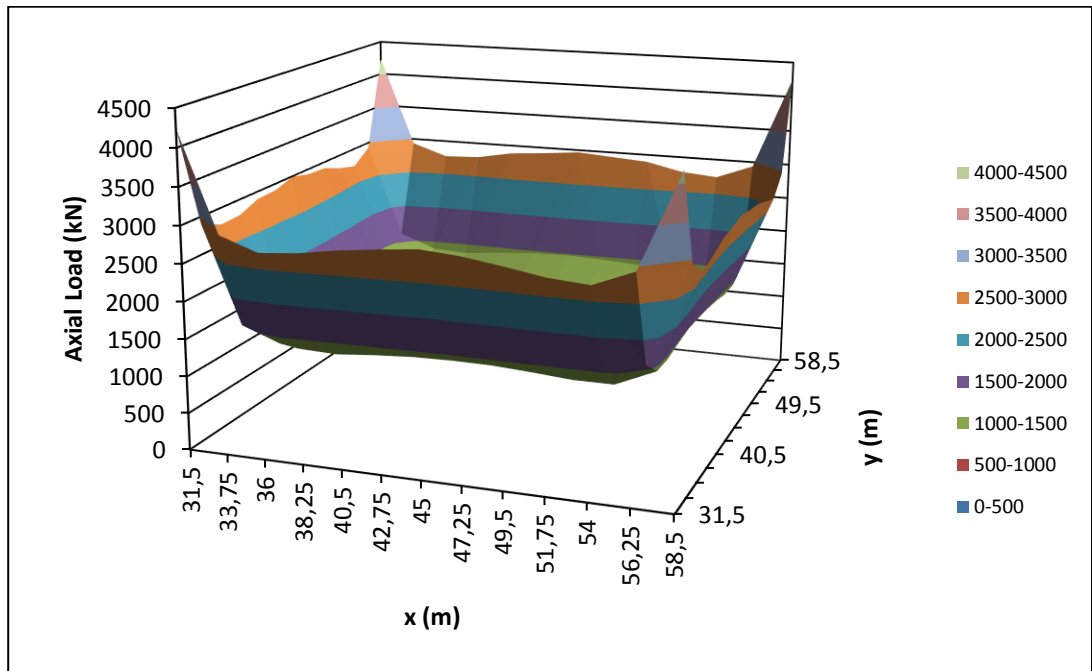

Figure 5.24. 3D axial load profile of piled raft foundation with L=40 m and s/d=2.25

101

Drained analyses are conducted for 1000 days by soft soil creep model in clay. In order to see the alteration of the each pile load in long term, one analysis with L=30 and s/d=7 is examined for 300 days, 600 days and 1000 days. Piles are numbered from 1 to 25 (Figure 5.25) and change of pile loads in long term are shown in Figure 5.26. As clay consolidates with time, loads on piles slightly increase.
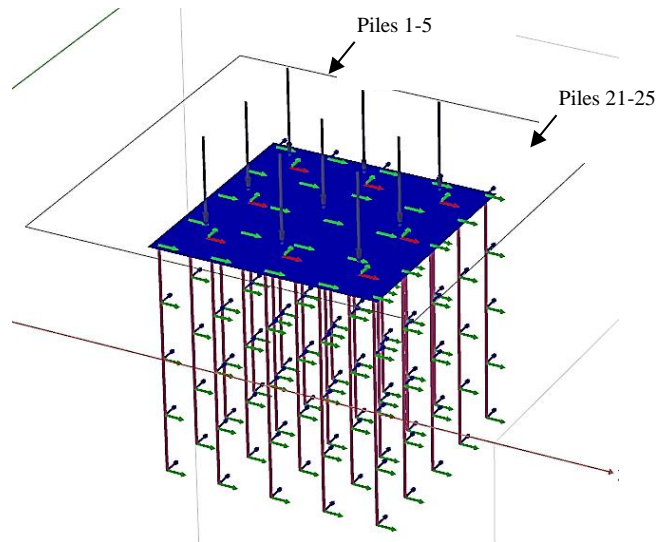

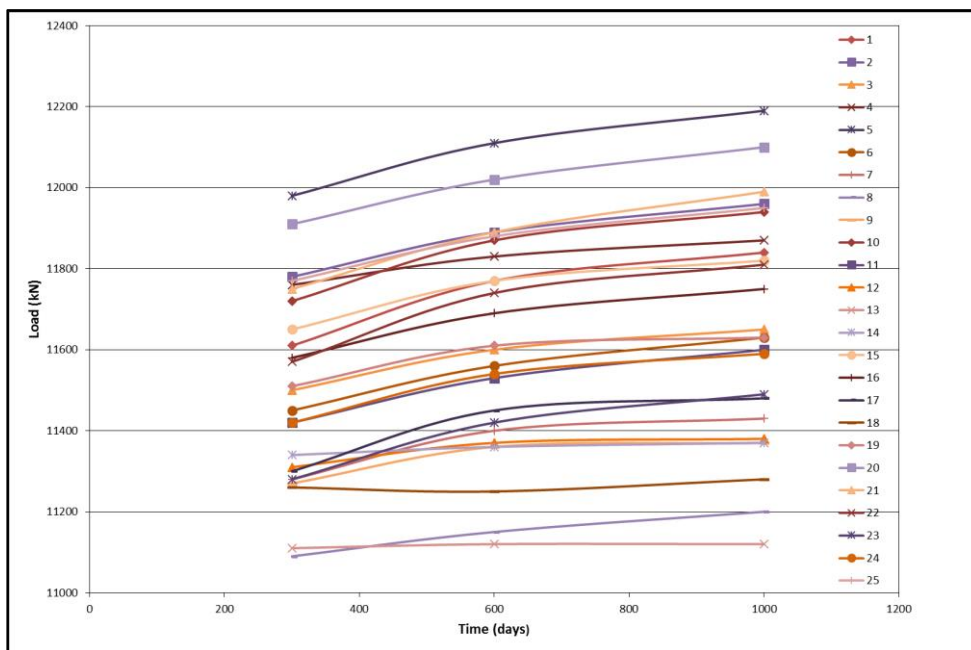*Figure 5.25.* Pile numbers of the model with L=30 and s/d=7

Figure 5.26. Change of pile loads in 300 days, 600 days and 1000 days

5.1. Implications of the Results

5.1.1. Implications of Mohr Coulomb and Hardening Soil Model Results for Sand

- According to Figure 5.1, SRR does not change significantly, where s/d is less than 3.5 indicating 9x9 configuration for single pile lengths of 20 m, 30 m and 40 m. This means that using more piles for this condition is unnecessary in terms of settlement reduction.

- According to Figure 5.2, SRR does not change significantly, where Total Length is more than:
  - ❖ nearly 1600 m indicating 9x9 configuration for single pile length of 20 m,
  - ❖ nearly 2400 m similarly indicating 9x9 configuration for single pile length of 30 m,
  - ❖ nearly 3200 m indicating 9x9 configuration for single pile length of 40 m. It must be noted that for single pile length of 40 m, SRR vs Total Length graph smoothens around 2000 m (7x7 configuration), yet becomes more stable at around 3200 m (9x9 configuration).

- If α vs s/d graph is interpreted on Figure 5.5, no distinct change is observed for α values where s/d is less than 3.5 for single pile lengths of 20 m, 30 m and 40 m. Furthermore, α value:
  - ❖ is around 0.9 for s/d = 3.5 which has 9x9 pile configuration,
  - ❖ decreases to as low as 0.35 for s/d=9 (4x4 configuration) for single pile length of 20 m,
  - ❖ decreases to as low as 0.55 for s/d=9 (4x4 configuration) for single pile length of 30 m,
  - ❖ decreases to as low as 0.75 for s/d=9 (4x4 configuration) for single pile length of 40 m,

- According to Figure 5.6, α does not change significantly and becomes nearly 0.9, where Total Length is more than:
  - ❖ nearly 1600 m indicating 9x9 configuration for single pile length of 20 m,

❖ nearly 2400 m similarly indicating 9x9 configuration for single pile length of 30 m,

❖ nearly 3200 m also indicating 9x9 configuration for single pile length of 40 m.

5.1.2. Implications of Mohr Coulomb and Hardening Soil Model Results for Clay

- According to Figure 5.7, SRR seems to have a stable trend, where s/d is less than 3,5 indicating 9x9 configuration for single pile lengths of 20 m, 30 m and 40 m. This means that using more piles beyond 9x9 for this condition is unnecessary in terms of settlement reduction.

- According to Figure 5.8, SRR does not change explicitly, where Total Length is more than:

  ❖ nearly 1600 m indicating 9x9 configuration for single pile length of 20 m,

  ❖ nearly 2400 m similarly indicating 9x9 configuration for single pile length of 30 m,

  ❖ nearly 3200 m also indicating 9x9 configuration for single pile length of 40 m.

- Figure 5.11 implies that the lower s/d, the higher α values are obtained. Therefore, an optimum point cannot be observed for α vs s/d graph.

- According to Figure 5.12, the lower Total Length, the higher α values are obtained. Therefore, an optimum point cannot be observed for α vs Total Length graph.

5.1.3. Implications of Soft Soil Creep Model Results for Clay

- There is an overall trend of increasing SRR with increasing s/d together with outliers in Figure 5.13. Moreover, SRR values are almost stable for three cases where s/d is less than 2.5.

- There is an overall trend of decreasing SRR with increasing Total Length together with outliers in Figure 5.14.

- From Figure 5.17, α values have tendency to decrease with increasing s/d which is more obvious in L=20 m cases.
- From Figure 5.18, α values have tendency to increase with increasing Total Length which is more obvious in L=20 m cases.
- In overall, it is important to state that abovementioned outliers are usually valid for L=30 m and L=40 m conditions. However, L=20 m cases do not show significant deviations.

5.1.4. Implications of 3D Axial Load Profile Results for Sand

Deductions from Appendix A for both Mohr Coulomb and Hardening Soil Model:

- As s/d decreases, the corner piles get more percentage of the total load for all pile lengths.
- For s/d=9, there are usually irregularities or concave down shapes in load sharing of the piles in different positions.
- Generally, for s/d=2.5 and s/d=4.5, load percentages increase from center piles to edge piles to corner piles. The difference between loads on corner and central piles could be also due to rigidity of the raft.

5.1.5. Implications of 3D Axial Load Profile Results for Clay

Deductions from Appendix A for both Mohr Coulomb and Hardening Soil Model:

- Similar to sand cases, as s/d decreases, the corner piles get more percentage of the total load for all pile lengths.
- Similar to sand cases, for s/d=9, there are usually irregularities or concave down shapes in load sharing of the piles in different positions.
- Different from sand cases, there happens to be a change in load percentage among edge and corner piles. Accordingly, the load percentage is higher in center compared to the edge in many cases. The difference between loads on corner and central piles could be also due to rigidity of the raft.

Deductions from Appendix A for Soft Soil Creep Model:

- Similar to sand cases, as s/d decreases, the corner piles get more percentage of the total load for all pile lengths.
- For s/d=9, there are usually irregularities in load sharing of the piles in different positions.
- Similar to sand cases, generally, for s/d=2.5 and s/d=4.5, load percentages increase from center piles to edge piles to corner piles. The difference between loads on corner and central piles could be also due to rigidity of the raft.

5.1.6. Implications of Change of Single Pile Loads in Long Term Results for Clay

- The representative analysis shows that, as can be expected, considering the consolidation in long term, the soil settles and exerts a down drag force on pile and this causes increase in axial loads on all piles in the Figure 5.26.

CHAPTER 6

CONCLUSIONS

It is known that piles serve for controlling total and differential settlement in addition to load carrying. In piled raft design, main criteria that governs the design are relative proportion of load carried by raft and by piles (represented by α factor) and reduction in settlements (represented by SRR). In this study, optimization of load sharing between piles and raft and settlement reduction ratio provided by piled raft is investigated via 3D finite element method. For different s/d ratios, for different total and single pile lengths, for different soil constitutive models in sand and in clay, the results indicate that:

- as s/d increases (as spacing increases), SRR increases for both Hardening Soil and Mohr Coulomb model, for both sand and clay.

- for a given length of piles, Mohr Coulomb model always gives larger SRR values than Hardening Soil model values for all s/d values.

- for a given soil constitutive model, as single pile length increases, SRR decreases for a given s/d ratio for both Hardening Soil and Mohr Coulomb model, for both sand and clay.

- for all single pile lengths (20 m, 30 m, 40 m), for all s/d ratios between 2 and 9, for both Hardening Soil and Mohr Coulomb models, SRR values are the range of 0.12 to 0.85.

- for all single pile lengths (20 m, 30 m, 40 m), for all s/d ratios between 2 and 9, for both Hardening Soil and Mohr Coulomb models, α values are the range of 0.3 to 1.

- as s/d increases (as spacing increases), α value decreases for all analyzed cases in this study.

- for a given s/d, as single pile length increases, α increases, which means in order to transfer more loads to raft, length of a single pile should be shorter for a given s/d ratio for all analyzed cases in this study.

- as total length of piles increase, α increases, for all cases analyzed in this study.

- as total length of piles increase, SRR values decrease for all analyzed cases in this study.

- an optimum value of "total length of piles / length of single pile" "80" provides benefit for all cases analyzed in this study.

RECOMMENDATIONS FOR FUTURE RESEARCHERS

- All of the conclusions in this study are based on three dimensional finite element analyses. Field measurements on settlement and loads on piles and/or centrifuge model test of piled raft with detailed instrumentation would verify the results.

- This study involves only vertical uniform load creating uniform pressure on the raft. Eccentric loading due to lateral forces such as in an earthquake or offshore wind and wave loading could be studied.

- Designs with variable pile lengths in the center and in the corners could be studied.

REFERENCES

Al-Mosawi, M. J., Fattah, M. Y., & Al-Zayadi, A. A. O. (2011). Experimental Observations on the Behavior of a Piled Raft Foundation, 17(4), 1–11.

Alver, O., & Özden, G. (2015). Tabakalı Zeminlerde Kazıklı Radye Temellerin Optimum Tasarımı. Dokuz Eylül Üniversitesi Mühendislik Fakültesi Fen ve Mühendislik Dergisi, 17(January), 13–26.

Bowles, L. E. (1996). Foundation analysis and design. McGraw-hill.

Brinkgreve, R. B. J. (2014). Efficient modelling of pile foundations in the Finite Element Method.

Butterfield, R. & Douglas, R.A. (1981). Flexibility coefficients for the design of piles and pile groups, CIRIA Technical Notes, 108

Clancy, P. & Randolph, M. F. (1993). An approximate analysis procedure for piled raft foundations. Int. J. Numer. Anal. Methods Geomech. 17, 849-869.

Clancy, P. and Randolph, M. F. (1996). Simple design tools for piled raft foundations. Géotechnique, 46(2), 313–328. https://doi.org/10.1680/geot.1996.46.2.313

Danish Standards Association. (1998). Norm for fundering (code of practice for foundation engineering). Danish standard DS415. 4th ed. Danish Standards Association, Copenhagen.

Dao, T. P. T. (2011). Validation of PLAXIS Embedded Piles For Lateral Loading. Delft University of Technology. Delft University of Technology.

Duncan, J. M. and Buchignani, A. L. (1976). An engineering manual for settlement studies, University of California at Berkeley, Berkeley, California.

El - Mossallamy, Y. M., El - Nahhas, F. M., & Essawy, A. S. (2006). Innovative use of piled raft foundation to optimize the design of high-rise buildings. In The 10th Arab Structural Engineering Conference, 13 -15 November 2006, Kuwait (pp. 347–358). Kuwait.

Elwakil, A. Z., & Azzam, W. R. (2016). Experimental and numerical study of piled raft system. Alexandria Engineering Journal, 55(1), 547–560. https://doi.org/10.1016/j.aej.2015.10.001

Engin, H. K., & Brinkgreve, R. B. J. (2009). Investigation of Pile Behaviour Using Embedded Piles. In Proceedings of the 17th International Conference on Soil Mechanics and Geotechnical Engineering: The Academia and Practice of Geotechnical Engineering (Vol. 2, pp. 1189–1192). https://doi.org/10.3233/978-1-60750-031-5-1189

Engin, H. K., Septanika, E. G., & Brinkgreve, R. B. J. (2008). Estimation of Pile Group Behavior using Embedded Piles. In 12th International Conference of International Association for Computer Methods and Advances in Geomechanics (IACMAG). Goa, India.

Garg, P., Singh, H., & Jha, J. (2013). Optimisation of Piled-Raft Foundation. In UKIERI Concrete Congress - Innovations in Concrete Construction (pp. 1724–1735).

Horikoshi, K., & Randolph, M. F. (1998). A contribution to optimum design of piled rafts. Géotechnique, 48(3), 301–317. https://doi.org/10.1680/geot.1998.48.3.301

Ismael N.F., Al-Sanad H.A. and Al-Otaibi F. (1994). Tension tests on bored piles in cemented desert sands. Canadian Geotechnical Journal, 31(4), 597-603.

Katzenbach, R., Arslan, U. & Moorman, C. (2000). Piled Raft Projects in Germany. In Hemsley (ed), Design Application of Piled Raft Foundations, 323-391. London: Thomas Telford.

Katzenbach, Rolf, P. D.-I., & Deepankar Choudhury, P. D. (2013). ISSMGE Combined Pile-Raft Foundation Guideline.

Kuwabara, F. (1989). An Elastic Analysis for Piled Raft Foundations in a Homogeneous Soil. Soils and Foundations, 29(1), 82–92.

Lambe, T. W., & Whitman, R. V. (1969), Soil Mechanics, 553 pp., John Wiley, New York.

Mali, S., & Singh, B. (2018). Behavior of large piled-raft foundation on clay soil. Ocean Engineering, 149, 205–216. https://doi.org/10.1016/j.oceaneng.2017.12.029

Mandolini, A., Di Laora, R., & Mascarucci, Y. (2013). Rational design of piled raft. Procedia Engineering, 57, 45–52. https://doi.org/10.1016/j.proeng.2013.04.008

Patil, J. D., Vasanwala, S. A., & Solanki, C. H. (2014). An experimental investigation on behavior of piled raft foundation. International Journal of Geomatics and Geosciences, 5(2), 300–311.

Plaxis 3D Tutorial, Reference, Material Models and Scientific Manuals (2013)

Poulos, H.G. & Davis, E.H. (1980). Pile foundation analysis and design. Wiley, New York.

Poulos, H. G. (2001). Piled raft foundations: design and applications. Géotechnique, 51(2), 95–113. https://doi.org/10.1680/geot.2001.51.2.95

Poulos, H. G. (2002). Simplified Design Procedure for Piled Raft Foundations. In Deep Foundations (pp. 441–458). Orlando, Florida, USA. https://doi.org/10.1061/40601(256)32

Prakoso, W. A., & Kulhawy, F. H. (2001). Contribution to Piled Raft Foundation Design. Journal Of Geotechnical and Geoenvironmental Engineering, 127(January), 17–24.

Randolph , M.F. (1994). Design methods for pile groups and piled rafts. S.O.A. Report, 13 ICSMFE, New Delhi, 5, 61-82.

Reul, O., & Randolph, M. F. (2003). Piled rafts in overconsolidated clay: comparison of in situ measurements and numerical analyses. Géotechnique, 53(3), 301–315. https://doi.org/10.1680/geot.2003.53.3.301

Ryltenius, A. (2011). FEM Modelling of Piled Raft Foundations in Two and Three Dimensions. Lund University.

Sheil, B. B., & Mccabe, B. A. (2012). Predictions of friction pile group response using embedded piles in PLAXIS. In 3rd International Conference on New Developments in Soil Mechanics and Geotechnical Engineering (pp. 679–686). North Cyprus.

Shen, W.Y., & Teh, C.I. (2002). Practical solution for group stiffness analysis of piles, Journal of Geotechnical and Geoenvironmental Engineering, Vol.128, No.8, pp.692-698

Sluis, J., Besseling, F., & Stuurwold, P. (2014). Modelling of a pile row in a 2D plane strain FE-analysis. In Numerical Methods in Geotechnical Engineering (pp. 277–282). https://doi.org/10.1201/b17017-51

Sorensen, K.K. & Okkels, N. (2013). Correlation between drained shear strength and plasticity index of undisturbed overconsolidated clays. Proc. 18th Intl. Conf. Soil Mech. & Geot. Engrg., Paris: 423-428.

Sönmez, N. (2013). A Study on Design of Piled Raft Foundation Systems. Middle East Technical University.

Stroud, M.A. 1988. The standard penetration test: its application and interpretation. Penetration Testing in the U.K., Thomas Telford, London: 29-49.

Terzaghi, K & B. Peck, R & Mesri, G. (1996). Soil Mechanics in Engineering Practice.

Yılmaz, B. (2010). An Analytical and Experimental Study on Piled Raft Foundations. Middle East Technical University.

APPENDIX

A. THREE DIMENSIONAL PILE LOAD PROFILES

For sand:
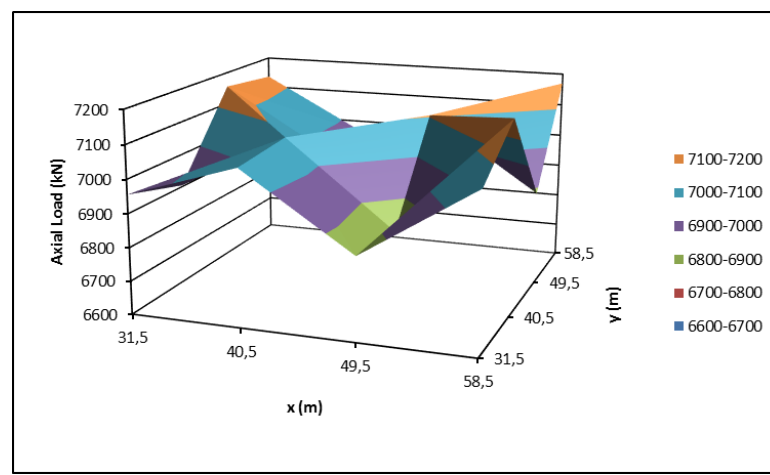
Mohr Coulomb Model Results for L=20 m
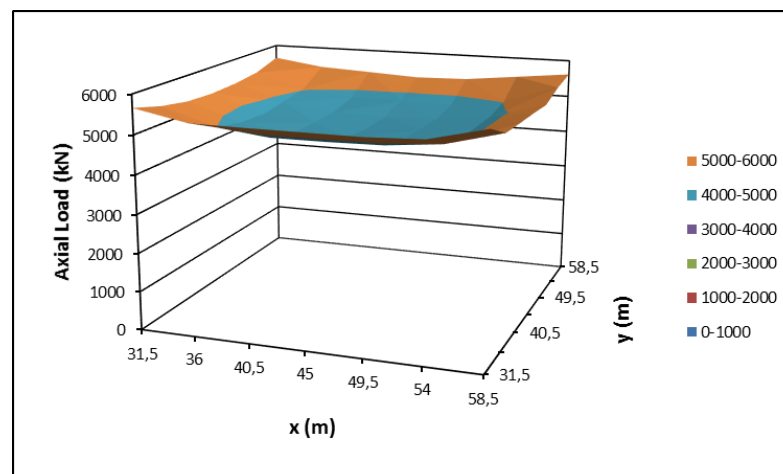

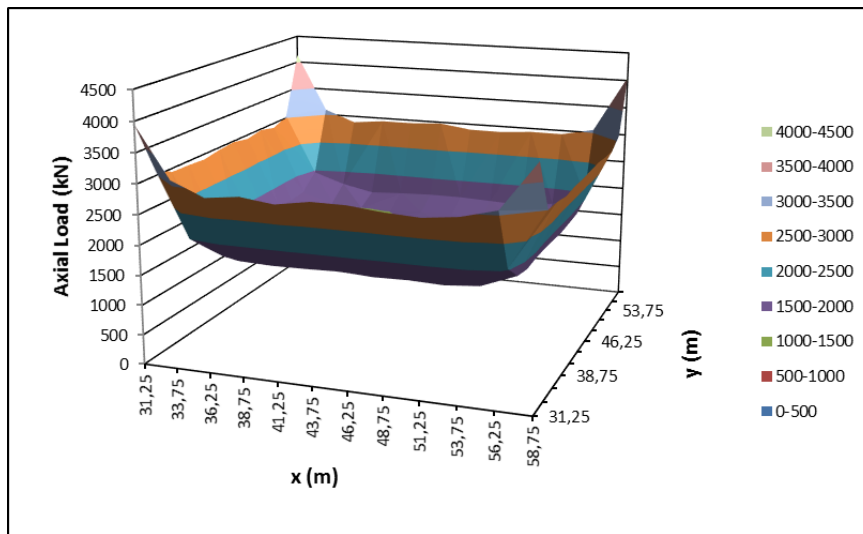*Figure A.1.* L=20 m s/d=9

Figure A.2. L=20 m s/d=4.5

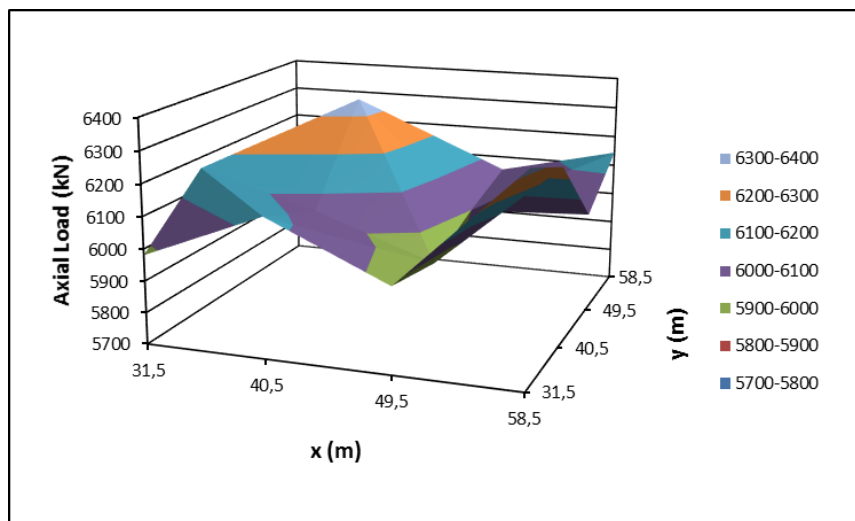*Figure A.3.* L=20 m s/d=2.5

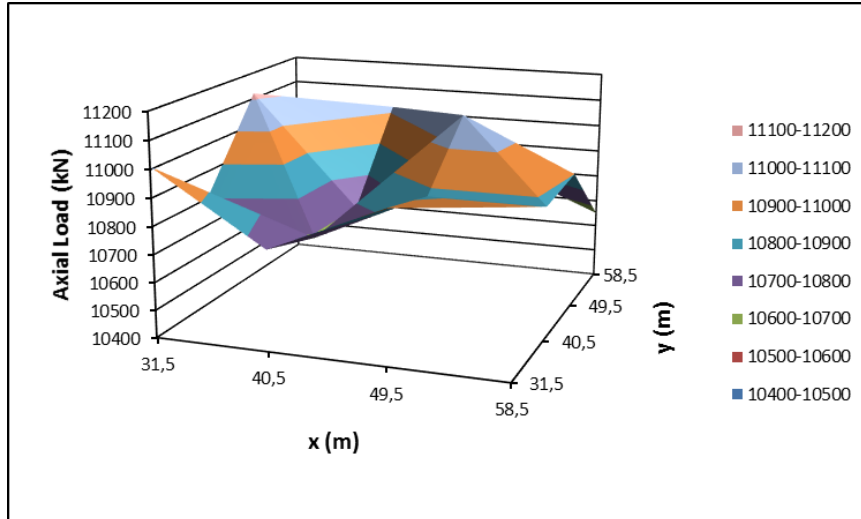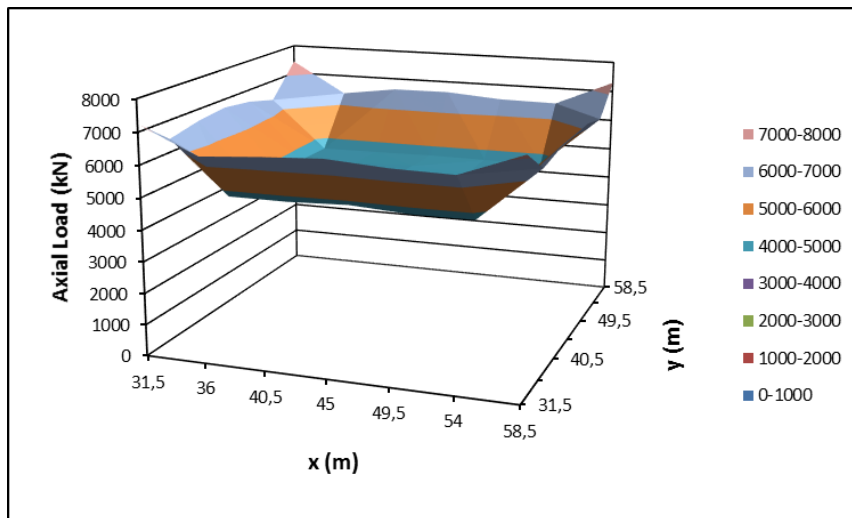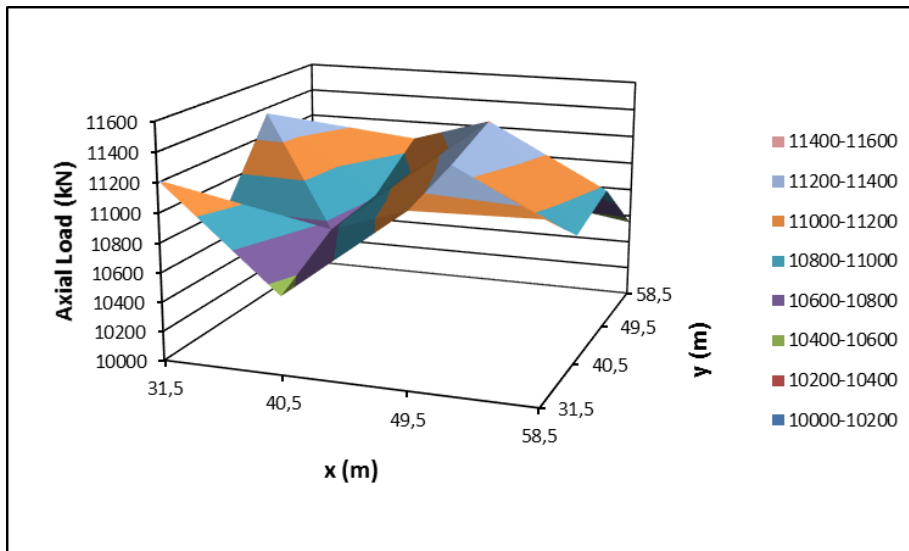## Hardening Soil Model Results for L=20 m

Figure A.4. L=20 m s/d=9
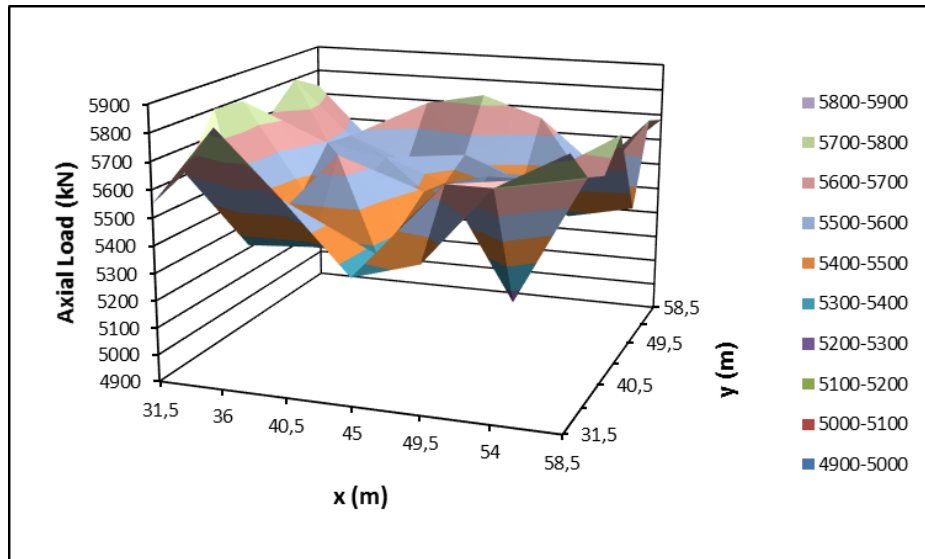
Figure A.5. L=20 m s/d=4.5
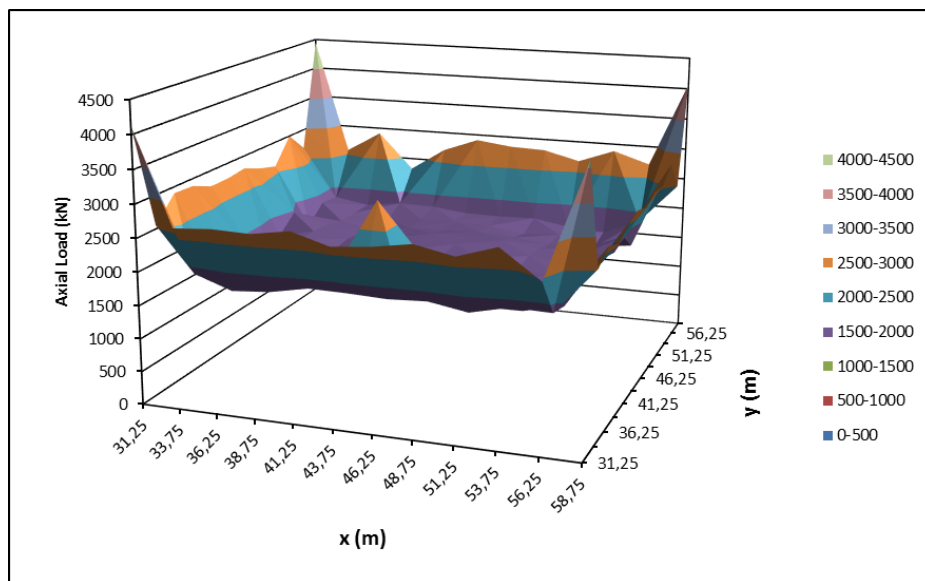
Figure A.6. L=20 m s/d=2.5

117

Mohr Coulomb Model Results for L=30 m

Figure A.7. L=30 m s/d=9

Figure A.8. L=30 m s/d=4.5
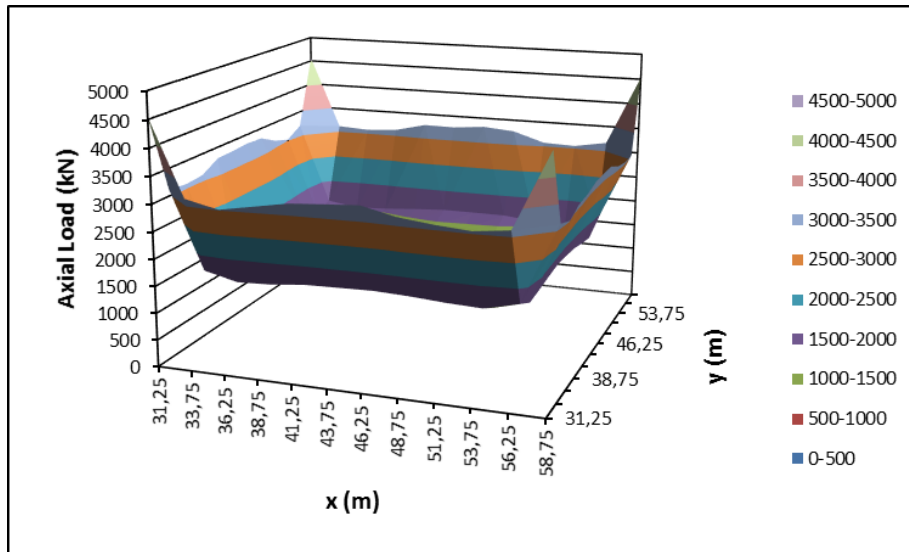
Figure A.9. L=30 m s/d=2.5

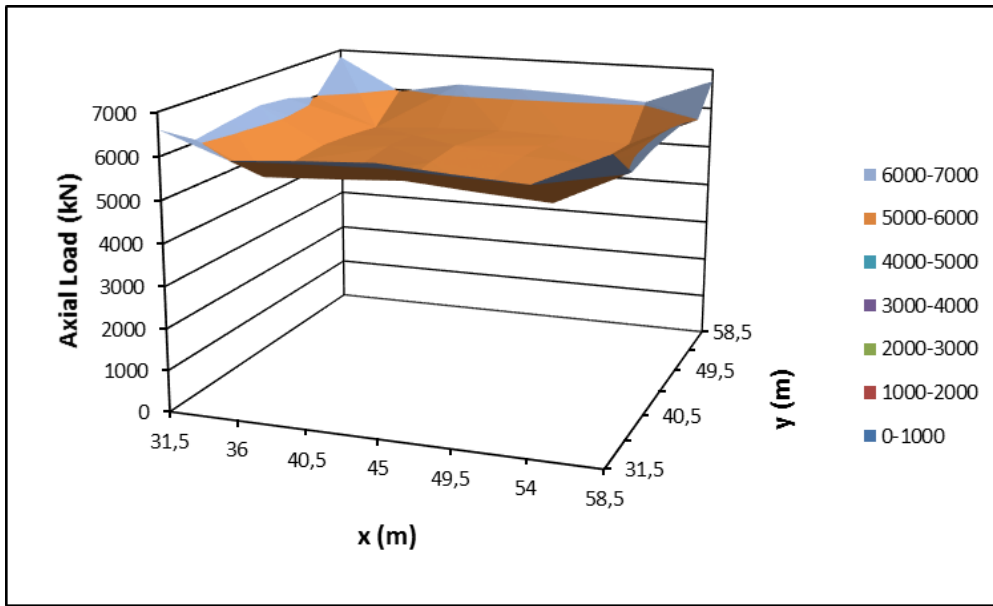**Hardening Soil Model Results for L=30 m**

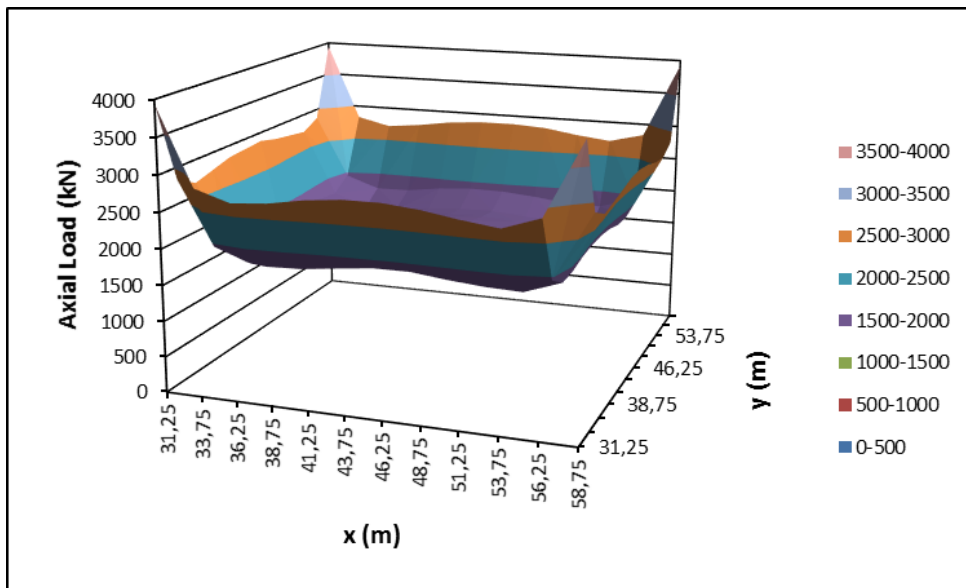*Figure A.10.* L=30 m s/d=9

Figure A.11. L=30 m s/d=4.5

Figure A.12. L=30 m s/d=2.5

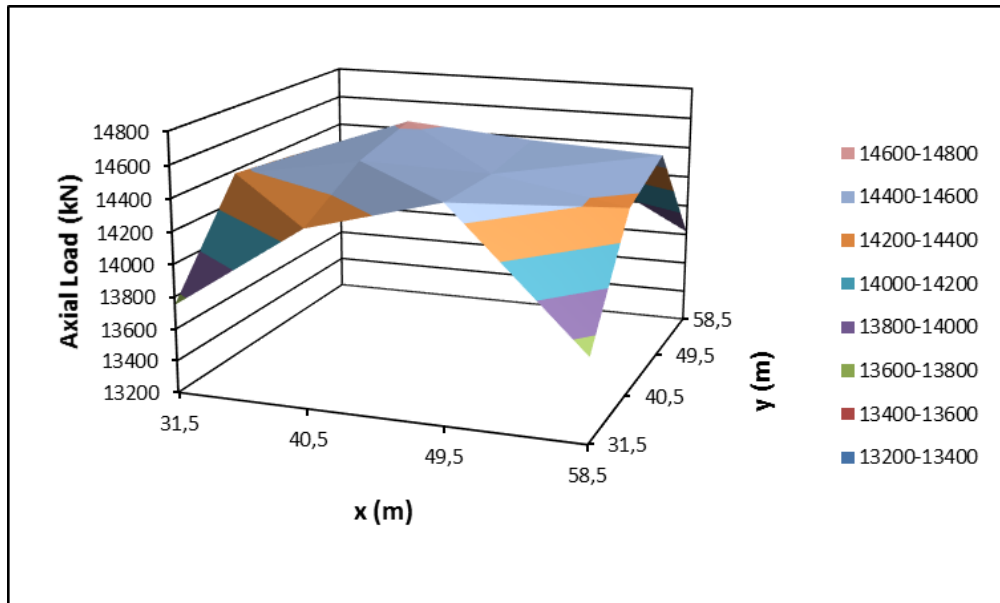**Mohr Coulomb Model Results for L=40 m**

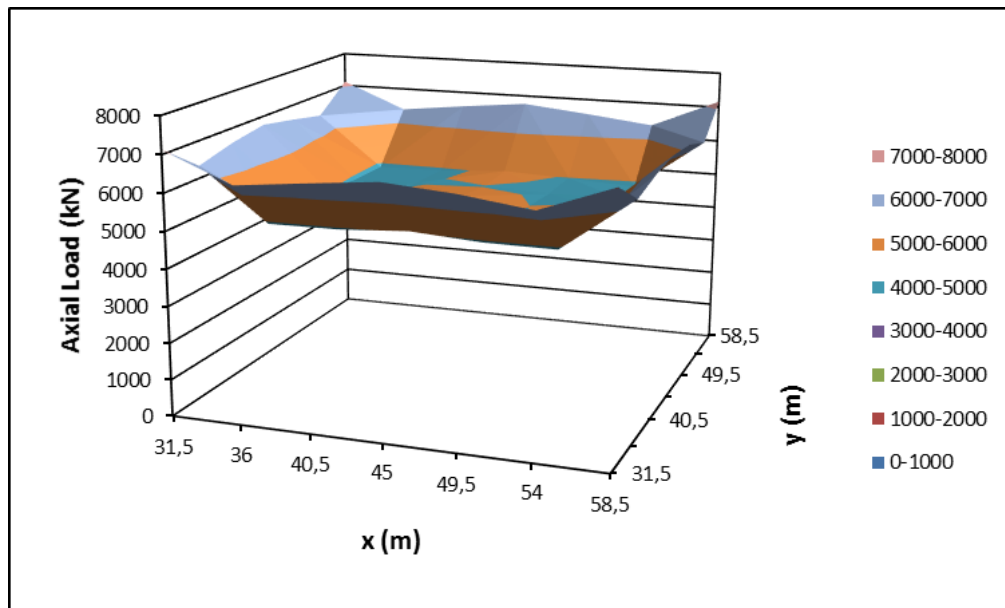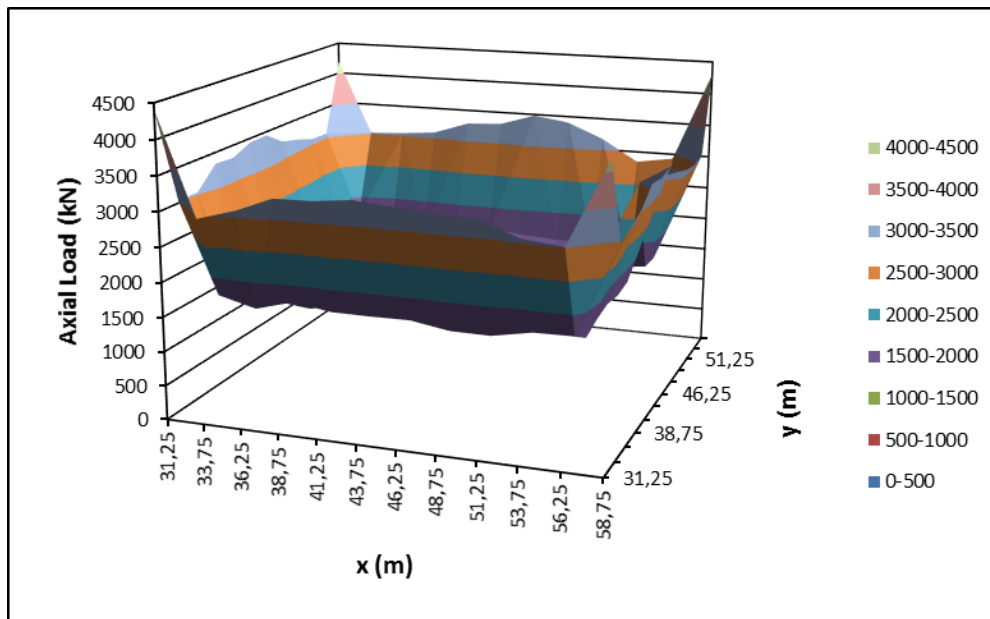*Figure A.13.* L=40 m s/d=9

Figure A.14. L=40 m s/d=4.5

121

Figure A.15. L=40 m s/d=2.5
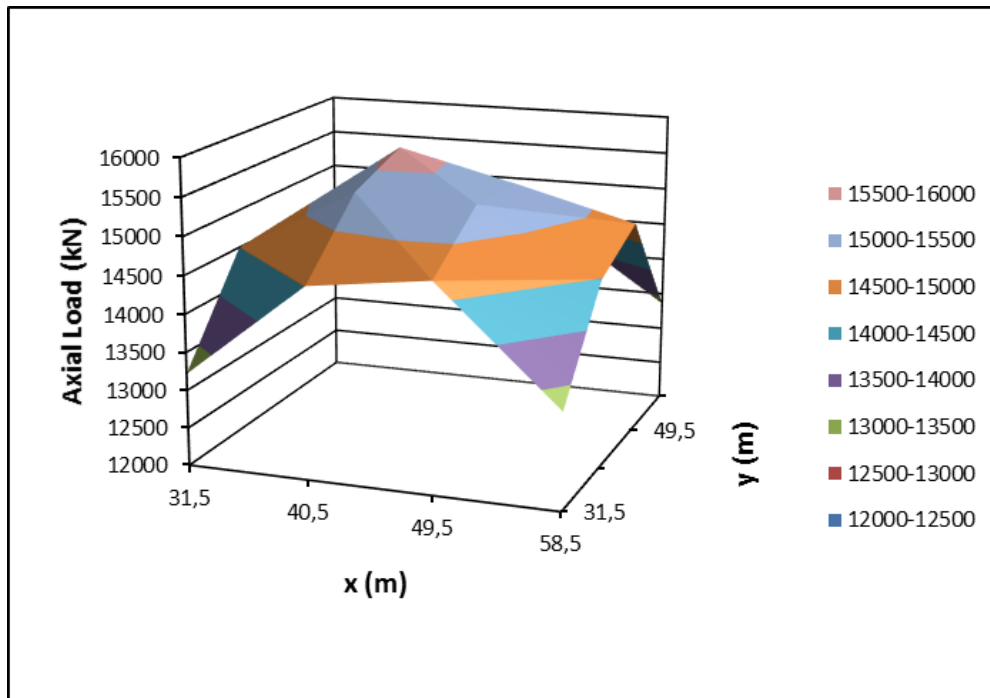
Hardening Soil Model Results for L=40 m
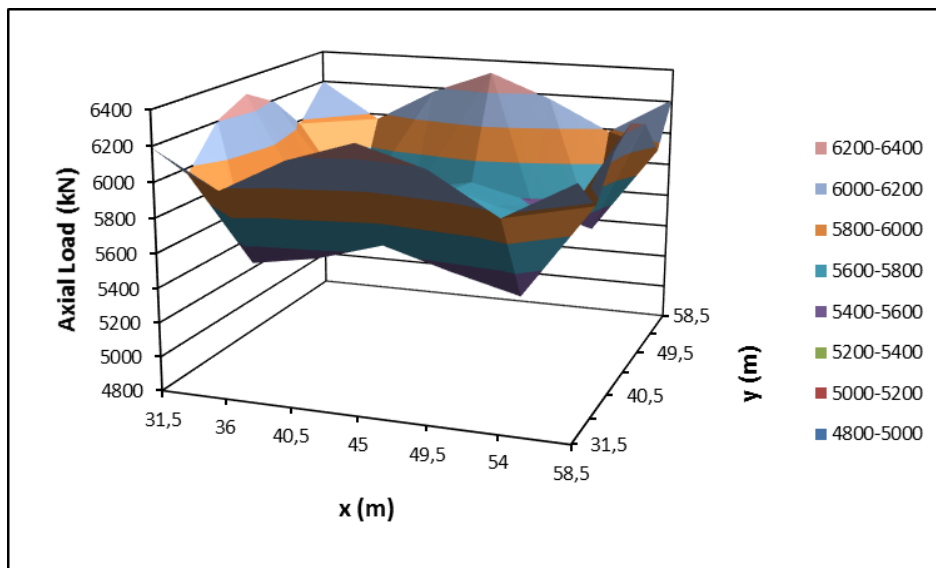

Figure A.16. L=40 m s/d=9

Figure A.17. L=40 m s/d=4.5

Figure A.18. L=40 m s/d=2.5

For clay:

Mohr Coulomb Model Results for L=20 m

Figure A.19. L=20 m s/d=9

Figure A.20. L=20 m s/d=4.5

124
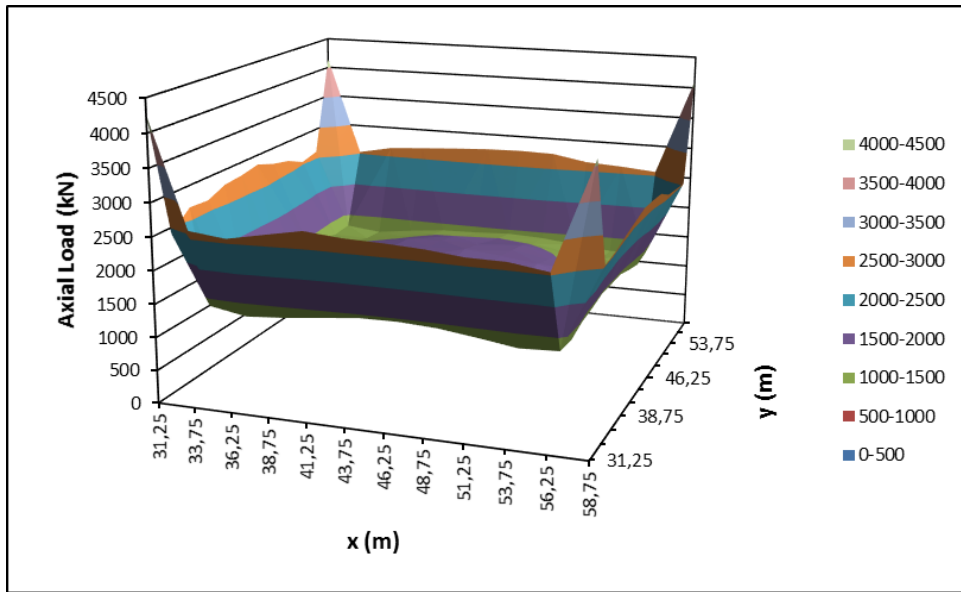
Figure A.21. L=20 m s/d=2.5

Hardening Soil Model Results for L=20 m
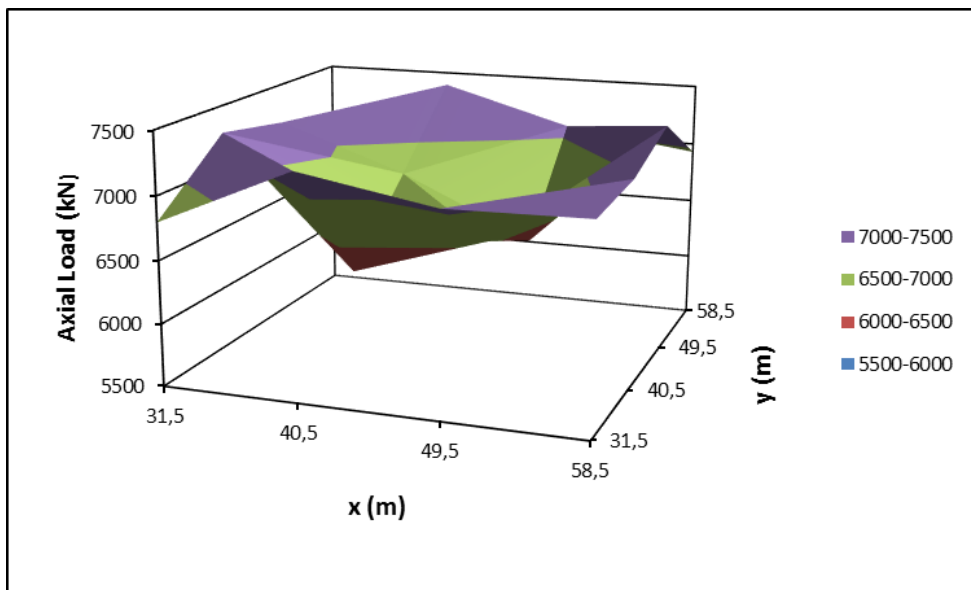
Figure A.22. L=20 m s/d=9
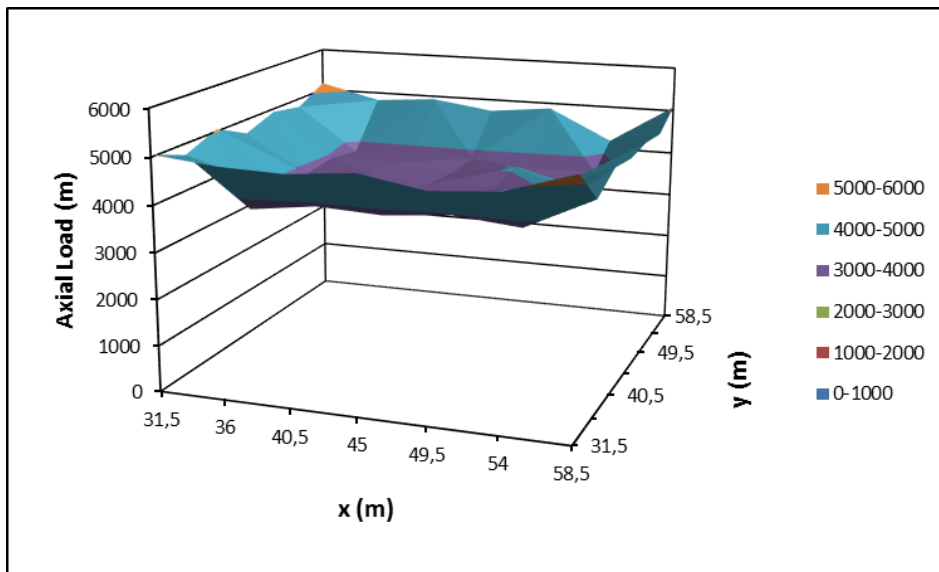
Figure A.23. L=20 m s/d=4.5
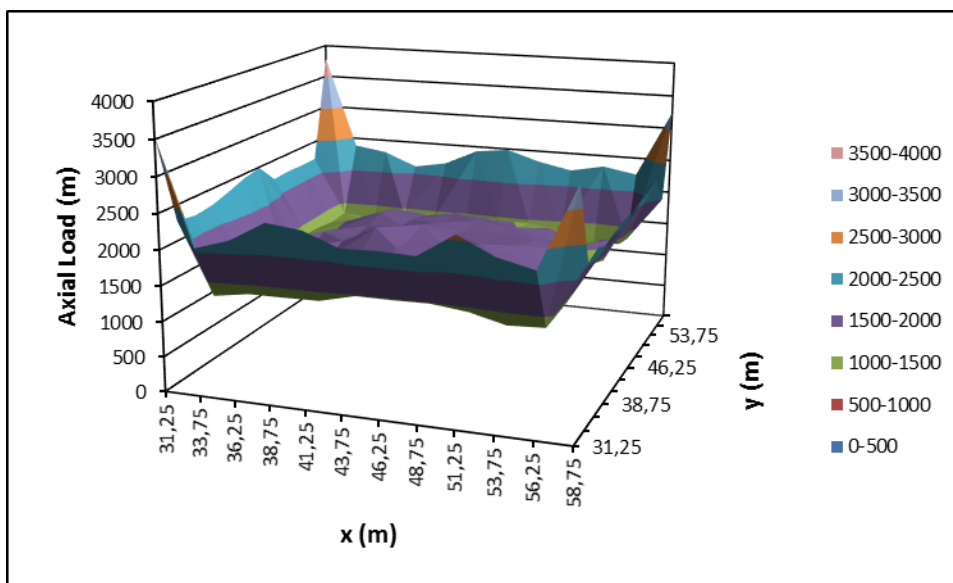
Figure A.24. L=20 m s/d=2.5

126

Mohr Coulomb Model Results for L=30 m
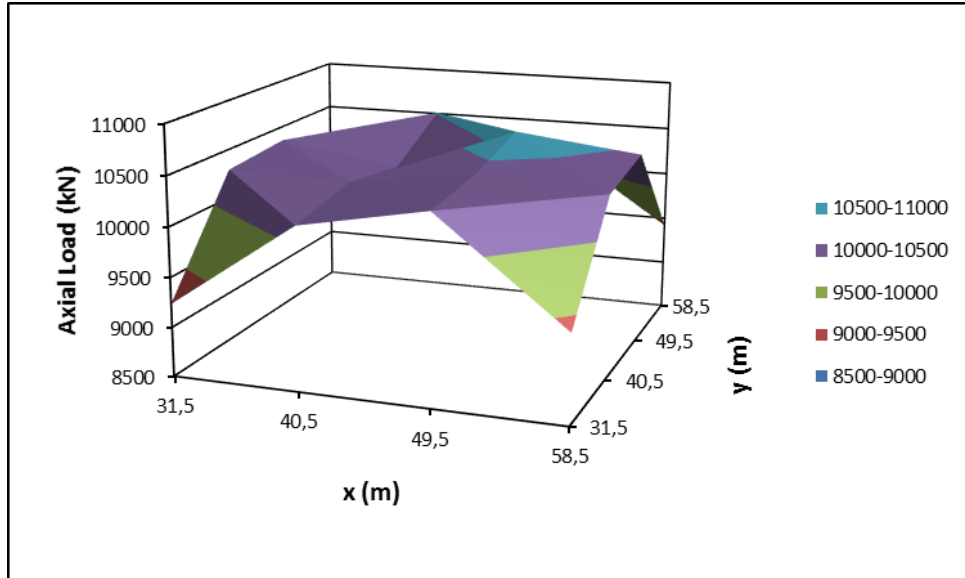
Figure A.25. L=30 m s/d=9
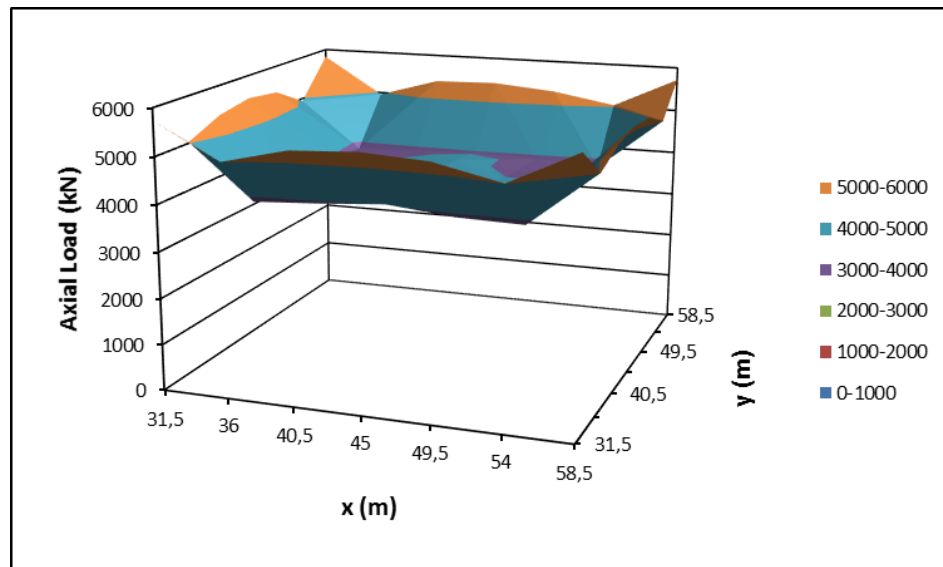
Figure A.26. L=30 m s/d=4.5
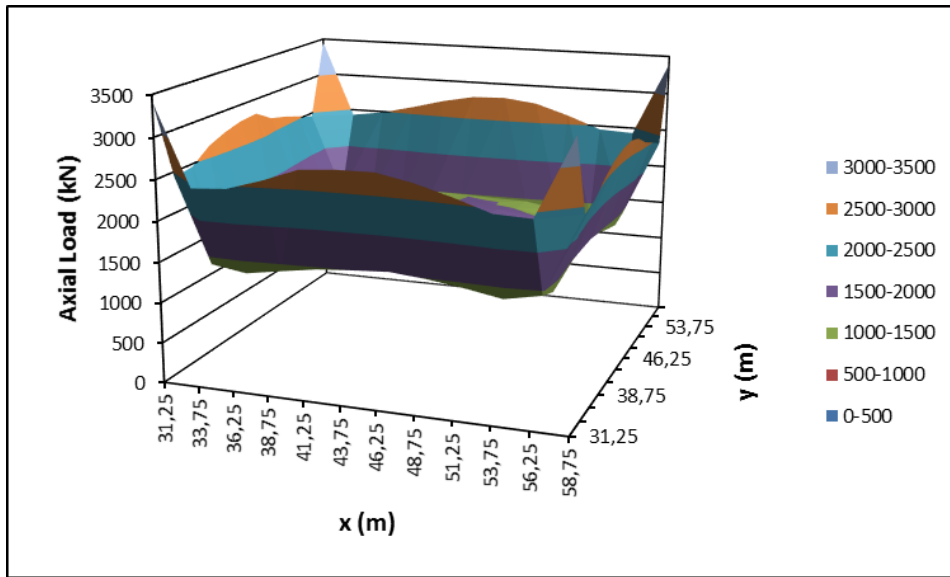
Figure A.27. L=30 m s/d=2.5

Hardening Soil Model Results for L=30 m
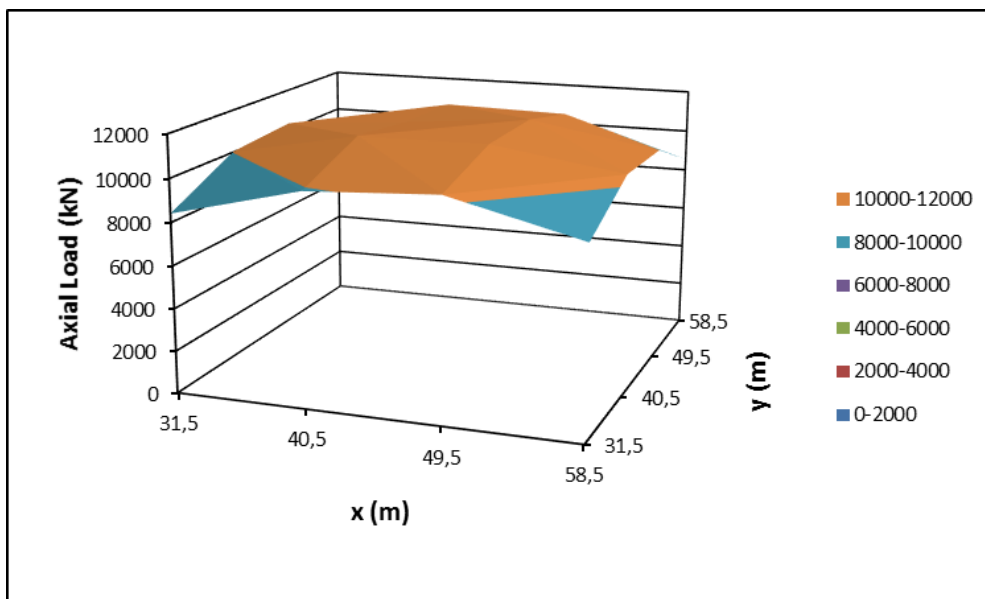
Figure A.28. L=30 m s/d=9
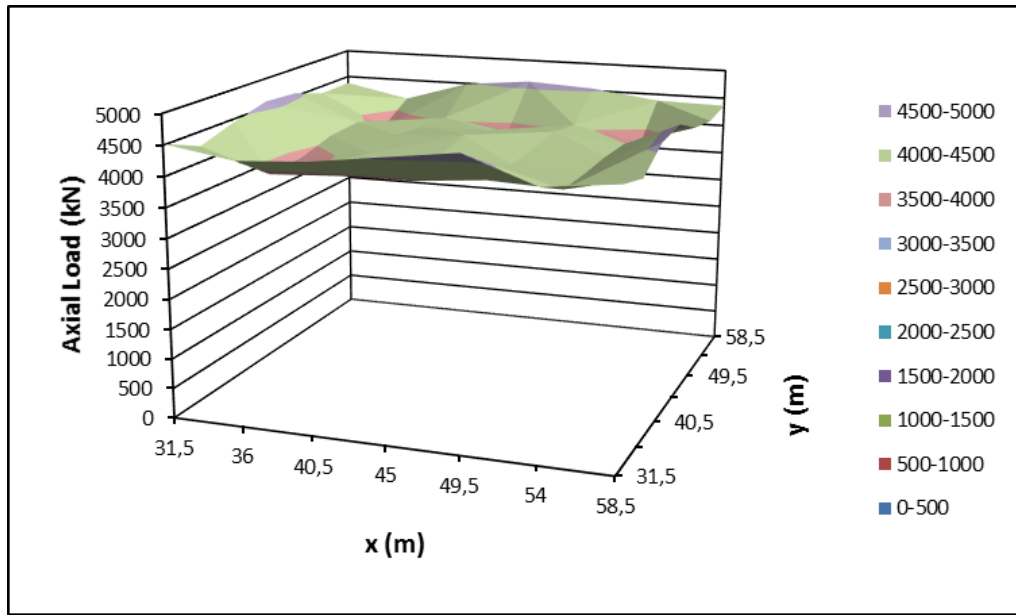
Figure A.29. L=30 m s/d=4.5
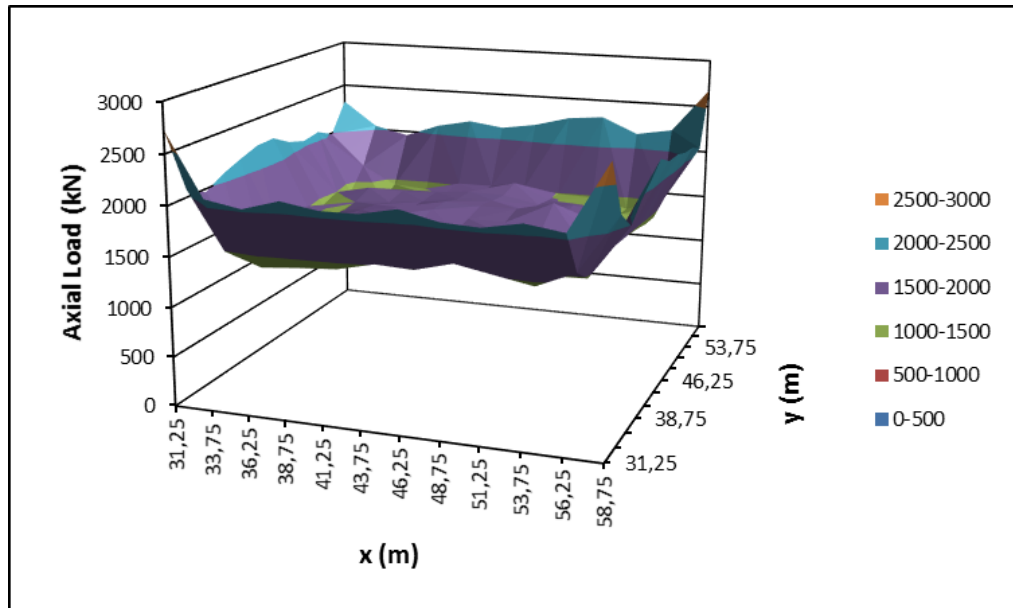
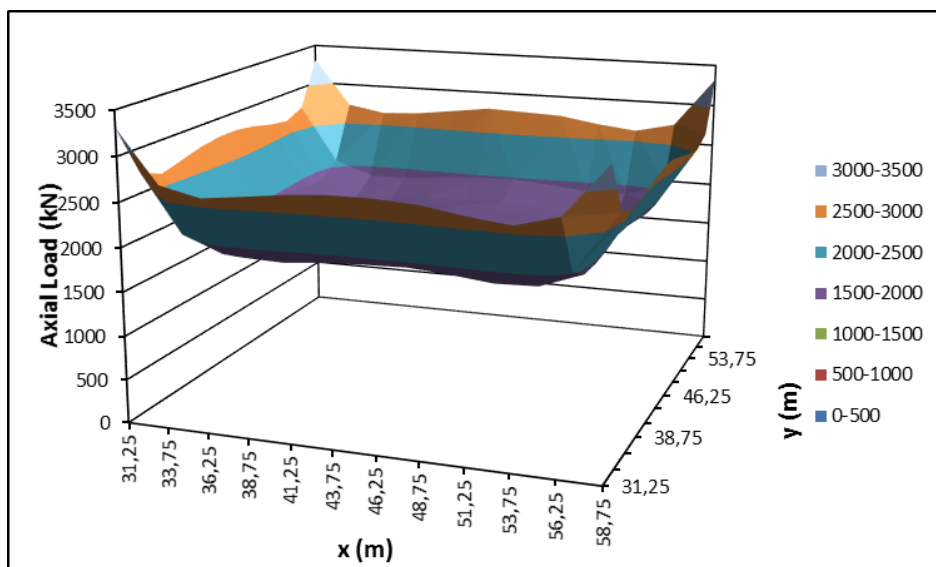*Figure A.30.* L=30 m s/d=2.5

Mohr Coulomb Model Results for L=40 m
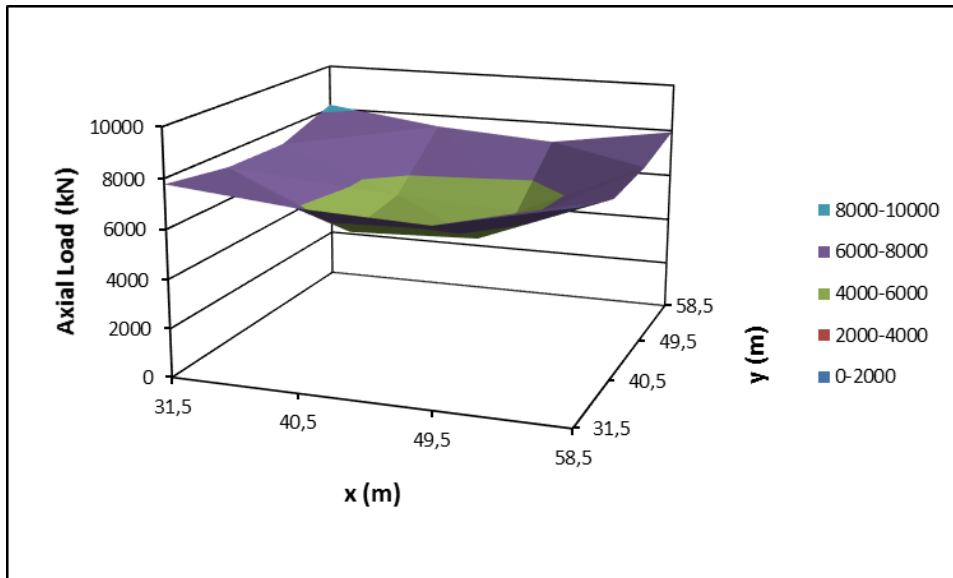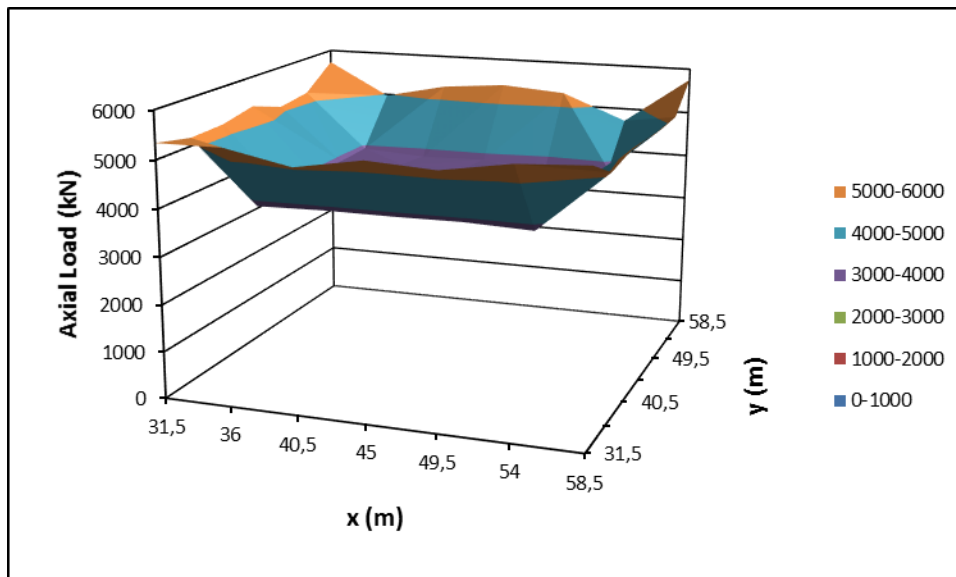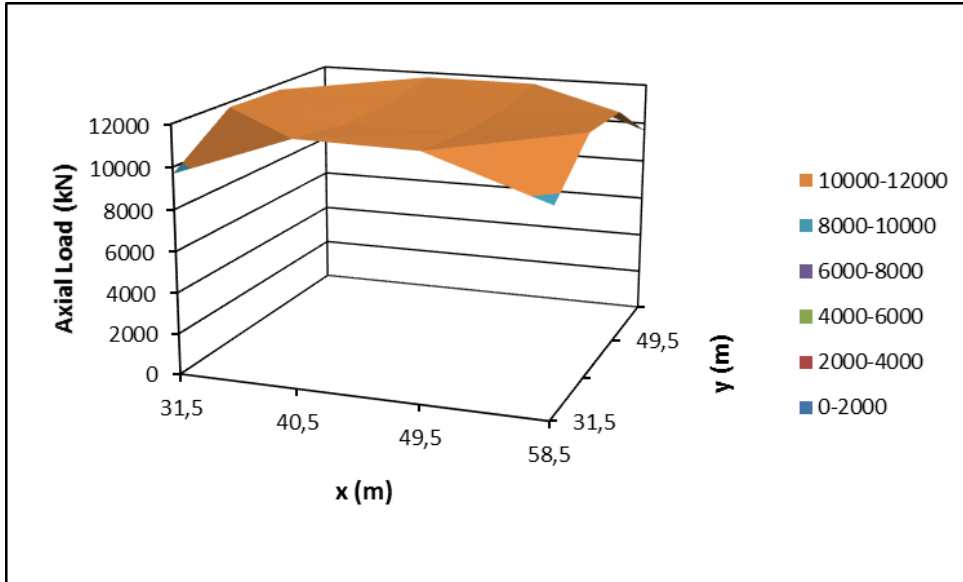

Figure A.31. L=40 m s/d=9
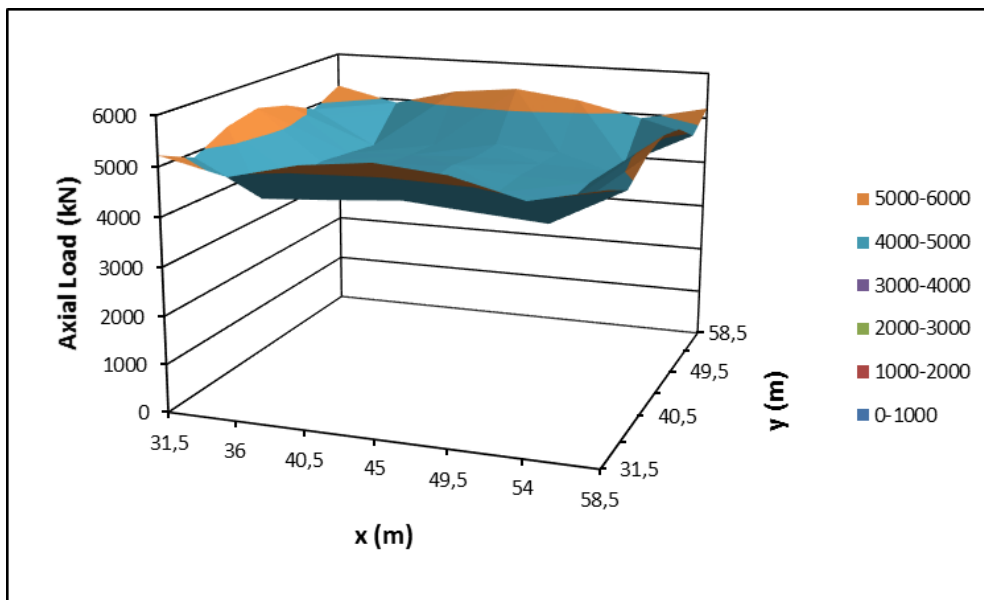
Figure A.32. L=40 m s/d=4.5
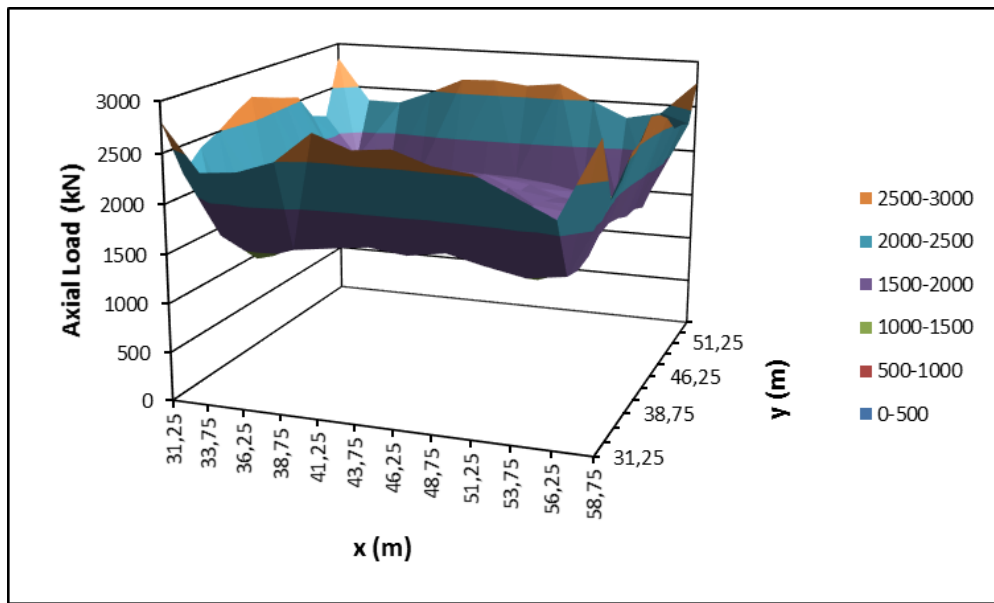
Figure A.33. L=40 m s/d=2.5

Hardening Soil Model Results for L=40 m
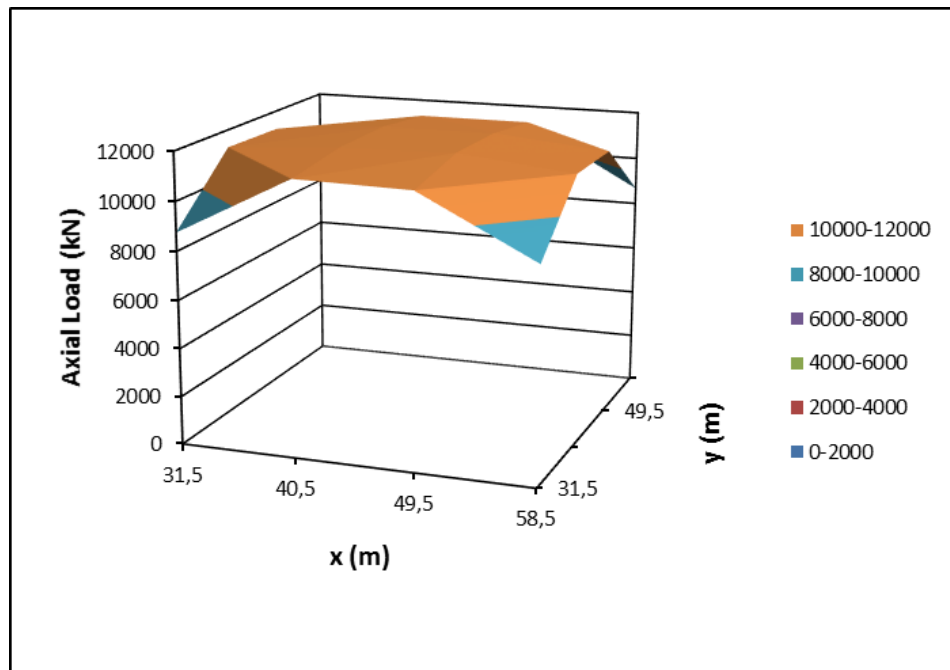
Figure A.34. L=40 m s/d=9

131
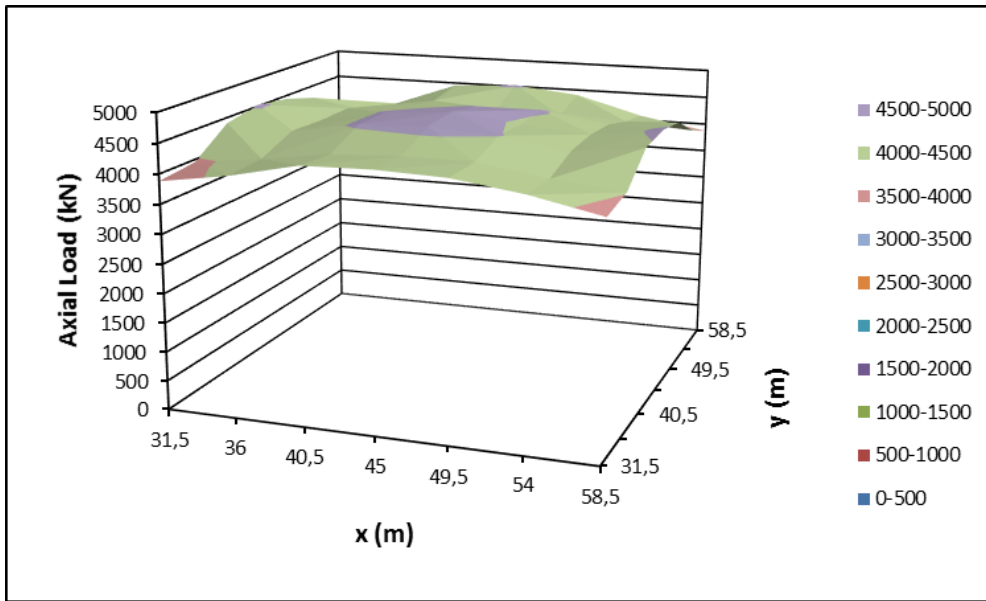
Figure A.35. L=40 m s/d=4.5
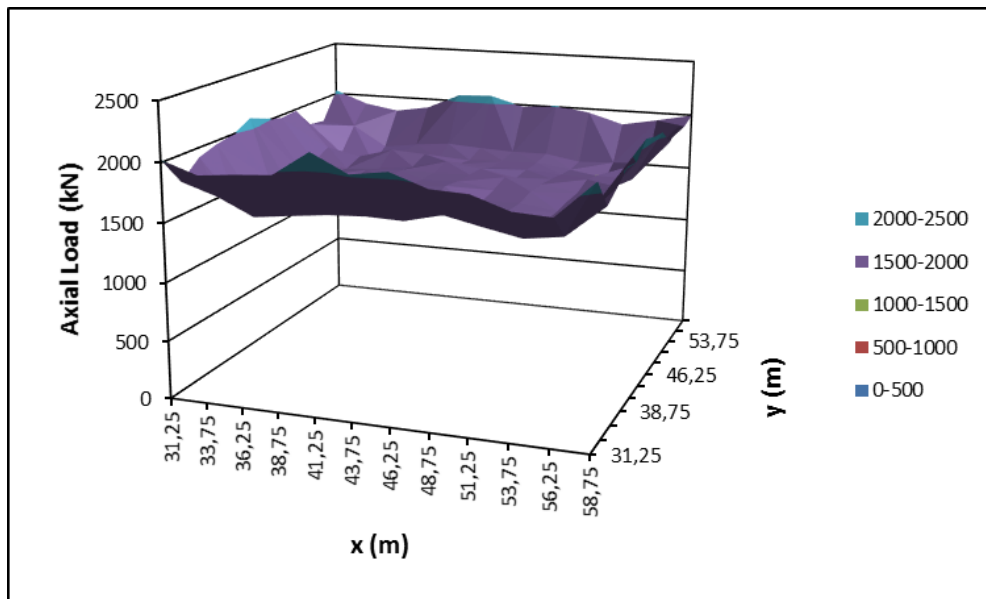
Figure A.36. L=40 m s/d=2.5

Soft Soil Creep Model Results for L=20 m
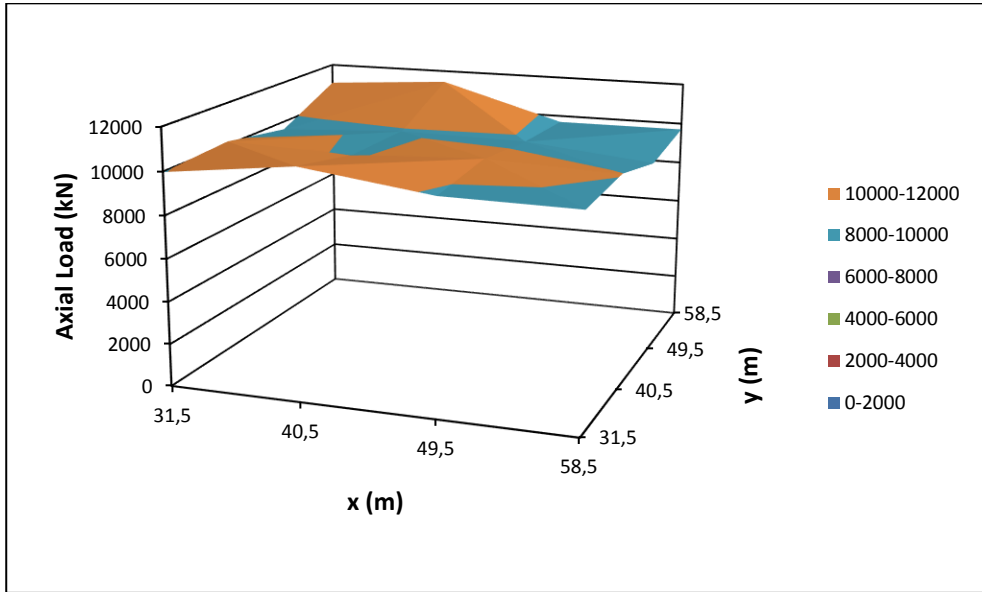
Figure A.37. L=20 m s/d=9
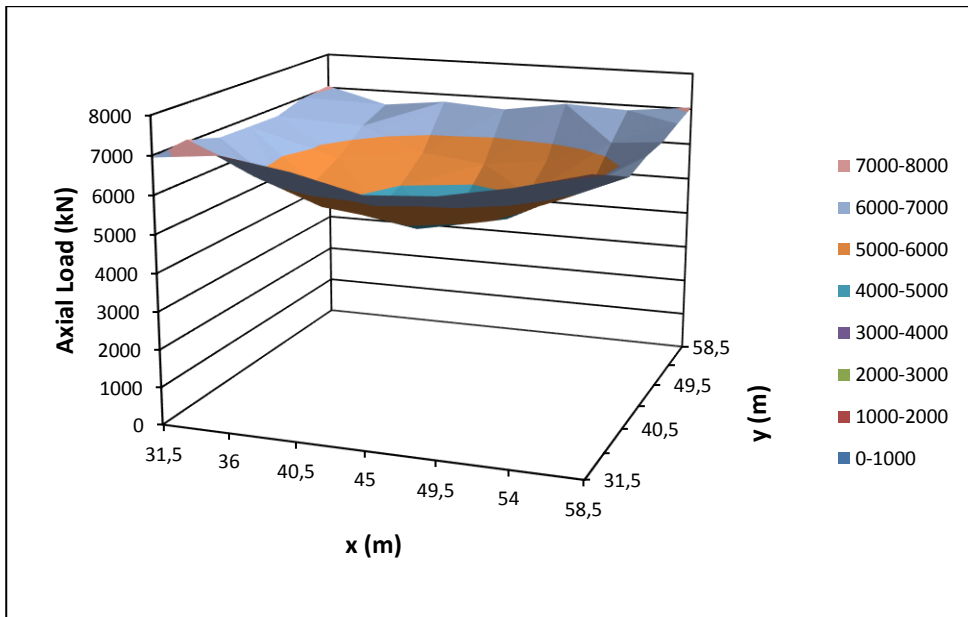
Figure A.38. L=20 m s/d=4.5

133
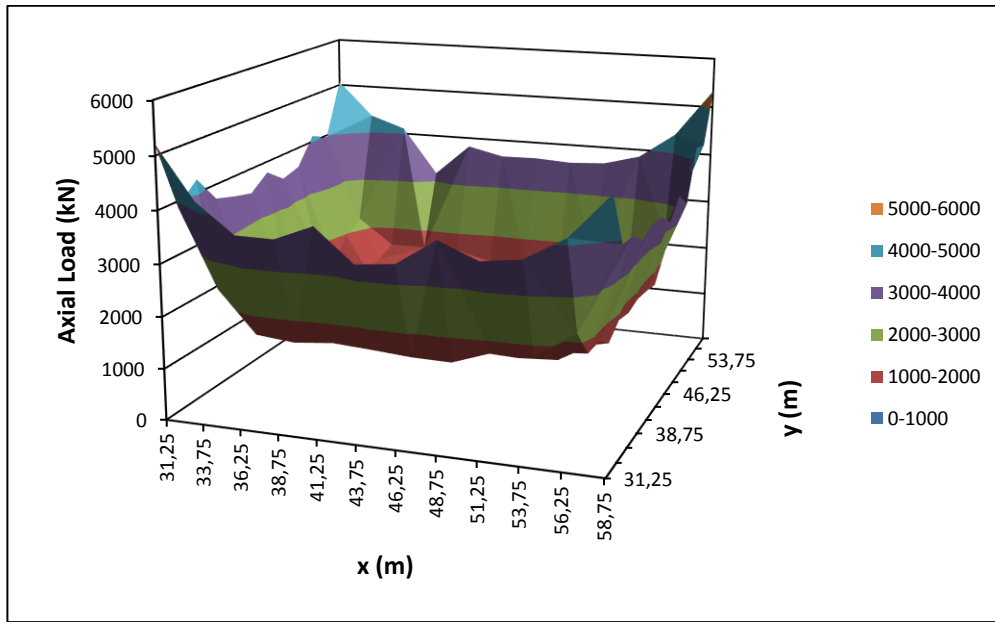
Figure A.39. L=20 m s/d=2.5

Soft Soil Creep Model Results for L=30 m
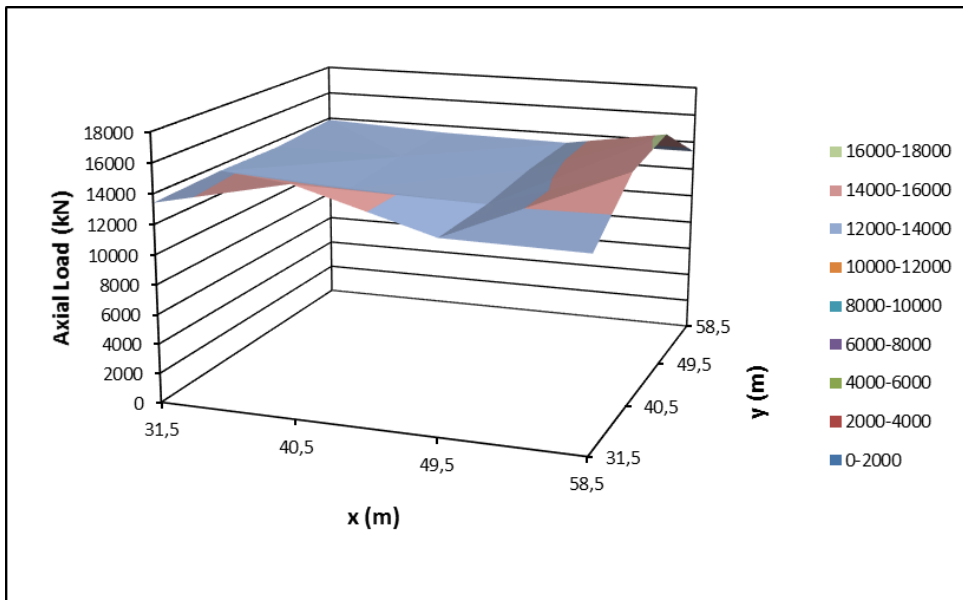
Figure A.40. L=30 m s/d=9
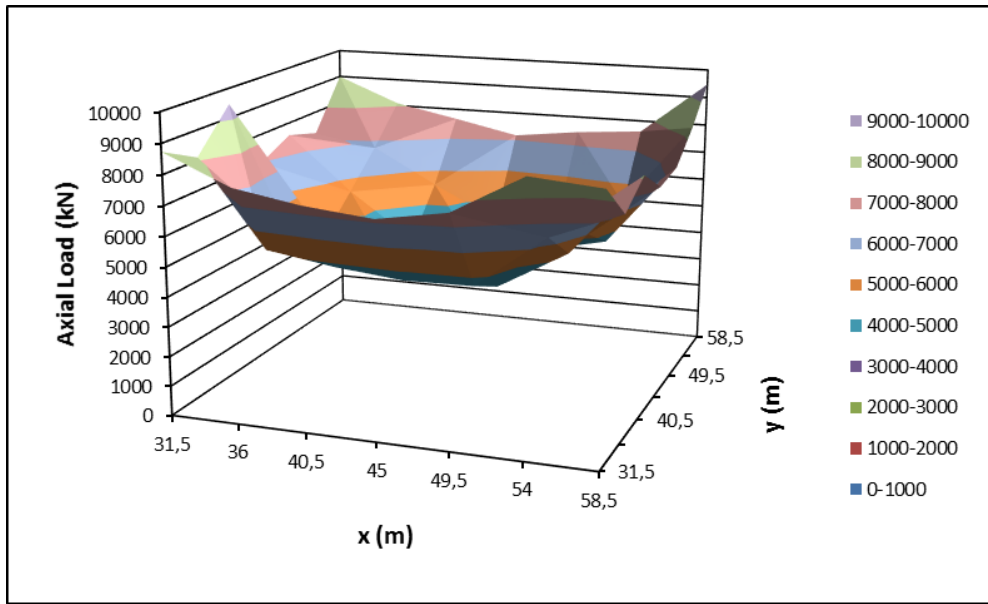
Figure A.41. L=30 m s/d=4.5
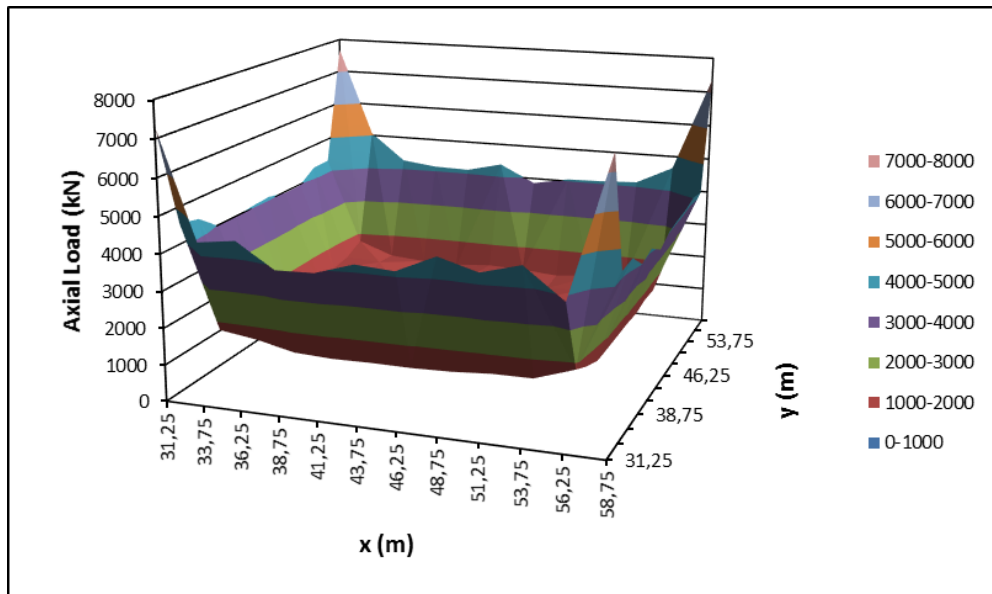
Figure A.42. L=30 m s/d=2.5

Soft Soil Creep Model Results for L=40 m
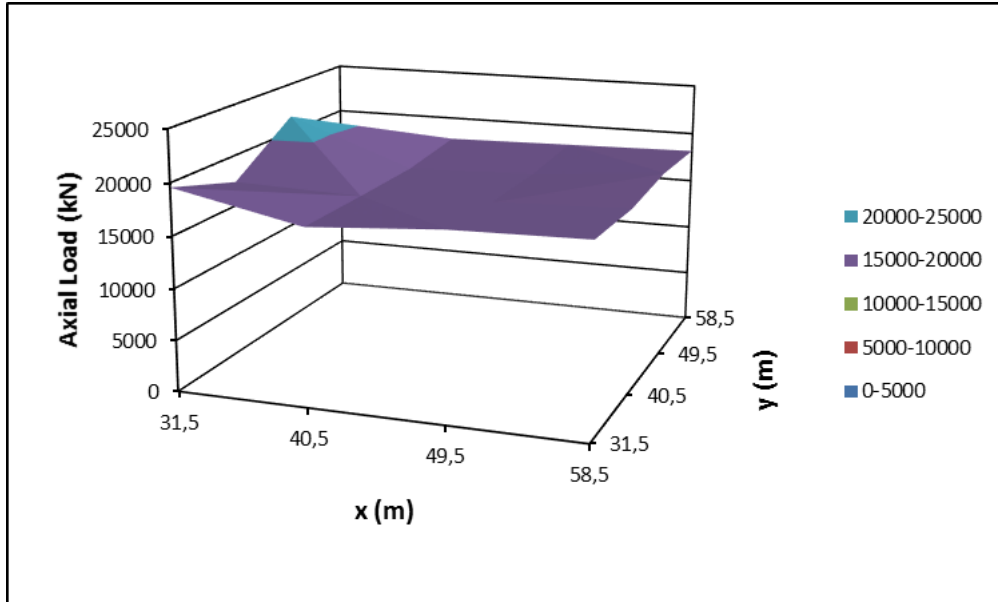
Figure A.43. L=40 m s/d=9
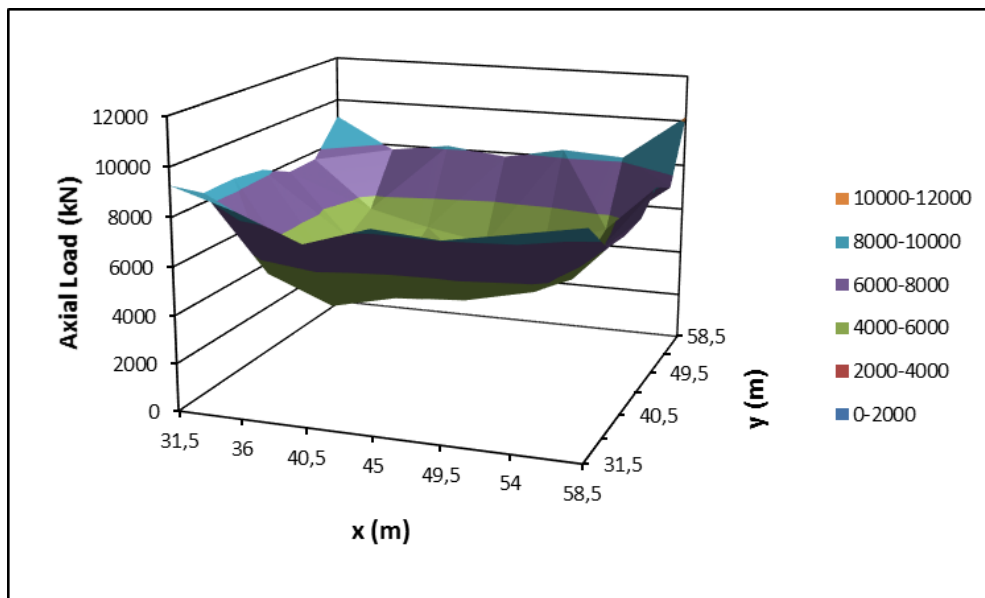
Figure A.44. L=40 m s/d=4.5

136
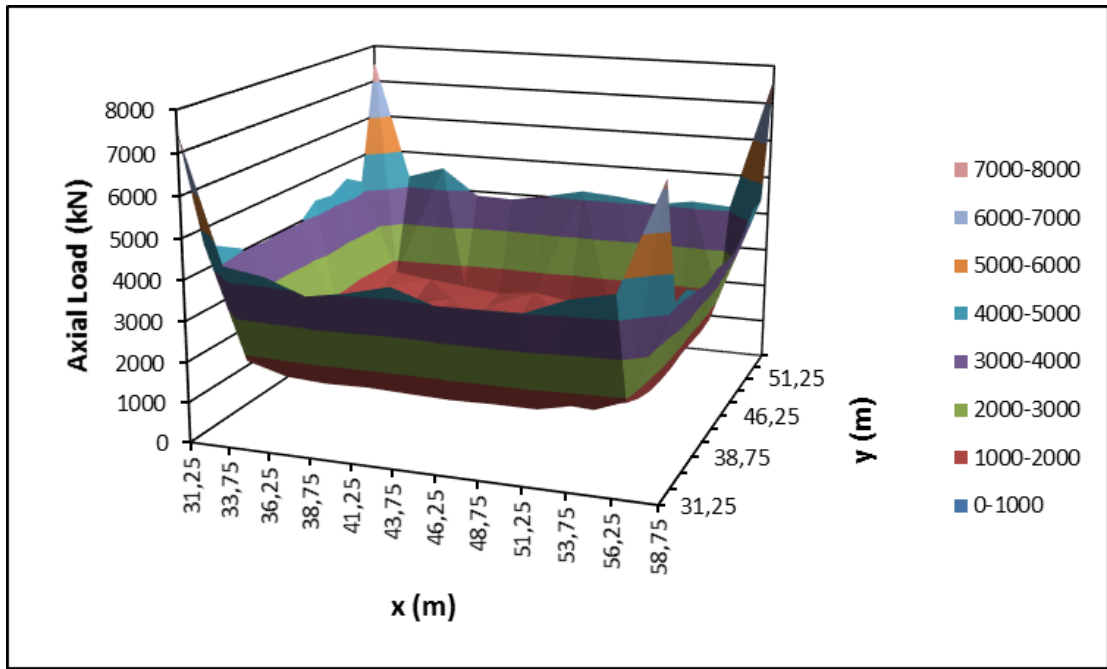
Figure A.45. L=40 m s/d=2.5

B. TABULATION OF ANALYSES RESULTS OF PARAMETRIC STUDY

Table B.1. *L=20, Mohr Coulomb Model results for sand*

s (m)	Settlement (m)	Axial Load, N (kN)	α	Total Pile Length (m)	s/d	SRR
2	0,136	309123,3	0,981	4500	2	0,596
2,25	0,142	292269	0,928	3380	2,25	0,625
2,5	0,140	294070	0,934	2880	2,5	0,613
3	0,141	287456	0,913	2000	3	0,620
3,5	0,141	290394	0,922	1620	3,5	0,618
4,5	0,158	250469	0,795	980	4,5	0,694
5,5	0,164	219037	0,695	720	5,5	0,717
7	0,179	158968	0,505	500	7	0,786
9	0,193	112329	0,357	320	9	0,844

Table B.2. *L=30, Mohr Coulomb Model results for sand*

s (m)	Settlement (m)	Axial Load, N (kN)	α	Total Pile Length (m)	s/d	SRR
2	0,110	309239,5	0,982	6750	2	0,481
2,25	0,109	294954	0,936	5070	2,25	0,477
2,5	0,108	295920	0,939	4320	2,5	0,471
3	0,107	291483	0,925	3000	3	0,467
3,5	0,107	292611	0,929	2430	3,5	0,468
4,5	0,112	277781	0,882	1470	4,5	0,491
5,5	0,120	270341	0,858	1080	5,5	0,526
7	0,138	238707	0,758	750	7	0,606
9	0,162	173970	0,552	480	9	0,709

Table B.3. *L=40, Mohr Coulomb Model results for sand*

s (m)	Settlement (m)	Axial Load, N (kN)	α	Total Pile Length (m)	s/d	SRR
2	0,093	308747,9	0,980	9000	2	0,410
2,25	0,092	300788	0,955	6760	2,25	0,401
2,5	0,089	305940	0,971	5760	2,5	0,392
3	0,089	293927	0,933	4000	3	0,390
3,5	0,089	297589	0,945	3240	3,5	0,388
4,5	0,091	283207	0,899	1960	4,5	0,401
5,5	0,096	276841	0,879	1440	5,5	0,421
7	0,105	263410	0,836	1000	7	0,462
9	0,128	228210	0,724	640	9	0,560

Table B.4. *L=20, Hardening Soil Model results for sand*

s (m)	Settlement (m)	Axial Load, N (kN)	α	Total Pile Length (m)	s/d	SRR
2	0,088	315376,1	1,001	4500	2	0,479
2,25	0,092	297983	0,946	3380	2,25	0,499
2,5	0,089	302892	0,962	2880	2,5	0,483
3	0,094	293646	0,932	2000	3	0,510
3,5	0,094	294855	0,936	1620	3,5	0,509
4,5	0,103	273018	0,867	980	4,5	0,558
5,5	0,119	220189	0,699	720	5,5	0,641
7	0,141	147828	0,469	500	7	0,764
9	0,155	97557	0,310	320	9	0,839

Table B.5. *L=30, Hardening Soil Model results for sand*

s (m)	Settlement (m)	Axial Load, N (kN)	α	Total Pile Length (m)	s/d	SRR
2	0,063	307440	0,976	6750	2	0,339
2,25	0,062	303480	0,963	5070	2,25	0,338
2,5	0,062	303401	0,963	4320	2,5	0,337
3	0,063	298772	0,948	3000	3	0,343
3,5	0,063	298816	0,949	2430	3,5	0,341
4,5	0,069	284685	0,904	1470	4,5	0,371
5,5	0,076	276676	0,878	1080	5,5	0,412
7	0,095	242180	0,769	750	7	0,512
9	0,120	175130	0,556	480	9	0,649

Table B.6. *L=40, Hardening Soil Model results for sand*

s (m)	Settlement (m)	Axial Load, N (kN)	α	Total Pile Length (m)	s/d	SRR
2	0,047	309824	0,984	9000	2	0,256
2,25	0,047	305119	0,969	6760	2,25	0,252
2,5	0,046	305396	0,970	5760	2,5	0,248
3	0,046	301423	0,957	4000	3	0,250
3,5	0,046	299583	0,951	3240	3,5	0,251
4,5	0,050	287649	0,913	1960	4,5	0,269
5,5	0,054	280077	0,889	1440	5,5	0,293
7	0,063	266793	0,847	1000	7	0,340
9	0,086	231180	0,734	640	9	0,467

Table B.7. *L=20, Mohr Coulomb Model results for clay*

s (m)	Settlement (m)	Axial Load, N (kN)	α	Total Pile Length (m)	s/d	SRR
2	0,048	302118,7	0,959	4500	2	0,433
2,25	0,050	275232	0,874	3380	2,25	0,455
2,5	0,050	270463	0,859	2880	2,5	0,451
3	0,053	248028	0,787	2000	3	0,476
3,5	0,052	249630	0,792	1620	3,5	0,470
4,5	0,055	224167	0,712	980	4,5	0,494
5,5	0,061	199227	0,632	720	5,5	0,555
7	0,075	153785	0,488	500	7	0,680
9	0,072	111422	0,354	320	9	0,652

Table B.8. *L=30, Mohr Coulomb Model results for clay*

s (m)	Settlement (m)	Axial Load, N (kN)	α	Total Pile Length (m)	s/d	SRR
2	0,033	305414,5	0,970	6750	2	0,295
2,25	0,033	272902	0,866	5070	2,25	0,303
2,5	0,033	268395	0,852	4320	2,5	0,303
3	0,034	250426	0,795	3000	3	0,311
3,5	0,035	247123	0,785	2430	3,5	0,316
4,5	0,038	226286	0,718	1470	4,5	0,348
5,5	0,042	214958	0,682	1080	5,5	0,383
7	0,049	195816	0,622	750	7	0,442
9	0,056	162198	0,515	480	9	0,506

Table B.9. *L=40, Mohr Coulomb Model results for clay*

s (m)	Settlement (m)	Axial Load, N (kN)	α	Total Pile Length (m)	s/d	SRR
2	0,027	301866,5	0,958	9000	2	0,245
2,25	0,027	278221	0,883	6760	2,25	0,243
2,5	0,027	276521	0,878	5760	2,5	0,240
3	0,027	254959	0,809	4000	3	0,249
3,5	0,028	253536	0,805	3240	3,5	0,252
4,5	0,031	231469	0,735	1960	4,5	0,279
5,5	0,034	219859	0,698	1440	5,5	0,305
7	0,038	202207	0,642	1000	7	0,348
9	0,047	177211	0,563	640	9	0,423

Table B.10. *L=20, Hardening Soil Model results for clay*

s (m)	Settlement (m)	Axial Load, N (kN)	α	Total Pile Length (m)	s/d	SRR
2	0,027	294680,9	0,935	4500	2	0,271
2,25	0,028	266780	0,847	3380	2,25	0,285
2,5	0,028	257720	0,818	2880	2,5	0,284
3	0,031	232124	0,737	2000	3	0,316
3,5	0,031	231424	0,735	1620	3,5	0,316
4,5	0,034	213470	0,678	980	4,5	0,339
5,5	0,039	199368	0,633	720	5,5	0,397
7	0,052	156165	0,496	500	7	0,521
9	0,062	111595	0,354	320	9	0,627

Table B.11. *L=30, Hardening Soil Model results for clay*

s (m)	Settlement (m)	Axial Load, N (kN)	α	Total Pile Length (m)	s/d	SRR
2	0,017	270305,8	0,858	6750	2	0,175
2,25	0,018	251526	0,798	5070	2,25	0,180
2,5	0,018	248909	0,790	4320	2,5	0,180
3	0,019	228448	0,725	3000	3	0,188
3,5	0,020	224357	0,712	2430	3,5	0,199
4,5	0,022	207430	0,659	1470	4,5	0,218
5,5	0,025	199185	0,632	1080	5,5	0,252
7	0,033	191332	0,607	750	7	0,330
9	0,038	161274	0,512	480	9	0,383

Table B.12. *L=40, Hardening Soil Model results for clay*

s (m)	Settlement (m)	Axial Load, N (kN)	α	Total Pile Length (m)	s/d	SRR
2	0,012	265844,2	0,844	9000	2	0,124
2,25	0,012	246737	0,783	6760	2,25	0,126
2,5	0,012	245986	0,781	5760	2,5	0,126
3	0,013	230735	0,732	4000	3	0,135
3,5	0,014	227069	0,721	3240	3,5	0,141
4,5	0,016	210201	0,667	1960	4,5	0,165
5,5	0,019	201370	0,639	1440	5,5	0,193
7	0,024	184407	0,585	1000	7	0,238
9	0,033	171319	0,544	640	9	0,331

Table B.13. *L=20, Soft Soil Creep Model results for clay*

s (m)	Settlement (m)	Axial Load, N (kN)	α	Total Pile Length (m)	s/d	SRR
2	2,416	325798,2	1,034	4500	2	0,555
2,25	2,467	317159,7	1,007	3380	2,25	0,567
2,5	2,445	317121	1,007	2880	2,5	0,562
3	2,45	311649	0,989	2000	3	0,563
3,5	2,415	309804	0,984	1620	3,5	0,555
4,5	2,577	299445	0,951	980	4,5	0,592
5,5	2,701	282008	0,895	720	5,5	0,620
7	3,057	222322	0,706	500	7	0,702
9	3,401	161202	0,512	320	9	0,781

Table B.14. *L=30, Soft Soil Creep Model results for clay*

s (m)	Settlement (m)	Axial Load, N (kN)	α	Total Pile Length (m)	s/d	SRR
2	2,058	329552,1	1,046	6750	2	0,473
2,25	2,072	337023,3	1,070	5070	2,25	0,476
2,5	2,041	326444	1,036	4320	2,5	0,469
3	2,044	316217	1,004	3000	3	0,470
3,5	2,785	335914	1,066	2430	3,5	0,640
4,5	2,111	309648	0,983	1470	4,5	0,485
5,5	2,974	312254	0,991	1080	5,5	0,683
7	2,391	289370	0,919	750	7	0,549
9	2,925	219650	0,697	480	9	0,672

Table B.15. *L=40, Soft Soil Creep Model results for clay*

s (m)	Settlement (m)	Axial Load, N (kN)	α	Total Pile Length (m)	s/d	SRR
2	1,845	332537	1,056	9000	2	0,424
2,25	1,839	329474,7	1,046	6760	2,25	0,422
2,5	1,824	331031	1,051	5760	2,5	0,419
3	2,5	383411	1,217	4000	3	0,574
3,5	1,797	341915	1,085	3240	3,5	0,413
4,5	1,834	311670	0,989	1960	4,5	0,421
5,5	1,855	309822	0,984	1440	5,5	0,426
7	1,918	306880	0,974	1000	7	0,441
9	2,262	287760	0,914	640	9	0,520